1035 354

7909280563

# FUEL ROD BOW EVALUATION

Edited by : J. Skaritka

July 1979

Contributors

| | |
|---|---|
| B. M. Argall | E. A. Dzenis |
| K. Bolewitz | W. J. Leech |
| S. Cerni | F. E. Motley |
| H. Chelemer | J. R. Reavis |

Approved: _L. H. Boman, Manager_
Fuel Performance Engineering
and Evaluation

Approved: _M. G. Arlotti, Manager_
Fuel Licensing Coordination

1035 058

## FOREWORD

Material that is proprietary to the Westinghouse Electric Corporation has been deleted from this document. Such deletions are marked by brackets. The basis for marking the material proprietary is identified by marginal notes referring to the standards in Section 8 of the affidavit of R. A. Wiesemann of record "In the Matter of Acceptance Criteria for Emergency Core Cooling Systems for Light Water Cooled Nuclear Power Reactors (Docket No. RM-50-1)" at transcript pages 3706 through 3710 (February 24, 1972).

## ACKNOWLEDGEMENT

ABSTRACT

The purpose of this document is to report the extent of fuel rod bowing in Westinghouse Low Parasitic (LOPAR) irradiated fuel assemblies and to present an evaluation of bowing effects for fuel performance and plant applications. Empirical bow correlations as a function of fuel assembly burnup are developed. The correlations are used to define the DNBR effect and the power peaking factor uncertainty ($F_Q^U$) effect as a function of burnup and assembly design. Based on fuel rod bowing data, the use of the $L^2$ rod bow scaling factor is justified, where L is the grid span length. Fretting of bowed rods is shown to be negligible and has no safety significance.

# TABLE OF CONTENTS

1035 062

## LIST OF FIGURES

1035 062

1035 064

# LIST OF TABLES

1035 065

# SECTION 1

## INTRODUCTION AND SUMMARY

Prior to 1973 a small amount of fuel rod bow was expected in fabricated fuel and was considered in core departure-from-nuclear boiling (DNB) evaluations by assigning reduced rod-to-rod spacing to the hot channel. In late 1972, a much larger fuel rod bowing was observed in Westinghouse irradiated low parasitic (Zircaloy thimbles and fuel cladding) 14x14 fuel assemblies. Since then, rod bow observations have been obtained from irradiated 14x14 and 15x15 low parasitic (LOPAR) assemblies during reactor refuelings, and more recently from 17x17 irradiated fuel. In 1975 sufficient rod bowing information was available to develop an empirical model to predict rod bow as a function of region average burnup. This information and the effects of predicted rod bowing on power peaking and DNBR analyses were presented in the original WCAP-8691, which was submitted for NRC review in January 1976. In August 1976 the NRC was informed of new DNB test results which showed larger DNBR effects caused by two heated rods in contact near an unheated thimble rod (thimble cell), compared to two heated rods in contact in a typical cell (presented in WCAP-8691). The NRC reviewed this and later information, and the DNBR effects due to rod bow were redefined. A chronology of the rod bow submittals and NRC reviews and approvals is given in Table 1-1.

The fuel rod bow data and evaluations in this report update the previous information on LOPAR fuel submitted to the NRC. Section 2 describes the fuel assembly and the rod bow nomenclature. Section 3 describes the rod bow data base and the procedures used to obtain rod bow data. Section 4 evaluates the data and uses this information to obtain a revised bow correlation related to fuel assembly burnup. The revised bow correlations in Section 4 are used to evaluate the DNBR effects in Section 5. Mechanical evaluations due to rod bowing are presented, and the use of the $L^2$ rod bow scaling factor is justified from irradiated 17 x 17 fuel assembly data which have a different grid span length (L). Section 6 shows how the revised rod bow correlations are applied to various fuel

1-1

TABLE 1-1

CHRONOLOGY OF EVENTS
WESTINGHOUSE AND NRC CORRESPONDENCE
ON REVIEW AND APPROVALS OF ROD BOW SUBMITTALS

January 1976        Submittal of WCAP-8691 to NRC

-   Empirical model predicts rod bow from 22 regions of
    fuel data (14x14, 15x15)

-   Rod bow $F_Q^B$ penalty of 5.6 % offset by
    statistical combination with other peaking factor
    uncertainties, "mini-convolution"

-   DNB penalty offset by generic DNBR design margins

-   Methodology presented for using 14x14 and 15x15 fuel
    data to predict 17x17 rod bowing.

April 1976          NRC Issues Interim SER[1] on WCAP-8691

-   Approval received on mini-convolution approach of
    $F_Q^B$ penalty.

-   Amount of 17x17 bow increased 40-50% compared to
    WCAP projections.

August 1976     -   Westinghouse informs NRC of new data[2] which
                    shows larger DNBR reduction effects than that
                    previously submitted. Westinghouse and NRC inform
                    operating plants to accommodate larger DNBR effects.

1035 269

TABLE 1-1 (Continued)

## CHRONOLOGY OF EVENTS
### WESTINGHOUSE AND NRC CORRESPONDENCE
### ON REVIEW AND APPROVALS OF ROD BOW SUBMITTALS

February 1977 — NRC issues Interim SER[3] on DNBR effects due to rod bowing. Plant $F_{\Delta H}$ limits are identified to accommodate rod bow DNBR effects. Also identified are generic DNBR margins and credits for increased reactor coolant flow and/or reduced core inlet temperature.

October 24, 1977 — Submittal of Westinghouse letter (NS-CE-1580) to NRC for reduction of rod bow DNBR effects on 15x15 and 17x17 fuel, based on partial rod bow DNBR test data and rod bow data from 17x17 demonstration assemblies.

April 1978 — NRC accepts application of rod bow data from 17x17 demonstration assemblies to reduce amount of rod bow and resultant DNBR effect, as documented in Westinghouse letter (NS-TMA-1760) to NRC.

October 13, 1978 — Westinghouse transmittal (NS-TMA-1976) responds to NRC questions on partial rod bow submittal of October 1977.

November 17, 1978 — Westinghouse transmittal (NS-TMA-1986) of additional partial rod bow information to NRC reviewer.

March 16, 1979 — Westinghouse transmittal (NS-TMA-2053) of additional partial rod bow information to NRC reviewer.

April 5, 1979 — NRC issues acceptance letter[17] on partial rod bow DNBR test results, based on Westinghouse Submittals[11] [16].

designs to assess the DNBR effects, and methods for accommodating these effects are discussed. Section 6 also gives the total power peaking factor uncertainty ($F_Q^U$), as a function of assembly burnup, needed to accommodate the rod bow power peaking factor uncertainty.

1035 069

## SECTION 2

## FUEL ASSEMBLY DESIGN AND NOMENCLATURE

### 2.1 FUEL ASSEMBLY DESIGN

Fuel rod bowing data were gathered fo three basic Low-Parasitic (LOPAR) Westinghouse fuel assembly designs having a 14x14, 15x15 or 17x17 square fuel rod pattern. Figure 2-1 shows the typical 15 x 15 fuel assembly. This figure is also representative of the 14x14 design, except for the number of fuel rods. The 14x14 and 15x15 design have identical fuel rod designs and an identical number of grids (7) at the same axial locations. Figure 2-2 shows the typical standard 17x17 fuel assembly, which has smaller diameter fuel rods and an additional grid compared to the 14x14 and 15x15 designs. The 16 x 16 fuel assembly design has the same relationship to the 17 x 17 fuel as the 14 x 14 fuel assembly has to the 15 x 15 fuel. All of the designs have their square array of 12 foot fuel rods supported and spaced by the Inconel grids. The fuel rods are loaded into the fuel assembly structure, which consists of the Inconel grids attached to an array of Zircaloy thimble tubes that are end-supported by the top and bottom nozzles. Since late 1972, all fuel assemblies have been manufactured with the fuel rods offset from the bottom nozzle. Additional information on the fitting together of the fuel assembly components can be obtained from RESAR-3S[4]. Other pertinent comparison information for the three designs and the 17x17 demonstration assemblies are presented in Table 2-1.

Specifically excluded from evaluations in this report are designs with stainless steel thimble tubes and pre-1973 designs with rods resting on the bottom nozzle. The few nuclear plants using fuel with stainless steel thimbles (HIPAR) have experienced much less fuel rod bowing than fuel using Zircaloy thimbles. The NRC has concluded[3] that rod bowing does not represent a safety concern in operating plants using HIPAR fuel assemblies.
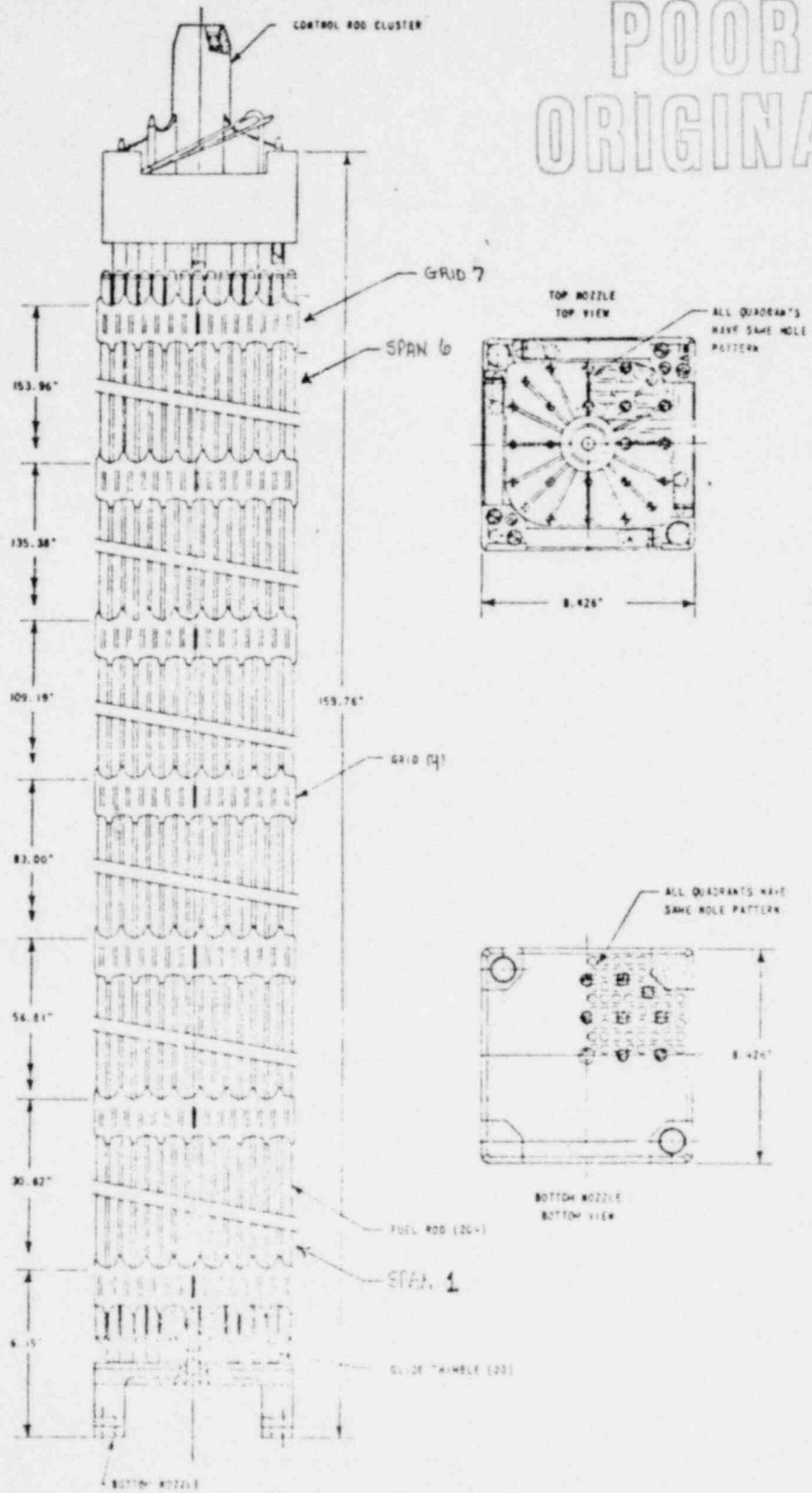
Figure 2-1  Typical 15x15 Fuel Assembly

1035 671
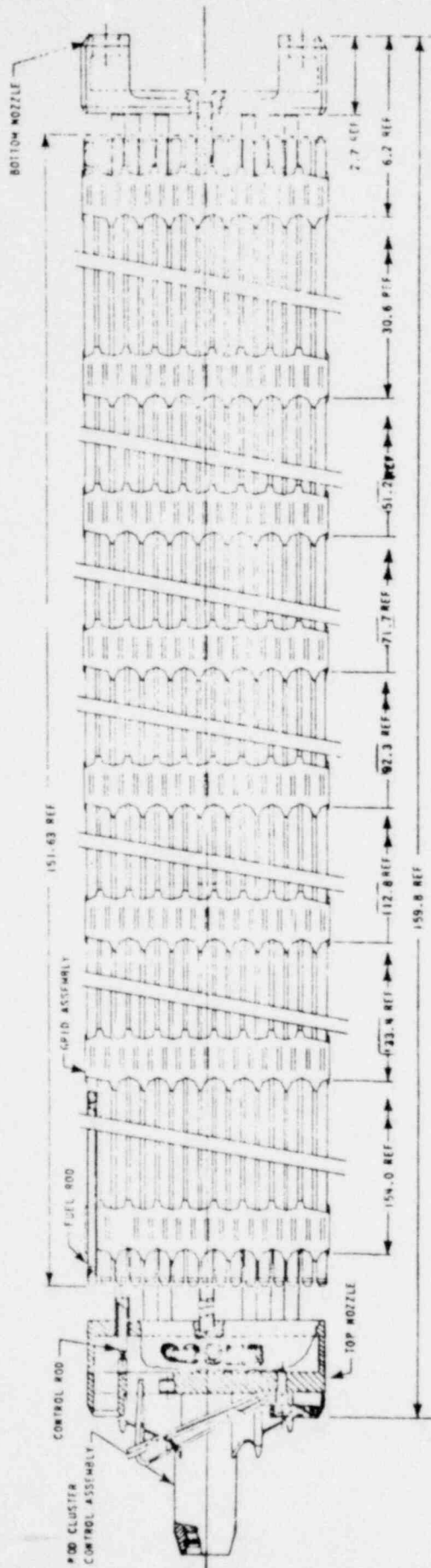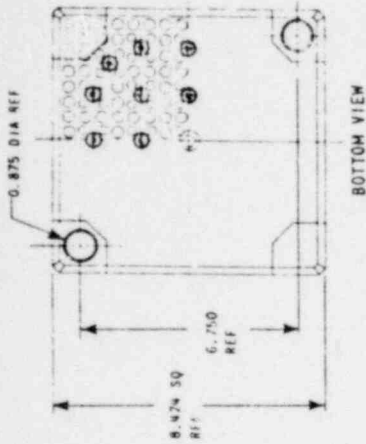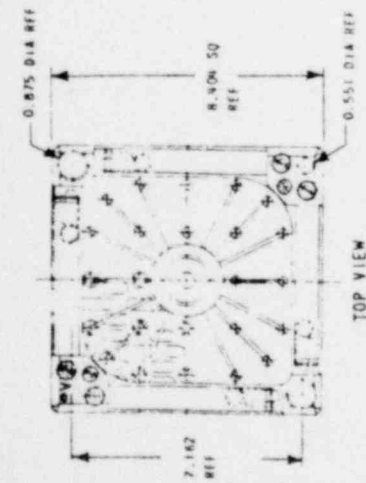
Figure 2-2  Typical 17x17 Fuel Assembly

1035

TABLE 2-1

COMPARISON OF FUEL ASSEMBLY DESIGNS

| | 14 x 14 and 15 x 15 Fuel Assemblies | Standard and Demonstration* 17 x 17 Fuel Assemblies |
|---|---|---|
| Rod OD (inches) | .422 | .374 |
| Rod - Rod Gap (inches) | .141 (15x15) .134 (14x14) | .122 |
| Pellet - Clad Diametral Gap (inches) | .007 | .0065 |
| Pellet Diameter (inches) | .366 | .323 |
| Rod Length (inches) | 151.6 | 151.6 |
| Nominal Fuel Length (inches) | 144 | 144 |
| Number of Grids (Inconel) | 7 | 8 (Standard) 7 (Demonstration) |

---

\*  Except for the number of grids, the demonstration assemblies were
equivalent to the standard 17x17 assemblies. The axial location of
the demonstration assembly grids were the same as for the 15x15
assemblies.

1035 073

## 2.2 FUEL ASSEMBLY NOMENCLATURE

For the remainder of this report, the following terms and identification schemes will be used:

Channel — The space between adjacent fuel rods. Channels are numbered from left to right when looking directly at the fuel assembly face (see Figure 2-3).

Gap — Lateral distance between the adjacent fuel rods or channel width.

Rod Bow — The lateral deformation of a fuel rod, assuming an initial straight (unbowed) rod in a given span.

Face — The surface fuel rods on the side of any assembly. These are numbered counter-clockwise from the Y Corner (reference) from 1 to 4 when looking down on the assembly (see Figure 2-3).

Span — The fuel rod region between grids. These are numbered from the bottom of the fuel assembly starting with Span 1 between Grids No. 1 and 2.

Burnup — Unless otherwise specified burnups reported are the best estimate average burnup for individual assemblies and not region average burnups.

Channel Closure — The difference between the nominal unbowed gap and the minimum gap (at a fixed elevation) between surfaces of the two fuel rods associated with a channel. It is expressed as a fraction of the unbowed gap. It is to be noted that no attempt is made to measure individual rod displacement.
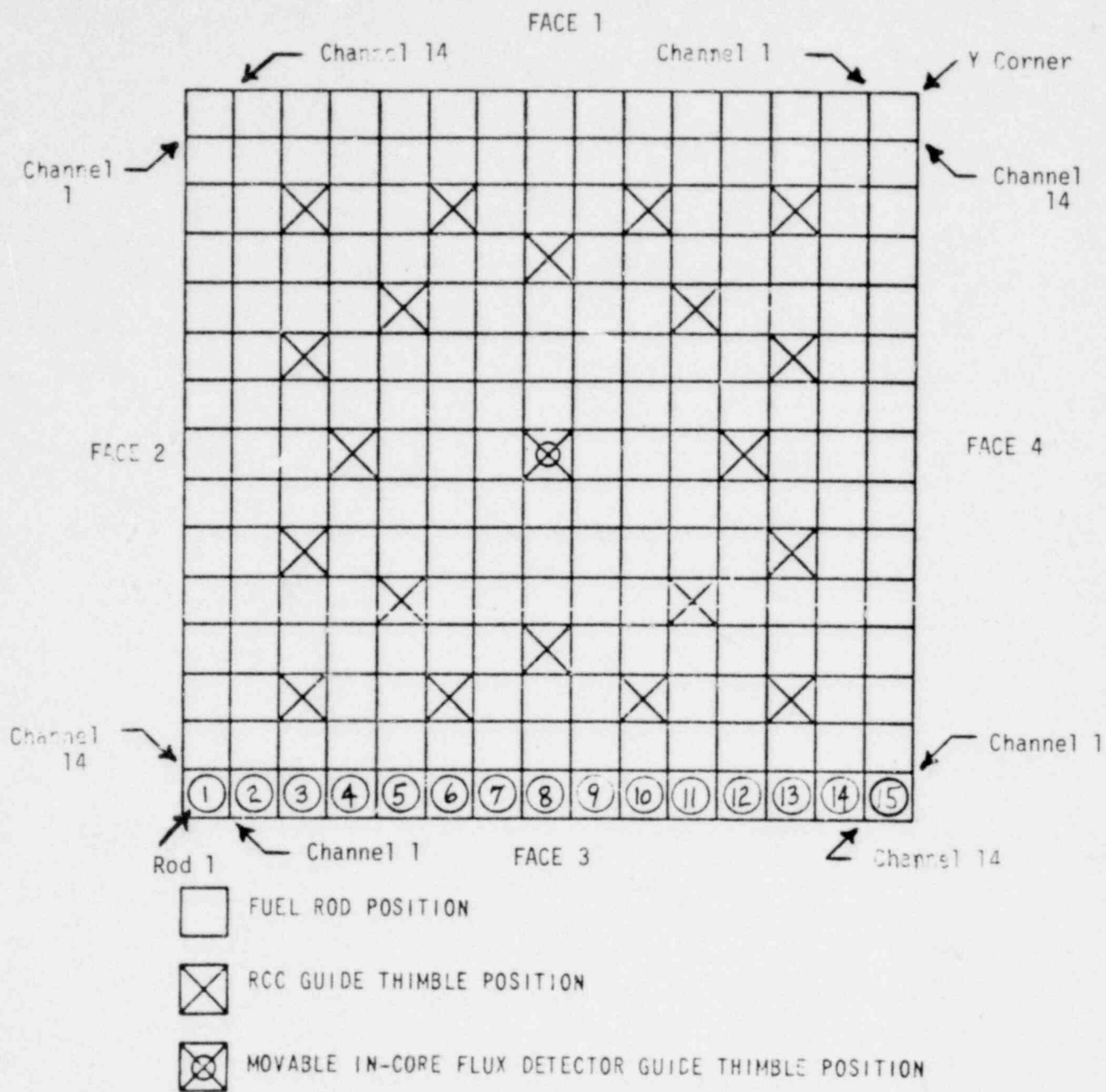
1035 074

Figure 2-3 Schematic of Assembly Face, Rod and Channel Position

1035 075

Worst Span   -   The distribution of channel closures is determined
for each span in an assembly. The worst span is the
one whose channel closure distribution results in
the largest standard deviation.

On-Bottom   -   Those fuel assembly designs with rods manufactured
in contact with the bottom nozzle assembly.

Off-Bottom   -   Those fuel assembly designs with a manufactured
offset between the rod bottom end plugs and the
bottom nozzle assembly (see Figures 2-1 and 2-2).

SECTION 3

ROD BOW OBSERVATIONS

Since late 1972 the phenomenon of rod bow has been observed in irra-
diated Westinghouse fuel assemblies. Fuel assemblies from a total of 14
nuclear plants have been examined for rod bow at various reactor cycle
shutdowns, and a total of 1656 assemblies with varied burnup experience
have been examined.

The Westinghouse rod bow performance database has been acquired from
irradiated fuel assemblies in two general ways. The bulk of data has
been reduced from television tapes made during on-site examinations of
irradiated assemblies in the spent fuel pits. The second method of
acquiring bow data is by the use of a strain gage, otherwise known as
the Channel Spacing Measurement System (CSMS). Television tapes allow
for the observation of peripheral rods only, while the CSMS enables the
measurement of all interior channels as well.

## 3.1 TV ROD BOW MEASUREMENTS

As experience in measuring rod bow has increased, several methods of
using the television tape have been developed. Earliest TV visuals
inspections were made at low magnification, such that one half the full
complement of rods for each assembly face were viewed at one time. Each
face was scanned in two vertical passes along its entire length.
Channel closures were either visually estimated or directly measured
from the TV screen using dividers and a ruler. Although this method of
TV taping has served the purpose of rod bow data reduction rather well,
the accuracy and precision of the measurements taken at each reactor
site were dependent on such factors as the water clarity in the spent
fuel pit, the existing lighting conditions, and television camera para-
meters and calibration. Therefore, a quality index has been designated
for each data set. There were cases in which low magnification tapes
did not allow for clear definition of individual rod edges, thus making

1035 074

accurate measurements difficult. These tapes have allowed only esti-
mates of channel closures and have been designated as data quality "1".
Data quality "2" has been assigned to those better quality low magnifi-
cation tapes where more accurate direct measurements were possible.

Later TV visual inspections have been improved through the use of high
magnification video tape equipment. To further improve measurements
using this method, only three rods at a time are viewed and scans are
made horizontally across each face of an assembly. These horizontal
scans are conducted just below each grid, just above each grid and at
each mid-grid elevation. Channel spacings are measured directly from
the TV screen, where high magnification allows clearer definition of
individual rod edges. Measurements can be taken from high magnification
TV tapes in either of two ways, depending on the particular TV equipment
used to inspect the irradiated assemblies on site. Data can be reduced
by measuring the channel spacing between adjacent rods in each hori-
zontal scan from the TV screen with dividers and a ruler. In those
cases where more sophisticated television equipment was used during the
on-site examination, it was possible to reduce data using a vertical
raster line in conjunction with a digital encoder. Encoder readings are
taken for each rod edge at each of the three key locations for each grid
span. These readings are then used to determine the channel closures.
Both types of high magnification data are designated as data quality "3".

## 3.2  CHANNEL CLOSURE DETERMINATION FROM TV OBSERVATIONS

Calculation of the percentage channel closure is the same for each of
the three methods of television data acquisition. It can be described
by the equation:

$$\% \text{ Channel Closure} = 100 \cdot \left[ 1 - \frac{C}{(A+B)/2} \right] \tag{3-1}$$

3-2

where:   A = measurement of gap above lower grid of span i

B = measurement of gap below upper grid of span i

C = measurement of gap at mid-grid of span i

Although both data of qualities 2 and 3 serve well in evaluating the relative extent of significant rod bow, analysis has indicated that low magnification may tend to overestimate individual channel closures. Reduction of individual channel closure data at low magnification indicated a positive mean bias when compared to the same channels viewed at high magnification. Generally speaking, for a given assembly, low magnification has also indicated a greater extent of significant rod bow than high magnification and, therefore, could be considered conservative.

## 3.3   PROBE CHANNEL SPACING MEASUREMENTS

The channel spacing measurement system, the second method of measuring rod bow performance, utilizes a strain gauge probe to measure rod-to-rod spacing. The probe is passed directly through each row of rods at the mid-grid span location. All channels, both interior and peripheral, within the range of 40 mils to 190 mils (fully depressed to fully open spring elements) can be measured. Percentage channel closure is then calculated, unlike TV tape measurements, with respect to nominal channel spacing. When measuring channel spacings, small measurement errors can occur due to the probe deflecting the rods as it is passed between them. The amount of this deflection is dependent on both the particulai stiffness of the rods involved and the size of the gap between them. A small correction was applied to the measured gaps to compensate for this effect. A most significant feature of the CSMS is its ability to provide data for interior as well as exterior rods. Data which have been obtained through use of the CSMS are classified as data quality "4".

## 3.4   ROD BOW DATA BASE

The rod bow correlations described in Section 4 are derived from the rod bow observations made on a total of 1656 irradiated fuel assemblies from

14 different Westinghouse Nuclear Plants. Table 2-1 lists the descriptive characteristics of the assemblies which currently comprise the Westinghouse rod bow performance database shown in Table 3-1. A summary of the channel closure data is presented in Section 4.

# TABLE 3-1

## SUMMARY OF WESTINGHOUSE ROD BOW PERFORMANCE DATA BASE

| Plant/ Fuel Rod Diameter (Inches) | Region * | Cycle | Assembly Avg. BU ($10^3$MWD/MTU) | Number of Assemblies | Data Quality |
|---|---|---|---|---|---|
| A (0.422) | 1 (OFF) | 1 | 18-20 | 2 | 2 |
| | 2 (OFF) | 1 | 20-22 | 2 | 2 |
| | 3 (OFF) | 1 | 16-18 | 3 | 2 |
| B (0.422) | 2 (ON) | 2 | 26-28 | 2 | 1 |
| | 3 (ON) | 2 | 20-22 | 4 | 1 |
| | 3 (ON) | 2 | 22-24 | 2 | 1 |
| | 3 (ON) | 2 | 24-26 | 4 | 1 |
| | 4 (OFF) | 2 | 6-8 | 28 | 1 |
| | 4 (OFF) | 2 | 8-10 | 1 | 1 |
| | 4 (OFF) | 2 | 10-12 | 15 | 1 |
| | 4 (OFF) | 2 | 12-14 | 8 | 1 |
| C (0.422) | 2 (OFF) | 1 | 18-20 | 10 | 2 |
| | 2 (OFF) | 2 | 30-32 | 7 | 2 |
| | 2 (OFF) | 2 | 30-32 | 2 | 3 |
| | 2 (OFF) | 2 | 32-34 | 1 | 3 |
| | 3 (OFF) | 1 | 8-10 | 4 | 2 |
| | 3 (OFF) | 1 | 10-12 | 1 | 2 |
| | 3 (OFF) | 1 | 14-16 | 3 | 2 |
| | 3 (OFF) | 1 | 16-18 | 2 | 2 |
| | 3 (OFF) | 2 | 22-24 | 1 | 2 |
| | 3 (OFF) | 2 | 22-24 | 1 | 3 |
| | 3 (OFF) | 2 | 26-28 | 1 | 2 |
| | 3 (OFF) | 2 | 30-32 | 1 | 2 |
| | 3 (OFF) | 2 | 30-32 | 2 | 3 |
| | 3 (OFF) | 3 | 38-40 | 3 | 3 |
| D (0.422) | 1 (OFF) | 1 | 10-12 | 2 | 2 |
| | 1 (OFF) | 1 | 12-14 | 1 | 2 |
| | 1 (OFF) | 1 | 14-16 | 8 | 2 |
| | 2 (OFF) | 1 | 14-16 | 3 | 2 |
| | 2 (OFF) | 1 | 16-18 | 17 | 2 |
| | 2 (OFF) | 2 | 22-24 | 2 | 1 |
| | 2 (OFF) | 2 | 24-26 | 8 | 1 |
| | 3 (OFF) | 1 | 8-10 | 8 | 2 |
| | 3 (OFF) | 1 | 10-12 | 2 | 2 |
| | 3 (OFF) | 1 | 12-14 | 6 | 2 |
| | 3 (OFF) | 1 | 14-16 | 4 | 2 |
| | 3 (OFF) | 3 | 26-28 | 9 | 2 |
| | 3 (OFF) | 3 | 30-32 | 6 | 2 |

---

* OFF - Fuel rods Off-Bottom
  ON  - Fuel rods On Bottom

TABLE 3-1 (Continued)

SUMMARY OF WESTINGHOUSE ROD BOW PERFORMANCE DATA BASE

| Plant/ Fuel Rod Diameter (Inches) | Region * | Cycle | Assembly Avg. BU ($10^3$MWD/MTU) | Number of Assemblies | Data Quality |
|---|---|---|---|---|---|
| D (cont) | 3 (OFF) | 3 | 32-34 | 4 | 2 |
| (0.422) | 4 (OFF) | 3 | 10-12 | 2 | 2 |
| | 5 (OFF) | 3 | 4-6 | 2 | 2 |
| | 5 (OFF) | 3 | 8-10 | 2 | 2 |
| | | | | | |
| E | 1 (ON) | 1A | 10-12 | 16 | 2 |
| (0.422) | 1 (ON) | 1A | 12-14 | 25 | 2 |
| | 1 (ON) | 1B | 18-20 | 7 | 2 |
| | 1 (ON) | 1B | 20-22 | 20 | 2 |
| | 2 (OFF) | 1A | 10-12 | 20 | 2 |
| | 2 (OFF) | 1A | 12-14 | 20 | 2 |
| | 2 (OFF) | 1B | 20-22 | 33 | 2 |
| | 2 (OFF) | 1B | 22-24 | 1 | 2 |
| | 2 (ON) | 2 | 28-30 | 24 | 2 |
| | 2 (ON) | 2 | 30-32 | 5 | 2 |
| | 3 (ON) | 1A | 6-8 | 20 | 2 |
| | 3 (ON) | 1A | 8-10 | 20 | 2 |
| | 3 (ON) | 1B | 12-14 | 6 | 2 |
| | 3 (ON) | 1B | 14-16 | 2 | 2 |
| | 3 (ON) | 1B | 16-18 | 18 | 2 |
| | 3 (ON) | 1B | 18-20 | 4 | 2 |
| | 3 (ON) | 1B | 20-22 | 6 | 2 |
| | 3 (ON) | 2 | 20-22 | 6 | 2 |
| | 3 (ON) | 2 | 22-24 | 2 | 2 |
| | 3 (ON) | 2 | 24-26 | 10 | 2 |
| | 3 (ON) | 2 | 26-28 | 8 | 2 |
| | 3 (ON) | 2 | 28-30 | 6 | 2 |
| | 3 (ON) | 2 | 6-8 | 2 | 2 |
| | 4 (OFF) | 1B | 6-8 | 24 | 2 |
| | 4 (OFF) | 2 | 12-14 | 8 | 2 |
| | 4 (OFF) | 2 | 14-16 | 4 | 2 |
| | 4 (OFF) | 2 | 16-18 | 10 | 2 |
| | 4 (OFF) | 2 | 4-6 | 10 | 2 |
| | 4 (OFF) | 2 | 6-8 | 6 | 2 |
| | 5 (OFF) | 2 | 4-6 | 4 | 2 |
| | 5 (OFF) | 2 | 6-8 | 2 | 2 |
| | 5 (OFF) | 2 | 8-10 | 14 | 2 |
| | | | | | |
| F | 1 (OFF) | 1 | 12-14 | 7 | 2 |
| (0.422) | 1 (OFF) | 1 | 14-16 | 46 | 2 |
| | 1 (OFF) | 2 | 16-18 | 5 | 2 |
| | 1 (OFF) | 2 | 18-20 | 4 | 2 |
| | 2 (OFF) | 1 | 14-16 | 32 | 2 |

---

* OFF - Fuel rods Off-Bottom
  ON  - Fuel rods On Bottom

1035 002

## SUMMARY OF WESTINGHOUSE ROD BOW PERFORMANCE DATA BASE

| Plant/<br>Fuel Rod<br>Diameter<br>(Inches) | Region * | Cycle | Assembly<br>Avg. BU<br>(10³MWD/MTU) | Number<br>of Assemblies | Data<br>Quality |
|---|---|---|---|---|---|
| F (cont)<br>(0.422) | 2 (OFF) | 1 | 16-18 | 20 | 2 |
| | 2 (OFF) | 2 | 18-20 | 1 | 2 |
| | 2 (OFF) | 2 | 20-22 | 31 | 2 |
| | 2 (OFF) | 2 | 22-24 | 19 | 2 |
| | 3 (OFF) | 1 | 8-10 | 27 | 2 |
| | 3 (OFF) | 1 | 10-12 | 4 | 2 |
| | 3 (OFF) | 1 | 12-14 | 28 | 2 |
| | 3(OFF) | 2 | 16-18 | 19 | 2 |
| | 3 (OFF) | 2 | 18-20 | 13 | 2 |
| | 3 (OFF) | 2 | 20-22 | 12 | 2 |
| | 3 (OFF) | 2 | 4-6 | 2 | 2 |
| | 4 (OFF) | 2 | 4-6 | 25 | 2 |
| | 4 (OFF) | 2 | 6-8 | 25 | 2 |
| G<br>(0.422) | 1 (OFF) | 1 | 10-12 | 8 | 2 |
| | 1 (OFF) | 1 | 12-14 | 24 | 2 |
| | 1 (OFF) | 1 | 14-16 | 21 | 2 |
| | 2 (OFF) | 1 | 12-14 | 22 | 2 |
| | 2 (OFF) | 1 | 14-16 | 30 | 2 |
| | 3 (OFF) | 1 | 6-8 | 3 | 2 |
| | 3 (OFF) | 1 | 8-10 | 22 | 2 |
| | 3 (OFF) | 1 | 10-12 | 13 | 2 |
| | 3 (OFF) | 1 | 12-14 | 14 | 2 |
| H<br>(0.422) | 1 (ON) | 1 | 10-12 | 2 | 1 |
| | 1 (ON) | 1 | 12-14 | 1 | 1 |
| | 1 (ON) | 1 | 14-16 | 14 | 1 |
| | 1 (ON) | 1 | 16-18 | 5 | 1 |
| | 2 (OFF) | 1 | 14-16 | 4 | 1 |
| | 2 (OFF) | 1 | 16-18 | 4 | 1 |
| | 2 (OFF) | 2 | 24-25 | 6 | 2 |
| | 2 (OFF) | 2 | 26-28 | 2 | 2 |
| | 3 (OFF) | 1 | 8-10 | 12 | 1 |
| | 3 (OFF) | 1 | 12-14 | 3 | 1 |
| | 4 (OFF) | 2 | 4-6 | 2 | 2 |
| I<br>(0.422) | 1 (ON) | 1 | 10-12 | 2 | 1 |
| | 1 (ON) | 1 | 12-14 | 2 | 1 |
| | 1 (ON) | 1 | 14-16 | 8 | 1 |
| | 2 (ON) | 1 | 12-14 | 4 | 1 |
| | 2 (ON) | 1 | 14-16 | 7 | 1 |
| | 2 (ON) | 1 | 16-18 | 9 | 1 |
| | 2 (ON) | 1 | 6-8 | 2 | 1 |

---

* OFF - Fuel rods Off-Bottom
  ON  - Fuel rods On Bottom

3-7

1035 083

TABLE 3-1 (Continued)

SUMMARY OF WESTINGHOUSE ROD BOW PERFORMANCE DATA BASE

| Plant/ Fuel Rod Diameter (Inches) | Region * | Cycle | Assembly Avg. BU ($10^3$MWD/MTU) | Number of Assemblies | Data Quality |
|---|---|---|---|---|---|
| I (cont) | 3 (ON) | 1 | 10-12 | 4 | 1 |
| (0.422) | 3 (ON) | 1 | 12-14 | 3 | 1 |
| | 3 (ON) | 3 | 18-20 | 3 | 2 |
| | 3 (ON) | 3 | 20-22 | 1 | 2 |
| | 3 (ON) | 3 | 22-24 | 8 | 2 |
| | | | | | |
| J | 1 (ON) | 1 | 16-18 | 5 | 1 |
| (0.422) | 1 (ON) | 1 | 18-20 | 4 | 1 |
| | 1 (ON) | 1 | 20-22 | 9 | 1 |
| | 2 (ON) | 1 | 18-20 | 8 | 1 |
| | 2 (ON) | 1 | 20-22 | 9 | 1 |
| | 2 (ON) | 2 | 28-30 | 11 | 1 |
| | 2 (ON) | 2 | 30-32 | 21 | 1 |
| | 2 (ON) | 2 | 32-34 | 8 | 1 |
| | 3 (ON) | 1 | 10-12 | 8 | 1 |
| | 3 (ON) | 1 | 12-14 | 1 | 1 |
| | 3 (ON) | 1 | 14-16 | 3 | 1 |
| | 3 (ON) | 1 | 16-18 | 5 | 1 |
| | 3 (ON) | 2 | -22 | 8 | 1 |
| | 3 (ON) | 2 | 22-24 | 8 | 1 |
| | 3 (ON) | 2 | 24-26 | 4 | 1 |
| | 3 (ON) | 2 | 26-28 | 10 | 1 |
| | 3 (ON) | 2 | 28-30 | 5 | 1 |
| | 4 (OFF) | 2 | 6-8 | 20 | 1 |
| | 4 (OFF) | 2 | 8-10 | 4 | 1 |
| | 4 (OFF) | 2 | 10-12 | 8 | 1 |
| | 4 (OFF) | 2 | 12-14 | 9 | 1 |
| | 4 (OFF) | 3 | 22-24 | 8 | 2 |
| | 4 (OFF) | 3 | 24-26 | 2 | 2 |
| | 4 (OFF) | 3 | 26-28 | 1 | 2 |
| | 4 (OFF) | 3 | 28-30 | 2 | 2 |
| | 4 (OFF) | 4 | 32-34 | 1 | 2 |
| | | | | | |
| | 6 (OFF) | 4 | 16-18 | 1 | 2 |
| | 7 (OFF) | 4 | 4-6 | 5 | 2 |
| | 7 (OFF) | 4 | 6-8 | 1 | 2 |
| | 7 (OFF) | 4 | 8-10 | 2 | 2 |
| | | | | | |
| J/K+ | 1 (ON) | 4 | 24-26 | 4 | 2 |
| (0.422) | 2 (ON) | 4 | 28-30 | 2 | 2 |

+ Contains combination of J and K irradiated fuel in Cycle 4 of plant J.
* OFF - Fuel rods Off-Bottom
  ON  - Fuel rods On Bottom

1035 084

TABLE 3-1 (Continued)

SUMMARY OF WESTINGHOUSE ROD BOW PERFORMANCE DATA BASE

| Plant/ Fuel Rod Diameter (Inches) | Region * | Cycle | Assembly Avg. BU ($10^3$MWD/MTU) | Number of Assemblies | Data Quality |
|---|---|---|---|---|---|
| K (0.422) | 1 (ON) | 1 | 16-18 | 4 | 1 |
| | 1 (ON) | 1 | 18-20 | 21 | 1 |
| | 1 (ON) | 1 | 20-22 | 8 | 1 |
| | 2 (ON) | 1 | 18-20 | 17 | 1 |
| | 2 (ON) | 1 | 20-22 | 9 | 1 |
| | 3 (ON) | 1 | 10-12 | 1 | 2 |
| | 3 (ON) | 1 | 14-16 | 4 | 2 |
| | 3 (ON) | 1 | 14-16 | 4 | 1 |
| | 3 (ON) | 1 | 16-18 | 4 | 2 |
| | 3 (ON) | 1 | 16-18 | 1 | 1 |
| | 3 (ON) | 3 | 34-36 | 8 | 1 |
| | 3 (ON) | 3 | 36-38 | 6 | 1 |
| | 3 (ON) | 3 | 38-40 | 4 | 1 |
| | 4 (OFF) | 3 | 18-20 | 2 | 1 |
| | 4 (OFF) | 3 | 20-22 | 4 | 1 |
| | 4 (OFF) | 3 | 24-26 | 2 | 1 |
| | 4 (OFF) | 3 | 26-28 | 2 | 1 |
| | 5 (OFF) | 3 | 6-8 | 2 | 1 |
| | 5 (OFF) | 3 | 8-10 | 4 | 1 |
| | 5 (OFF) | 3 | 12-14 | 2 | 1 |
| L (0.374) | 1 (OFF) | 1 | 14-16 | 1 | 3 |
| | 1 (OFF) | 1 | 16-18 | 1 | 3 |
| | 1 (OFF) | 1 | 18-20 | 4 | 3 |
| | 2 (OFF) | 1 | 16-18 | 1 | 3 |
| | 2 (OFF) | 1 | 18-20 | 5 | 3 |
| | 3 (OFF) | 1 | 8-10 | 2 | 3 |
| | 3 (OFF) | 1 | 12-14 | 2 | 3 |
| | 3 (OFF) | 1 | 16-18 | 1 | 3 |
| H (0.374) | 4 (ON) | 2 | 6-8 | 2 | 2 |
| | 4 (ON) | 3 | 14-16 | 2 | 2 |
| I (0.374) | 4 (ON) | 2 | 8-10 | 2 | 2 |
| | 4 (ON) | 3 | 16-18 | 2 | 2 |
| M (0.422) | 3 (ON) | 3 | 22-24 | 3 | 2 |
| | 3 (ON) | 3 | 26-28 | 3 | 2 |
| | 3 (ON) | 3 | 28-30 | 6 | 2 |
| | 3 (ON) | 3 | 30-32 | 8 | 2 |
| | 4 (OFF) | 3 | 14-16 | 3 | 2 |
| | 4 (OFF) | 3 | 16-18 | 2 | 2 |
| | 4 (OFF) | 3 | 18-20 | 3 | 2 |

* OFF - Fuel rods Off-Bottom
  ON - Fuel rods On Bottom

1035 085

TABLE 3-1 (Continued)

SUMMARY OF WESTINGHOUSE ROD BOW PERFORMANCE DATA BASE

| Plant/ Fuel Rod Diameter (Inches) | Region * | Cycle | Assembly Avg. BU ($10^3$ MWD/MWD) | Number of Assemblies | Data Quality |
|---|---|---|---|---|---|
| M (cont) | 5 (OFF) | 3 | 4-6 | 7 | 2 |
| (0.422) | 51 (OFF) | 4 | 16-18 | 2 | 3 |
| | 52 (OFF) | 4 | 14-16 | 6 | 3 |
| | 6 (OFF) | 4 | 4-6 | 2 | 3 |
| | 6 (OFF) | 4 | 6-8 | 3 | 3 |
| | 6 (OFF) | 4 | 8-10 | 1 | 3 |
| | | | | | |
| L | 1 (OFF) | 1 | 14-16 | 2 | 4 |
| (0.374) | 1 (OFF) | 1 | 16-18 | 2 | 4 |
| | 1 (OFF) | 1 | 18-20 | 1 | 4 |
| | 2 (OFF) | 1 | 18-20 | 3 | 4 |
| | 3 (OFF) | 1 | 8-10 | 1 | 4 |
| | 3 (OFF) | 1 | 10-12 | 1 | 4 |
| | 3 (OFF) | 1 | 16-18 | 1 | 4 |
| | | | | | |
| C (0.422) | 2 (OFF) | 2 | 30-32 | 5 | 4 |
| | | | | | |
| I | 3 (ON) | 3 | 18-20 | 2 | 4 |
| (0.422) | 3 (ON) | 3 | 20-22 | 1 | 4 |
| | 3 (ON) | 3 | 22-24 | 2 | 4 |
| | | | | | |
| I (0.374) | 4 (ON) | 3 | 16-18 | 2 | 4 |
| | | | | | |
| N (0.422) | 4 (OFF) | 4 | 28-30 | 11 | 2 |

---

* OFF - Fuel rods Off-Bottom
ON - Fuel rods On Bottom

1035 086

## SECTION 4

## EMPIRICAL BOW CORRELATION

### 4.1 DATA ANALYSIS

### 4.1.1 REDUCTION OF ROD BOW DATA

Since rod bow data were obtained using a number of techniques described in Section 3, it was necessary to process the raw data in order to obtain estimates for the bow distribution parameters. Rod bow behavior exhibited by 14x14 and 15x15 fuel assemblies was similar. As these assemblies differ only in the number and spacing of rods in the assembly lattice, such results were expected. Consequently, the 14x14 and 15x15 fuel assembly bow data were combined into a single set, referred to by their common 0.422 inch fuel rod diameter.

### 4.1.1.1  Low Magnification TV Tape (Quality 1 and 2 Data)

A threshold value of channel closure was chosen (50%) and the location of each gap (mid-span) having a closure greater or equal to this value was noted. For each assembly the relative frequency of this significant closure was determined span-by-span by totalling the number of such closures for a span and dividing by the total number of observed gaps at that span. This value represented the best estimate value for the fraction of the gap population having closures greater than or equal to the threshold value. A frequency of 50 percent was assigned "a priori" for zero closure (i.e., half the gaps were considered to be smaller than the nominal value). Justification for this value is based on the manufacturing procedure whereby the total assembly width is controlled to within a very close tolerance of the value determined with all nominal rod gaps. Furthermore, probe and high magnification TV data analyses indicate that sample mean values do not differ significantly from the assigned value of zero closure.

As is indicated in Section 4.1.2, the closure population can be considered normally distributed. The standard deviation of a normal distribution represented by the aforementioned closure frequencies is readily determined. Graphically the procedure used is shown in Figure 4-1. On a normal probability plot, frequency of closure is represented on the vertical probability scale and fractional closure on the horizontal arithmetic scale. The observed frequency of significant closures is plotted, in the case shown a frequency of 0.62 percent being observed for closures of 50 percent or more. This point is joined to the 50 percent frequency value at zero percent closure by a straight line representing the best estimate normal distribution curve for the observed closure frequency. The standard deviation is found by reading off the closure value corresponding to a frequency of 15.87 percent. This frequency value, obtained from standard normal distribution tables, represents the fraction of the population that is at least one standard deviation greater than the mean. For the case shown in the figure, the standard deviation value obtained is 20 percent closure.

In practice, a tabular procedure using normal distribution values is used. Referring to the example, the frequency value of 0.62 percent is found from normal distribution tables to correspond to a value of 2.5 in standardized units. The standard deviation is obtained by dividing the fractional closure value of 50 percent by 2.5 giving, as before, 20 percent as the standard deviation value.

If no significant closures are observed in a span, a non-zero estimate of the distribution standard deviation is obtained as follows:

An upper tolerance limit on the frequency of significant closures based on observing x such closures in a random sample of n corresponds to the value of f satisfying the following equation: [5]

$$\sum_{i=0}^{x} \frac{x!}{(x-i)!i!} \ f^{i}(1-f)^{n-i} = 1-\gamma \qquad (4-1)$$
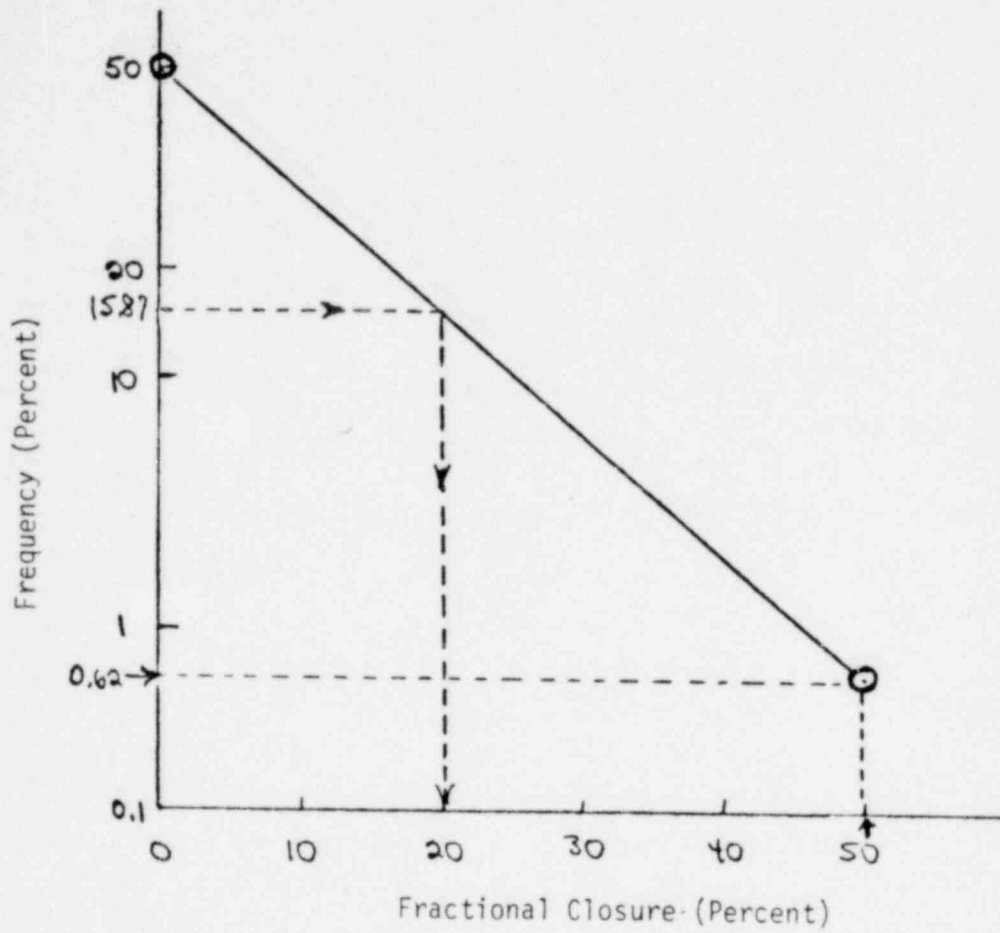
where $\gamma$ represents the confidence level.

4-2

1035 008

Figure 4-1  Frequency versus Fractional Closure
of Channel Gaps

If no significant closures are observed, x=0. The value of f can then be explicitly found from the equation, and $\gamma=0.5$ will give a value comparable to a best estimate value. The resulting relation is:

$$f = 1 - (0.5)^{1/n} \qquad (4-2)$$

This equation is used to determine the frequency value assigned to the chosen fractional closure, the standard deviation being calculated as indicated above.

## 4.1.1.2 High Magnification TV Tape (Visual Reduction-Quality 3 Data)

All mid-span gaps which were less than the nominal value were measured and their fractional closures determined based on the nominal gap closure corrected for cladding creepdown. The standard deviation was obtained from the expression

$$s = \Sigma_i \left[ x_i^2/(n-1) \right]^{1/2} \qquad (4-3)$$

where the $x_i$ are the closure values and n is the total number of measured closures. This equation corresponds to the familiar expression for the standard deviation with the average closure value being set to the "a priori" mean value of zero.

## 4.1.1.3 High Magnification TV Tape (Encoder Reduction-Quality 3 Data)

The fractional closure at each mid-span location was determined by dividing the mid-span gap value by the average of the gap values at the two grid elevations bounding the span (equation 3-1). The standard deviation is obtained from the conventional expression

$$s = \left[ \sum_i (x_i - \bar{x})^2/(n-1) \right]^{1/2} \qquad (4-4)$$

where the $x_i$ are the closure values, $\bar{x}$ is the mean of the $x_i$, and n is the number of observed gaps.

1035 090

## 4.1.1.4 Probe Data

Channel spacing values obtained using the strain gage probe were corrected to account for the deflection of the rods by the probe. The insertion of the probe between two rods resulted in a lateral force being exerted and, as a result, a lateral deflection of the rods. This necessitated correcting the values indicated by the probe to account for the increased deflection by comparing the actual mean gap for an assembly with the mean value given by the probe readings. Using this difference and the free probe width, a correction curve which varied linearly with the measured gap was produced for each assembly.

The corrected spacings were then converted to values of fractional closure based on the nominal closure corrected for cladding creepdown. As many as four sets of data were reported for an assembly at each span elevation: inner and outer rods obtained with the probe entering from each of two faces of the assembly. For each data set, the mean and standard deviation obtained using equation (4-4) were determined.

## 4.1.2 NORMALITY OF GAP DISTRIBUTION

The channel spacing probe data were obtained in a manner which permitted testing the validity of the assumption that gaps are normally distributed. The test is defined in the American National Standards Institute's assessment on the assumption of normality[6], which has been accepted by the NRC[7].

The procedure involves using the individual data points to calculate a "statistic", and then to compare this quantity with tabulated values which define an interval indicative of a statistically significant departure from normality. This test is representative of other significant tests in that a hypothesis concerning the distribution is made and then either rejected or not rejected on the basis of the outcome of the test.

A tabulation of the gap data and the results of the normality test are indicated in Table 4-1. Of the 260 distributions obtained from the probe data analysis, well over 90 percent were found to satisfy the normality assumption at the 5% significance level. Thus, the assumption of normality is well justified and in subsequent analyses, normal distributions of gaps will be used.

### 4.1.3 COMPARISONS BETWEEN INNER AND OUTER GAP DISTRIBUTIONS

The data obtained using the channel spacing probe were used to compare the distributions of fuel rod gaps on the periphery of the fuel assembly ("outer") with those for the remaining gaps within the assembly ("inner"). As is shown in the preceding section, the distributions satisfy normality, and consequently the F distribution[8] can be used to perform significant tests using the ratio of the sample standard deviations determined from the measurement.

A comparison of the sample standard deviation for inner and outer rods are shown in Figures 4-2 and 4-3. Each point represents a pair of standard deviation values obtained fom measurements taken from one face of a fuel assembly midway between two grids. The dashed lines represent limits, determined from the F distribution, beyond which significant differences between the $\sigma$ values are indicated at the five percent significance level.

For the 0.422" rod data shown in Figure 4-2, it is evident that the outer gap $\sigma$ values are generally greater than the inner gap values. In only a single case is the standard deviation of the inner gaps significantly greater than that of the outer gaps.

Figure 4-3 shows the results obtained for the 0.374" rod data. Again it is evident that most of the data shows no significant difference between inner and outer gap distributions, with the cases in which the outer gap standard deviation is significantly greater than the inner value being more numerous than for the converse effect.

1035 092

## TABLE 4-1

## NORMALITY CHECK ON GAP DISTRIBUTIONS
### (Quality 4 Data)

| Plant | Rod Diameter Inches | Number of Assemblies Observed | Total Number of Inner and Outer Gap Distributions | Number of Distributions Satisfying Normality at 5% Significance Level |
|-------|---------------------|-------------------------------|---------------------------------------------------|----------------------------------------------------------------------|
| I | 0.422 | 5 | 42 | 39 |
| C | 0.422 | 5 | 68 | 62 |
| I | 0.374 | 2 | 26 | 25 |
| L | 0.374 | 11 | 124 | 113 |
| TOTALS | | 23 | 260 | 239 |

(b,c)

$\sigma_o$, Standard Deviation of Outer Gaps (Percent)

50

40

30

20

10

0

10    20    30    40    50

$\sigma_i$, Standard Deviation of Inner Gaps (Percent)
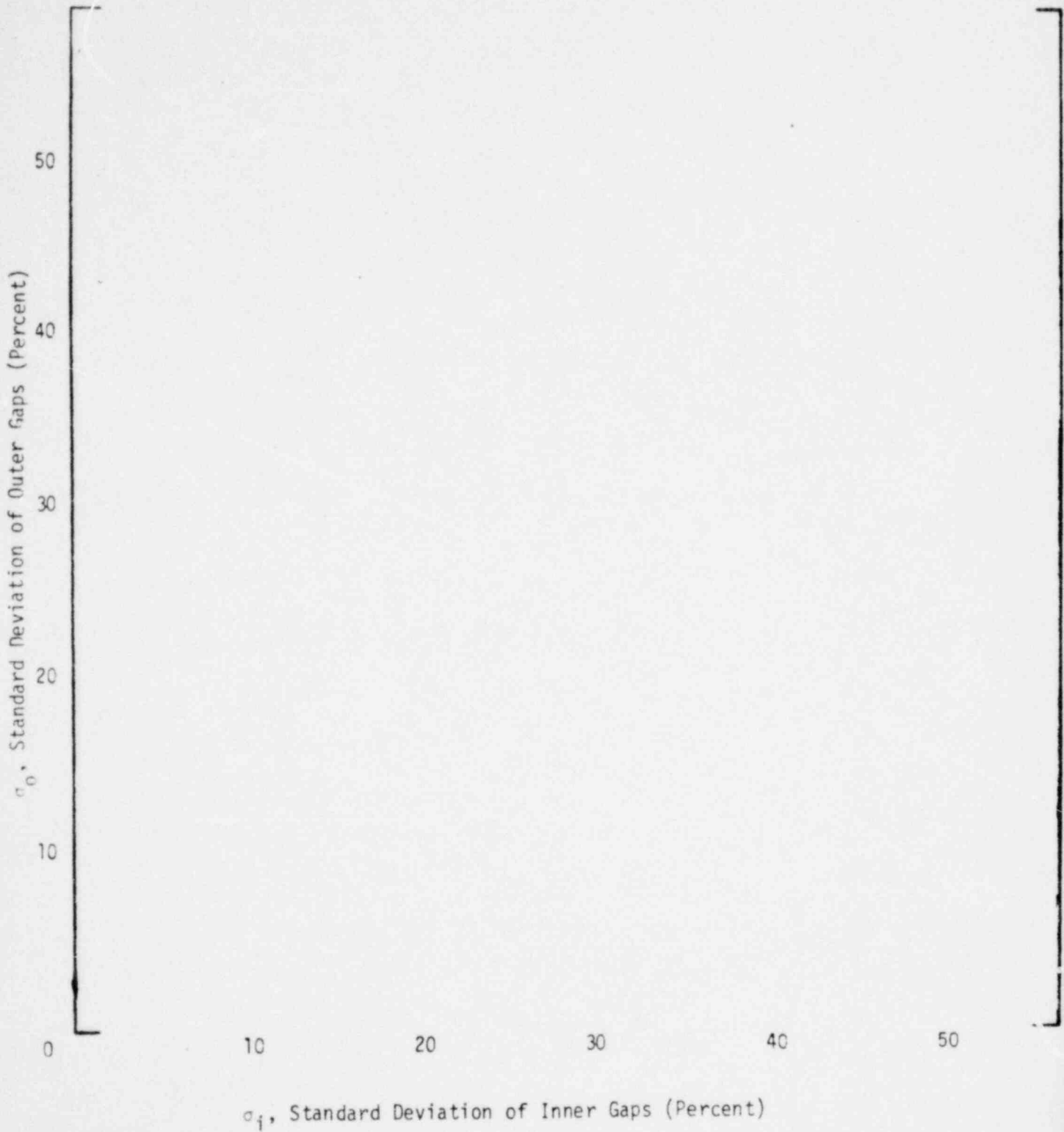
Figure 4-2    Comparison of Inner and Outer
Gap Distributions - 0.422 Inch O.D. Fuel Rods

1035 094

(b,c)

50

40

30

20

10

0

10      20      30      40      50

$\sigma_i$, Standard Deviation of Inner Gaps (Percent)
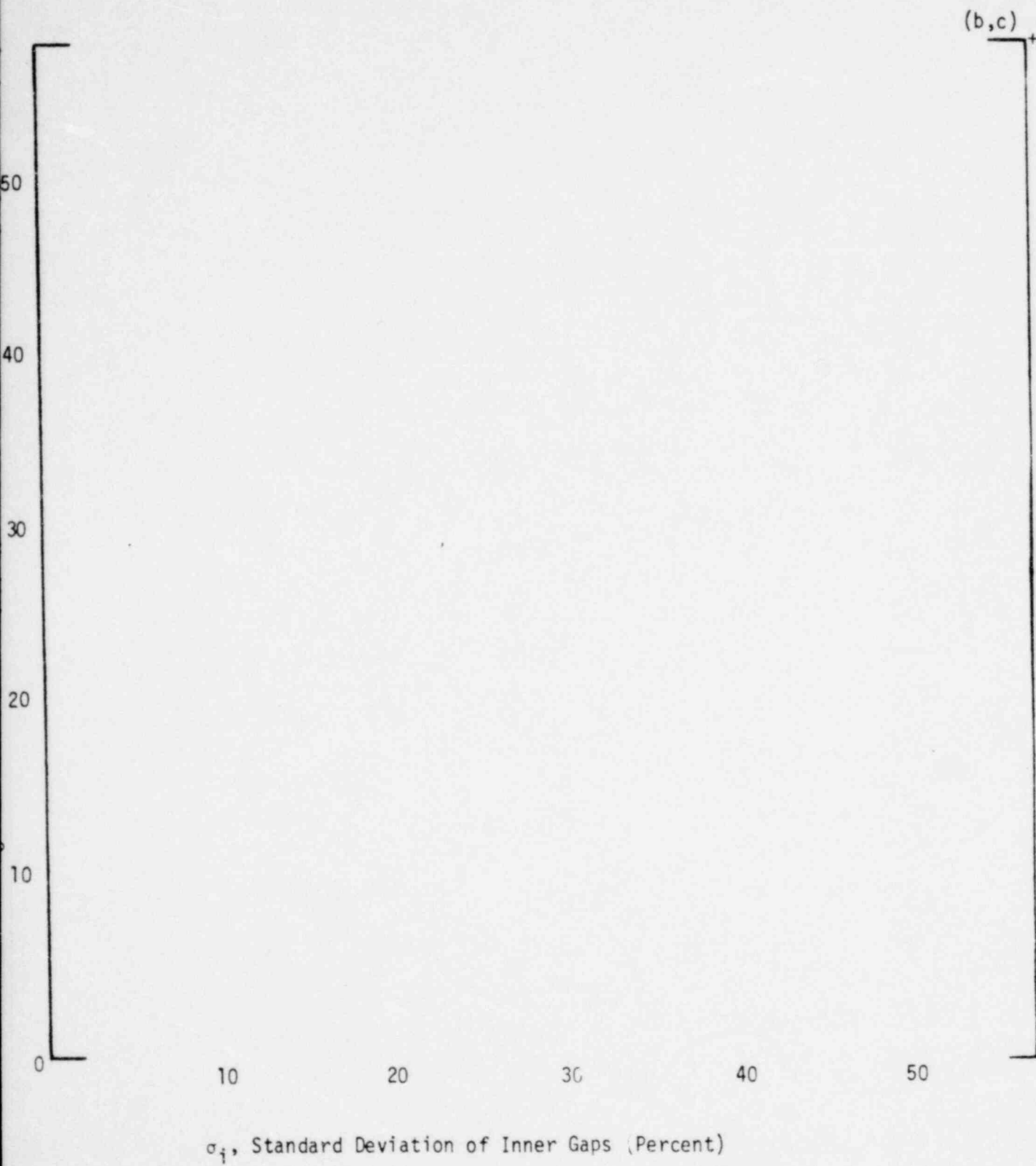
Figure 4-3   Comparison of Inner and Outer
Gap Distributions - 0.374 Inch O.D. Fuel Rods

1035 095

Based on these results, the analysis in the remainder of this report will consider data for any of the gaps at a mid-span location on an assembly to be representative of all gaps at that location. As the bulk of the data is based on outer gap measurements, the data presented in Figures 4-2 and 4-3 indicate that this procedure leads to conservative results.

## 4.2 ROD BOW CORRELATIONS

Using the techniques described in 4.1 to quantify rod bow, the effects of various parameters on channel closure were evaluated. Fuel assembly burnup was found to be the most significant parameter. After separation of the burnup effects, another significant variable was identified. Earlier design fuels had fuel rods in contact with the bottom nozzle. This condition was identified as "on bottom." In 1972 the design was altered to provide an axial offset of the fuel rod from the bottom nozzle. This condition is representative of current production and is identified as "off bottom." Separation of the two groups of data (Quality 2 and 3 only) is illustrated in Figure 4-4. Assembly burnups were grouped to eliminate scatter due to small sample sizes. From these figures, it is clear that the older design "on bottom" assemblies have inferior bow performance when compared to the current design. The "on bottom" design results in increased grid forces from the grid springs via a staircase effect. For the bottom span (Span 1) to accommodate irradiation growth or thermal expansion, it must force the remainder of the rod through all the remaining grids. Net grid force will, as a result, lessen toward the top of the assembly. With rods "off bottom", the rod expansion can be relieved by downward motion and the staircasing does not occur to the same extent. This explanation is supported by the data in Figure 4-4, which shows that the newer "off bottom" design has reduced bow by the reduction of these forces.

The change-over from the "on bottom" to the "off bottom" rod design occurred over a short time interval. The improvement in bow performance may be the result of concurrent improved fabrication procedures or

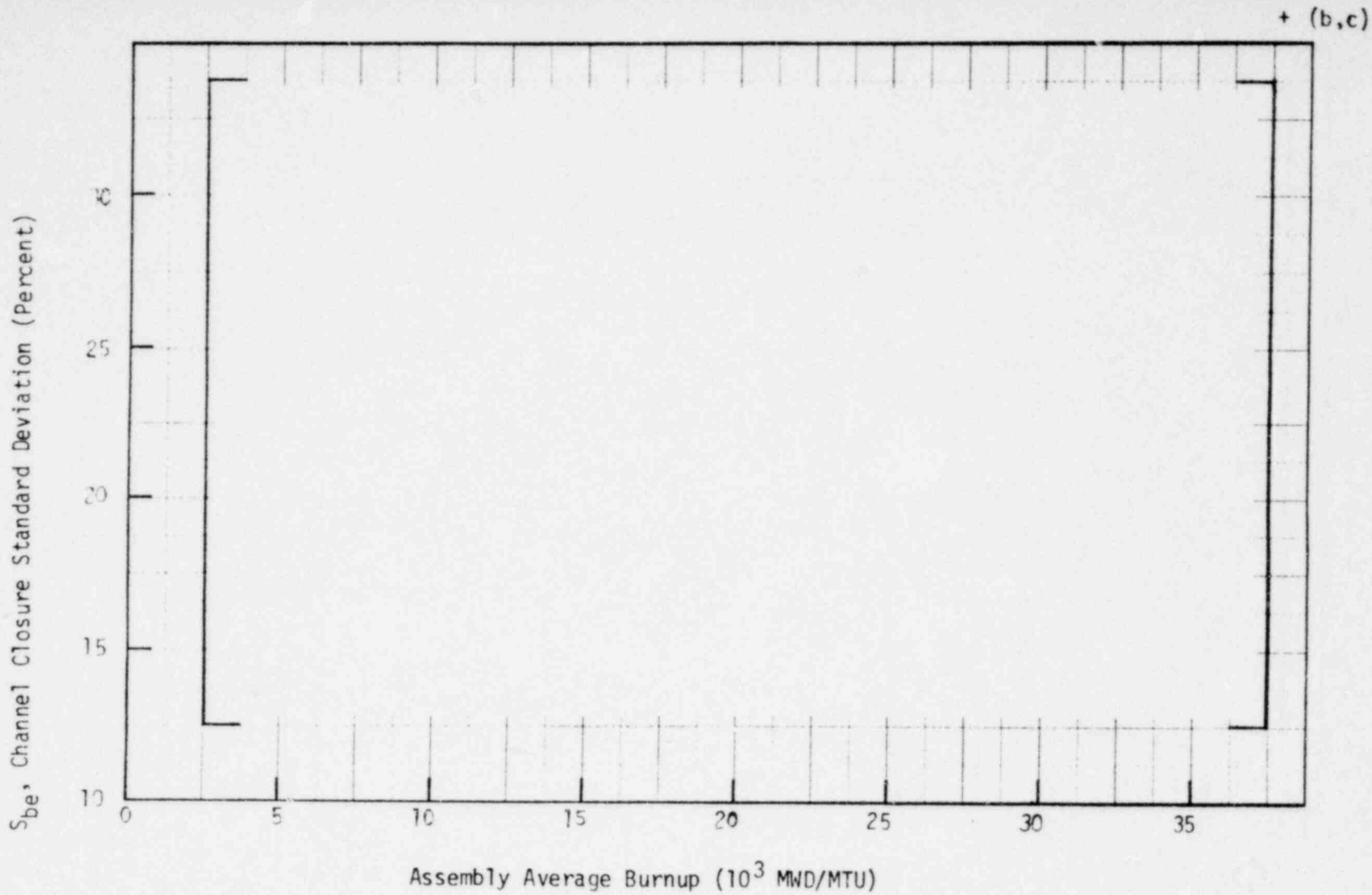1035 096

Figure 4-4  Comparison of Channel Closures for
Rods-On-Bottom and Rods-Off-Bottom
(0.422 Inch Rods, Worst Span)

LEGEND

- - - ⊖ - - -    Rods-On-Bottom

——— ⊖ ———    Rods-Off-Bottom

design changes. In any case, the older "on bottom" assemblies are no longer representative of the Westinghouse product and will not be included in further discussions or analyses of channel closures.

Regression analysis of the "off bottom" data was performed utilizing various equation forms. For conservatism, only the worst span was utilized. Only the 17x17 standard assemblies (8 grids) were used for the 0.374 inch rod bow data. The best fit to the data was obtained using an equation of the form:

$$S_{be} = A_1 + B_1 x \qquad\qquad (4-5)$$

where:

$S_{be}$ = best estimate standard deviation of channel closure for the worst span of each assembly

$A_1$ = [      ]$^+$ for 0.422 inch fuel rods (14x14, 15x15 assemblies)

= [      ]$^+$ for 0.374 inch fuel rods (17x17 assemblies)      (a,c)

$x$ = assembly average burnup ($10^3$ MWD/MTU)

$B_1$ = [      ]$^+$ for 0.422 inch fuel rods

[      ]$^+$ for 0.374 inch fuel rods      (a,c)

The resultant equations are shown with the grouped data in Figures 4-5 and 4-6. These equations represent the best estimate of the standard deviation of channel closure in the worst span as a function of burnup for current product Westinghouse fuel.

In order to show the relationship more clearly for the 0.422" rod data, the observations for a group of assemblies (each having nearly the same burnup) were combined to determine a single value plotted in Figure 4-5. Thus, the ordinate of each point represents a best estimate for the channel closure standard deviation, based on the total of the number significant closures observed in the worst span of each of the twenty or twenty-one assemblies in the group. The abscissa value is the average of the burnup values for the assemblies in the group.

4-12

1035 098

Assembly Average Burnup, BU ($10^3$ MWD/MTU)

Figure 4-5  Correlation of Worst Span Channel Closure with
Assembly Burnup - for 0.422 Inch Rods Off Bottom

S, Channel Closure Standard Deviation (Percent)

24
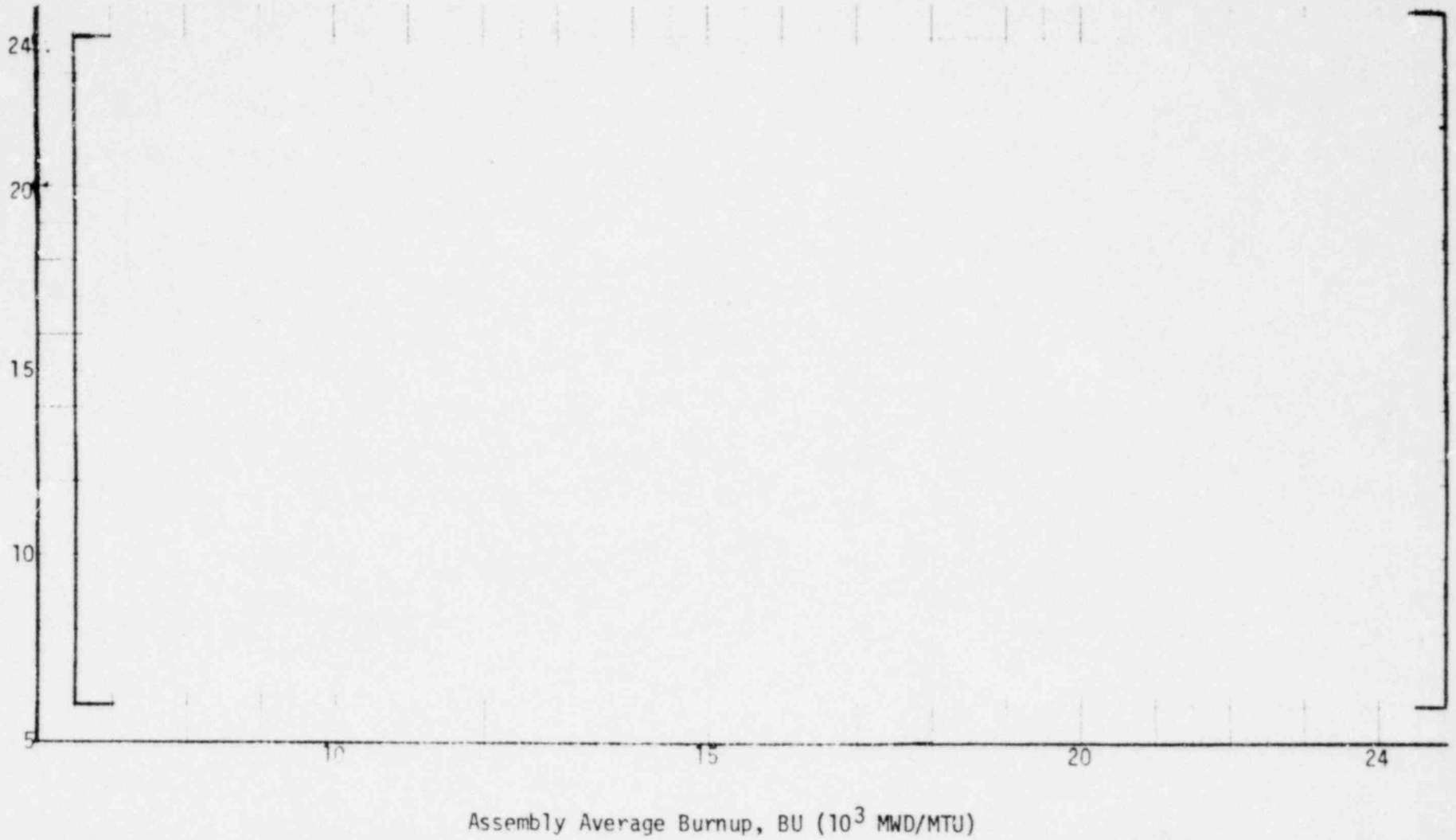
20

15

10

5

10            15            20            24

Assembly Average Burnup, BU ($10^3$ MWD/MTU)

Figure 4-6   Correlation of Worst Span Channel Closure with
Assembly Burnup - for 0.374 Inch Rods Off Bottom

Using the distribution of the differences between the observed and predicted standard deviations, a tolerance limit factor was determined. Applying this factor to the best fit line resulted in a tolerance limit line which represents an upper 95 percent tolerance limit for the channel closure standard deviation with a 95 percent confidence. Using this method the equation obtained is:

$$S_w = A_2 + B_2 x \qquad\qquad (4\text{-}6)$$

where:

$S_w$      =   upper 95 percent tolerance limit for the standard deviation of channel closure for the worst span

$A_2$      = $[ \qquad ]^+$ for 0.422 inch fuel rods (14x14, 15x15      (a,c)
     assemblies)

       $[ \qquad ]^+$ for 0.374 inch fuel rods (17x17 assemblies)      (a,c)

$x$      =   assembly average burnup ($10^3$ MWD/MTU)

$B_2$      = $[ \qquad ]^+$ for 0.422 inch fuel rods      (a,c)

       $[ \qquad ]^+$ for 0.374 inch fuel rods      (a,c)

Equations 4-5 and 4-6 are the closure correlations used in Chapters 5 and 6 to evaluate the effects of rod bow.

1035 107

SECTION 5

ROD BOW EVALUATIONS

## 5.1 MECHANISTIC CONSIDERATIONS

### 5.1.1 FUEL ROD FRETTING

Clad fretting wear could occur for the unlikely event of rods bowed to
contact. Fuel rod fretting is caused by small amplitude oscillatory
motion of mating surfaces. Due to motion, "adhesive wear" (or wear
caused by attraction between the surface atoms of two contacting sliding
surfaces) occurs. The Archard wear equation[9] derived for unlubri-
cated sliding surfaces relates the worn volume to the normal force and
the sliding distance. The Archard equation has been previously used to
evaluate rod to grid fretting. The Archard wear model has been extended
to rod-to-rod wear in a conservative manner. Details of this study are
given in Appendix A, where it is shown that the forces are small, the
amplitudes of vibration low, and the resulting fretting negligible.
Therefore, fuel rod clad failure due to fretting wear is not predicted
for those rods bowed to contact.

### 5.1.2 COLD-TO-HOT BOW CORRECTION

The rod bow correlation equations in Section 4.2 were obtained using
cold rod bow data. Appendix B considers the effects on rod bowing at
hot fuel operating conditions and presents a hot-to-cold correction
(equation B-2) to the rod bow correlation equations. Appendix B was
evaluated by the NRC[1] who replaced equation B-2 by the following
conservative equation:

$$\sigma_{HOT} = 1.2 \; \sigma_{COLD} \qquad (5-1)$$

This NRC approved equation is being used to adjust all calculated rod
bow channel closures to hot channel closures in operating reactors.

1035 102

### 5.1.3 ROD BOW SCALING

In the absence of rod bow data for a particular design, it is frequently necessary to extrapolate or scale the bow behavior of a different geometrical design. This was necessary when the 17x17 design was introduced several years ago with no available rod bow data for that design.

A scaling factor is derived in Appendix C from basic engineering mechanics principles for the bending of a creep sensitive rod under the action of an arbitrary bending moment. This derived scaling factor is $L^2/I$, where L is the span length and I is the moment of inertia of the clad. The validity of the $L^2$ factor is also supported by bow data which have recently become available for the 17x17 fuel rod design where span length was the only variable. The grid design, rod design and manufacturing processes for these two applications were virtually identical giving support to the assumption that the same bending moment is applied in both cases. An evaluation of the bow data for determination of the span length dependence is presented in Appendix D.

### 5.2 THERMAL-HYDRAULIC EVALUATON

One of the design criteria for pressurized water reactor cores is the prevention of departure from nucleate boiling (DNB) during Condition I or II events*. This criterion is shown to be met for any particular case by calculating a minimum DNB ratio (DNBR) which is greater than the appropriate limit DNBR for that case. It is the intent of this section to show how to include the effects of rod bow on DNB in determining the appropriate limit DNBR.

### 5.2.1 CRITICAL HEAT FLUX (CHF) EFFECTS

Changes in flow geometry due to fuel rod bowing can result in a reduction in the critical heat flux (CHF) at which DNB occurs. The rod bow

---

*Condition I (Normal Operation) and Condition II (Faults of Moderate Frequency) are described in Chapter 15 of Reference 4.

effects on DNBR is based on DNB tests with a heater rod bowed from its nominal position to approach or contact adjacent rods. The critical heat flux at the DNB condition with rod bow is compared to a corresponding data point obtained previously without any bow. This pair of runs is matched as closely as possible in inlet temperature, pressure and flow.

The parameter used to quantify the penalty due to the bow is:

$$\delta_{bow} = \frac{(M/P)_{NO\ BOW} - (M/P)_{BOW}}{(M/P)_{NO\ BOW}} \tag{5-2}$$

where

    P      =    predicted critical heat flux based on no bow geometry input for both BOW and NO BOW Conditions

    M      =    measured critical heat flux

$$(M/P) = \frac{1}{minimum\ DNBR} \tag{5-3}$$

    NO BOW  =    inlet temperature pressure, flow, and power level from an unbowed test run.

    BOW     =    inlet temperature, pressure, flow, and power level from a bowed test run.

The bow DNB effect has been found to be strongly related to the amount of closure, with DNB tests of rods bowed to contact giving significantly larger values of $\delta_{bow}$ than tests with some slight gap. The form of $\delta_{bow}$ as a function of fractional closure is given in Figure 5-1 with the points based on DNB test results indicated by circles. Figure 5-1 shows this form conceptually; the values used in the analysis are discussed later in the report.

Contact
DNBR
Penalty

1.0

0.85 Closure Point
Not Scaled to DNBR Penalty

Fraction of Contact DNBR Penalty

0

0    0.5    0.85    1.0
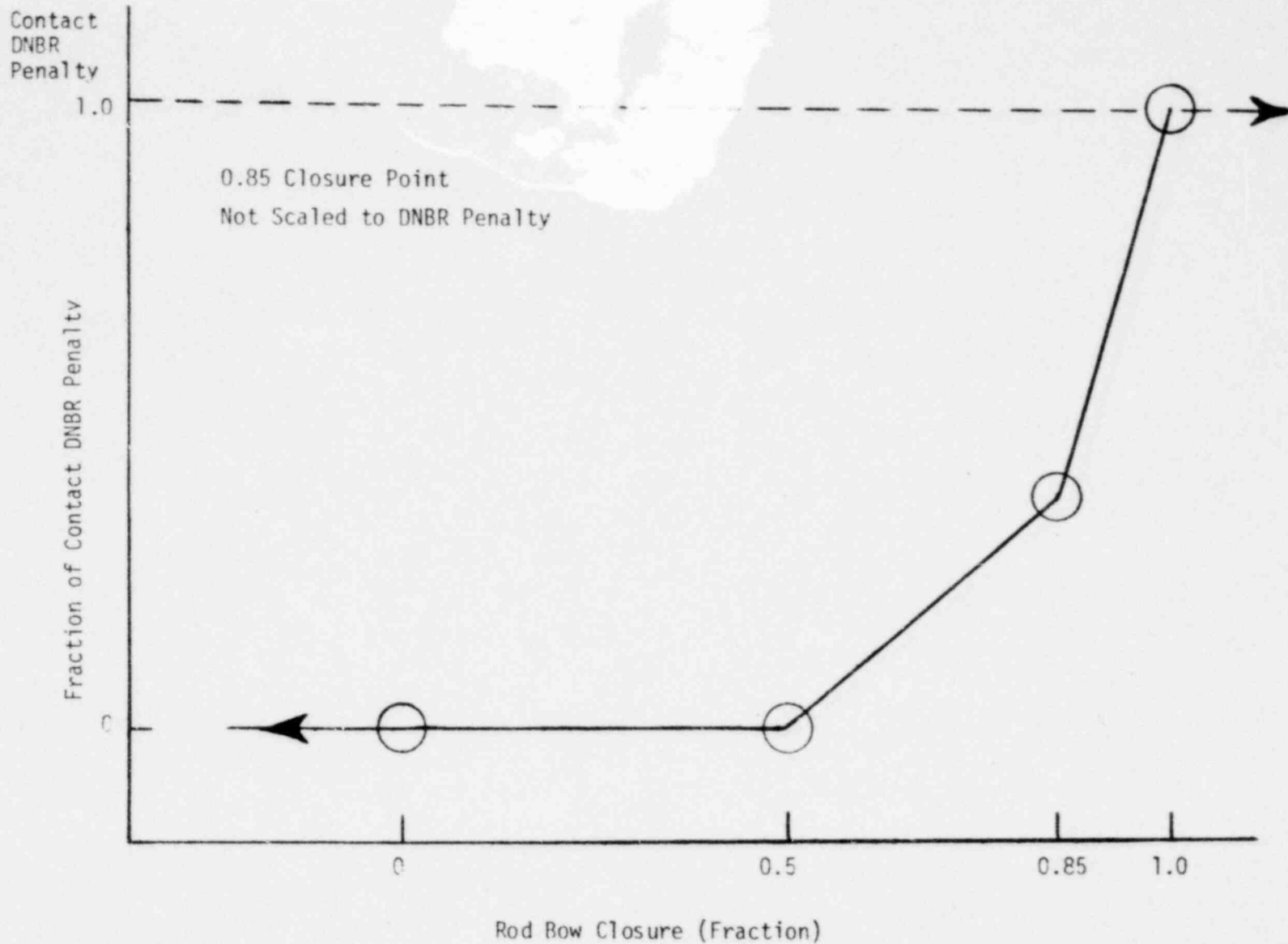
Rod Bow Closure (Fraction)

Figure 5-1   Rod Bow DNBR Penalty Versus Fractional Closure

The circle located at zero closure and zero penalty represents the rod bundle DNB test data with nominal spacing which is used to develop DNB correlations. The continuation to the left of that circle indicates that no penalty is assigned to a gap which is greater than the nominal value. Similarly no penalty is assigned for a closure of 50% of nominal gap. This is based on the results of DNB testing at 50% closure described in References 10 and 16, which show no adverse effect on CHF unless the clearance between heated rods is reduced by more than 50%.

The values used for $\delta_{bow}$ at closure values of .85 and 1.0 are based on the correlations for 85% closure partial bow and contact DNB test penalties as described in References 11 and 16. These submittals to the NRC and the NRC acceptance letter[17] are given in Appendix H. The continuation of the value of the contact penalty for closure values greater than 1.0 is indicated because the analytical treatment of rod bow as a normal distribution requires defining a bow penalty function for all values of bow ($-\infty <$ closure $<+\infty$).

Statistical comparisons of the mean and standard deviations of the 85% closure and contact DNB test data sets, including the appropriate $\delta_{bow}$ correction, with the corresponding unbowed DNB test set statistics indicate that all of the sets are from the same population.

5.2.2  LIMIT DNBR DETERMINATION

The appropriate limit DNBR to assure a 95% probability that DNB will not occur at a 95% confidence level is derived from the results of DNB testing as follows:

$$\text{LIMIT DNBR} = \frac{1}{(\overline{M/P}) - K_{95 \times 95}\ \hat{\sigma}(M/P)} \qquad (5-4)$$

where:

$(\overline{M/P})$ = average ratio of measured to predicted CHF for the correlated data.

1035 106

$\hat{\sigma}(M/P)$ = unbiased estimate of standard deviation for the correlated data.

$$= \left[ \frac{\Sigma \left[ (M/P)_i - \overline{(M/P)} \right]^2}{n-1} \right]^{1/2}$$

n = number of data points in set used to derive the correlation.

$K_{95x95}$ = a tabulated[12] factor, as a function of n (or degrees of freedom = n-1), for a one-sided tolerance limit for a normal distribution. This factor is such that at least 95% of the population of M/P values is greater than $\overline{(M/P)} - K_{95x95}\hat{\sigma}(M/P)$ with 95% confidence.

Values of these parameters and the corresponding limit DNBR's for some DNB correlations in use are:

| Correlation | $\overline{(M/P)}$ | $\hat{\sigma}(M/P)$ | n | $K_{95x95}$ | Limit DNBR |
|---|---|---|---|---|---|
| WRB-1[13] | 1.0043 | .0873 | 1147 | 1.723 | 1.17 |
| 17x17 R-grid[14] | .9813 | .109 | 199 | 1.838 | 1.28 |
| 15x15 L-grid[15] | 1.0184 | .1093 | 91 | 1.942 | 1.24 |

In order to determine the limit DNBR (including the effects of rod bow) to assure 95% probability with 95% confidence that DNB will not occur, each of the parameters of Equation 5-4 must include the effect of rod bow.

The DNBR calculations for both DNB test geometry and reactor core geometry are based on the fluid conditions of the flow cell (defined by four fuel rods or three rods and a thimble) and the heat flux of the

1035 104

hottest rod associated with that cell. Thus, the DNB effect of rod bow on that DNBR calculation would be determined by the gap closure associated with the hottest rod in the cell. The penalty to that rod should be based on the lesser of the two gaps between it and its neighbors in that cell.

Thus, the distribution of bow DNBR penalties can be generated by choosing two random gaps from a normal distribution of gap closure and assigning the appropriate penalty from the penalty function in Figure 5-1 based on the larger closure of the two gaps chosen. To accomplish this, a Monte Carlo type calculation was used to generate a distribution of DNB penalties based on 100,000 random selections of two gaps.

The normal distribution used for selection of gaps is a distribution with a mean of zero closure and a conservative value for the standard deviation of channel closure, as given by the tolerance limit values in Figures 4-5 and 4-6. The values are multiplied by a factor of 1.2 for cold-to-hot bow corrections as discussed in Section 5.1.2.

The penalty function magnitudes are calculated based on a combination of conditions which are attainable within the protection setpoints for events protected against DNB and which maximize rod bow DNBR penalties (maximum pressure, maximum hot rod average heat flux, minimum local mass velocity).

The calculated average ($\overline{\delta}$) and standard deviation ($\hat{\sigma}_\delta$) of the DNBR penalty distribution can be combined with the DNB correlation (M/P) statistics to obtain total effect parameters as follows:

$$(\overline{M/P})_B = (M/P)(1-\overline{\delta})$$

$$\hat{\sigma}_B^2 = (1-\overline{\delta})^2 \left[\hat{\sigma}(M/P)\right]^2 + (\overline{M/P})^2 \hat{\sigma}_\delta^2$$

(5-5)

(5-6)

1035 108

$$n_B - 1 = \frac{(\hat{\sigma}_B^{\,4})}{\dfrac{(1-\bar{\delta})^4 \left[\hat{\sigma}(M/P)\right]^4}{n-1} + \dfrac{(\overline{M/P})^4 \, \hat{\sigma}_\delta^{\,4}}{n_\delta - 1}}$$

(5-7)

These equations and the definitions of the terms used are explained in Appendix E.

Thus the limit DNBR including the effect of rod bow on DNB is:

$$\text{LIMIT DNBR}_B = \frac{1}{(\overline{M/P})_B - K_{95 \times 95}^B \, \hat{\sigma}_B}$$

(5-8)

where $K_{95 \times 95}^B$ is based on $n_B$.

Using a relationship corresponding to Equation (5-2) and making use of Equation (5-3), the DNBR penalty for the effect of rod bow is:

$$\delta_{DNBR} = 1 - \frac{\text{LIMIT DNBR (Equation 5-4)}}{\text{LIMIT DNBR}_B \text{ (Equation 5-8)}}$$

(5-9)

PLANT APPLICATIONS

## 6.1 ROD BOW DESIGN CORRELATIONS

The correlations of rod bow as a function of assembly burnup are given
in Table 6-1 for the fuel assembly types listed. These correlations
represent a conservative value for the standard deviation of channel
closure, as given by the tolerance limit values in Figures 4-5 and 4-6.
They also include a conservative cold-to-hot multiplier of 1.2 for all
burnups which bounds the derived cold-to-hot variability given in
Appendix B.

TABLE 6-1

ROD BOW DESIGN CORRELATIONS

| Fuel Assembly Type | $S_w$ Correlation (%) (Hot) | Number of Gap Measurements Used to Derive Correlation $(n_\delta)$ | |
|---|---|---|---|
| .422 rod, 7 grids .374 rod, 8 grids | $\left[ \qquad \right]^+$ | $\left[ \qquad \right]^+$ | (a,b,c) |

where:  BU = Fuel Assembly Average Burnup ($10^3$ MWD/MTU)

## 6.2 POWER PEAKING EFFECTS OF ROD BOW

An extensive discussion of the effect of local moderation variations due
to rod bowing and their impact on peaking factors was previously
reviewed by the NRC[1] and is contained in Appendix F.  The resultant
rod bow peaking factor uncertainty ($F_Q^B$) as a function of the
standard deviation of rod displacement was approved by the NRC[1] and
is shown in Figure F-8.  This figure, in conjunction with the rod bow
correlations of Table 6-1, determines the appropriate $F_Q^B$ as a

1035 10

function of assembly burnup by using the values of $S_w$ in fractional closure. Since the rod bow peaking factor uncertainty is independent of the other uncertainties which are included in the evaluation of the total power peaking factor uncertainty ($F_Q^U$), the uncertainties can be statistically combined as was approved by the NRC[1]. Combining $F_Q^B$ with a nuclear power distribution uncertainty ($F_N^U$) of 1.05 and an engineering hot channel factor ($F_Q^E$) of 1.03, the following relation would apply:

$$F_Q^U = 1 + \left[ (.05)^2 + (.03)^2 + (F_Q^B-1)^2 \right]^{1/2}$$

This function is shown on Figure 6-1 for the rod bow correlations given in Table 6-1. This total uncertainty must be accounted for in the analysis of peaking factors for each plant application.

## 6.3 DNBR EFFECTS OF ROD BOW

Using the method of calculating rod bow DNBR effects as described in Section 5.2 and the design rod bow correlations of Table 6.1, the DNBR reduction as a function of assembly burnup were calculated. The results are shown in Figures 6-2, 6-3 and 6-4. Each figure shows two curves which consider the 35% closure DNB reduction as given in Reference 16 and Appendix H. One curve is for the [                                                  ]⁺         (a,c)
and the other for the [                                                  ]⁺.        (a,c)
The rod bow design correlation and DNB correlation used in the calculation are noted in the title of each figure.

These reductions must be accounted for in the analysis of each plant application. Applicable generic credits for margin resulting from retained conservatism in the evaluation of DNBR and/or margin obtained from measured plant operating parameters (such as $F_{\Delta H}^N$ or flow), which are more restrictive than those required by the safety analysis, can be used to offset these reductions.

Figure 6-1  Total Power Peaking Factor Uncertainty (Including Rod Bow) versus Assembly Average Burnup
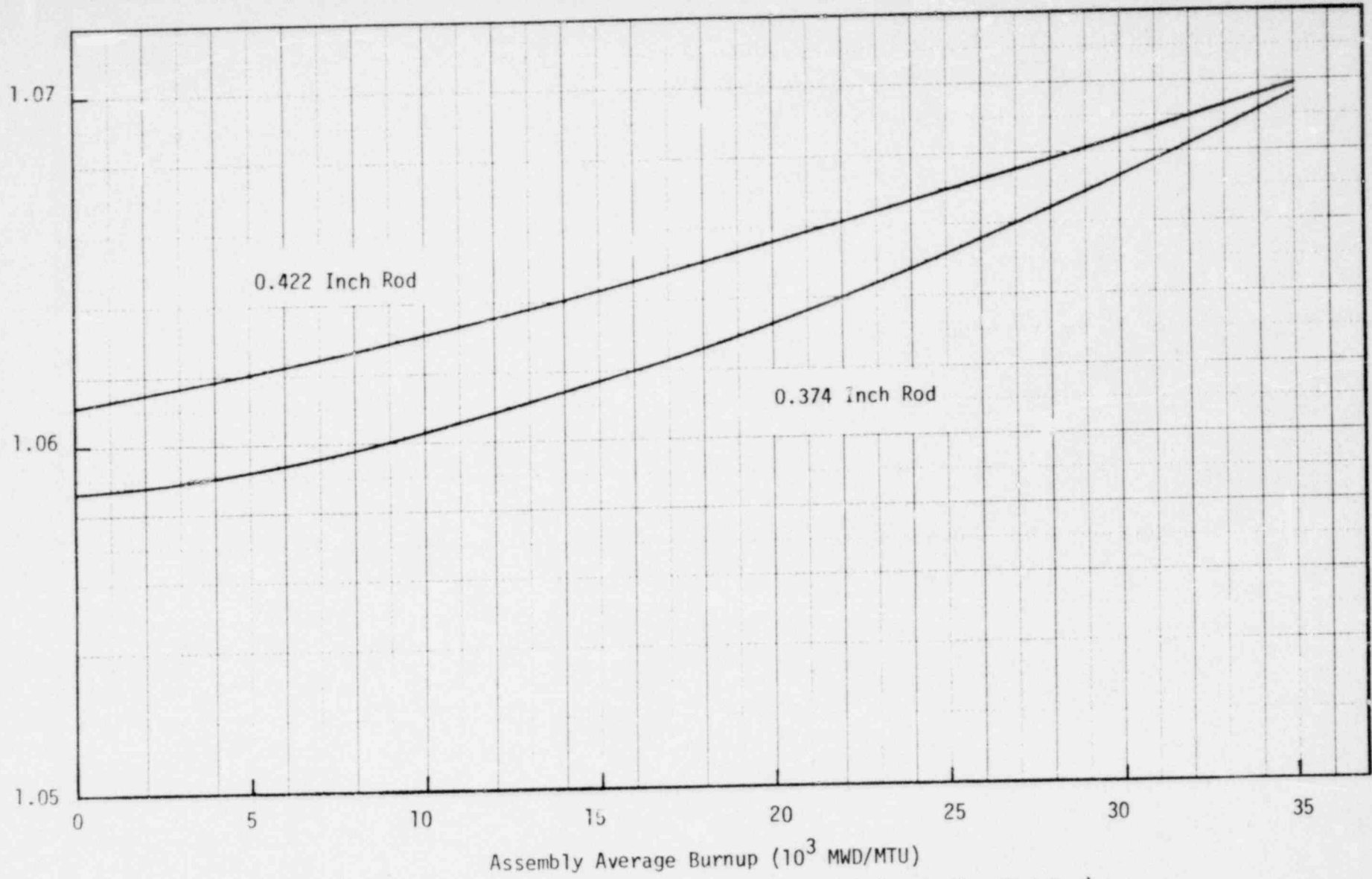
+ (a,c)

6

5

4

3

2

1

0

DNBR Penalty (Percent)

0       5       10      15      20      25      30      35
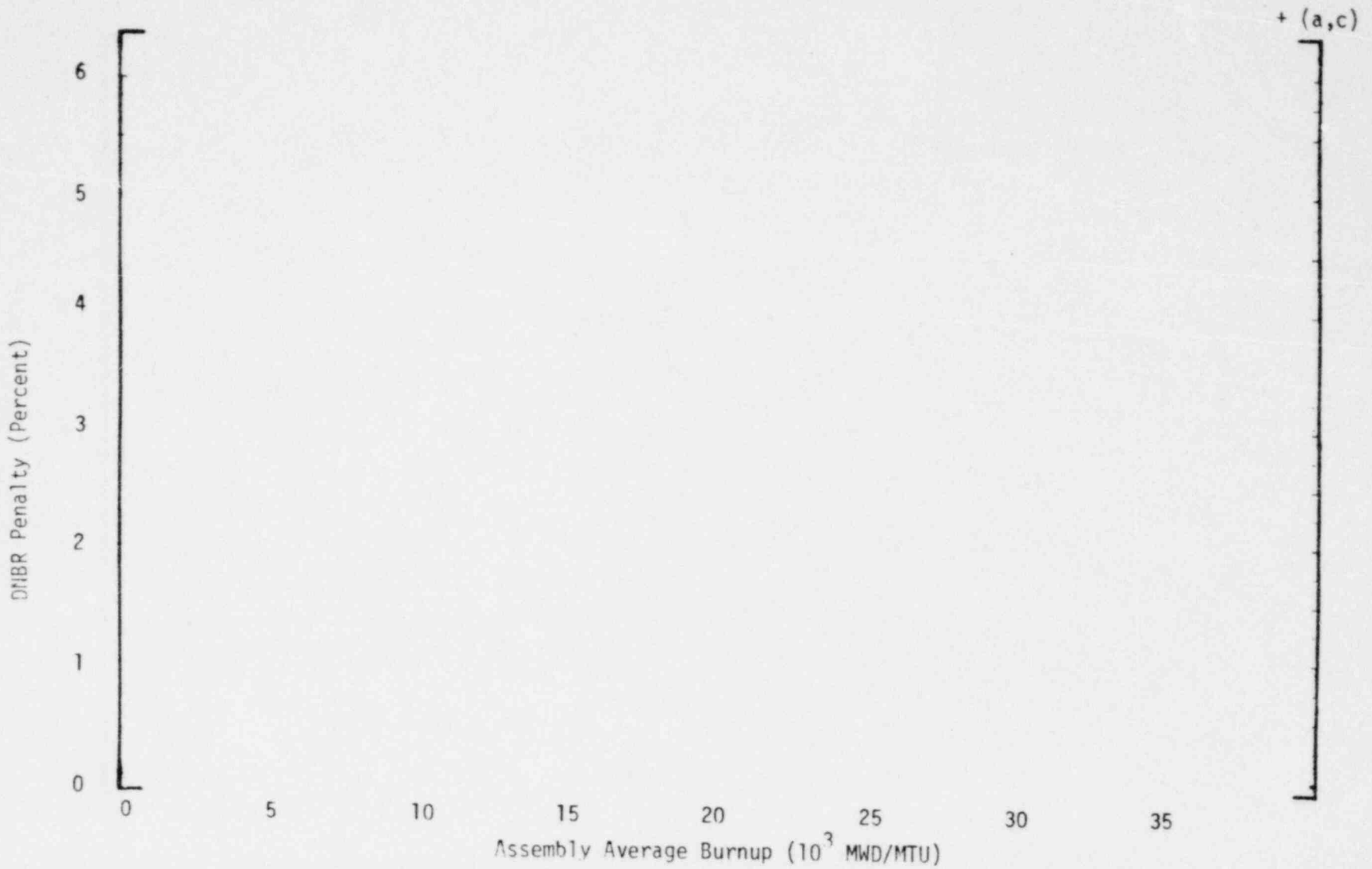
Assembly Average Burnup ($10^3$ MWD/MTU)

Figure 6-2   Rod Bow DNBR Reduction as a Function of Fuel Assembly Average Burnup
(0.374 Rod, WRB-1)

6-4

1035 113

DNBR Penalty (Percent)

6

5

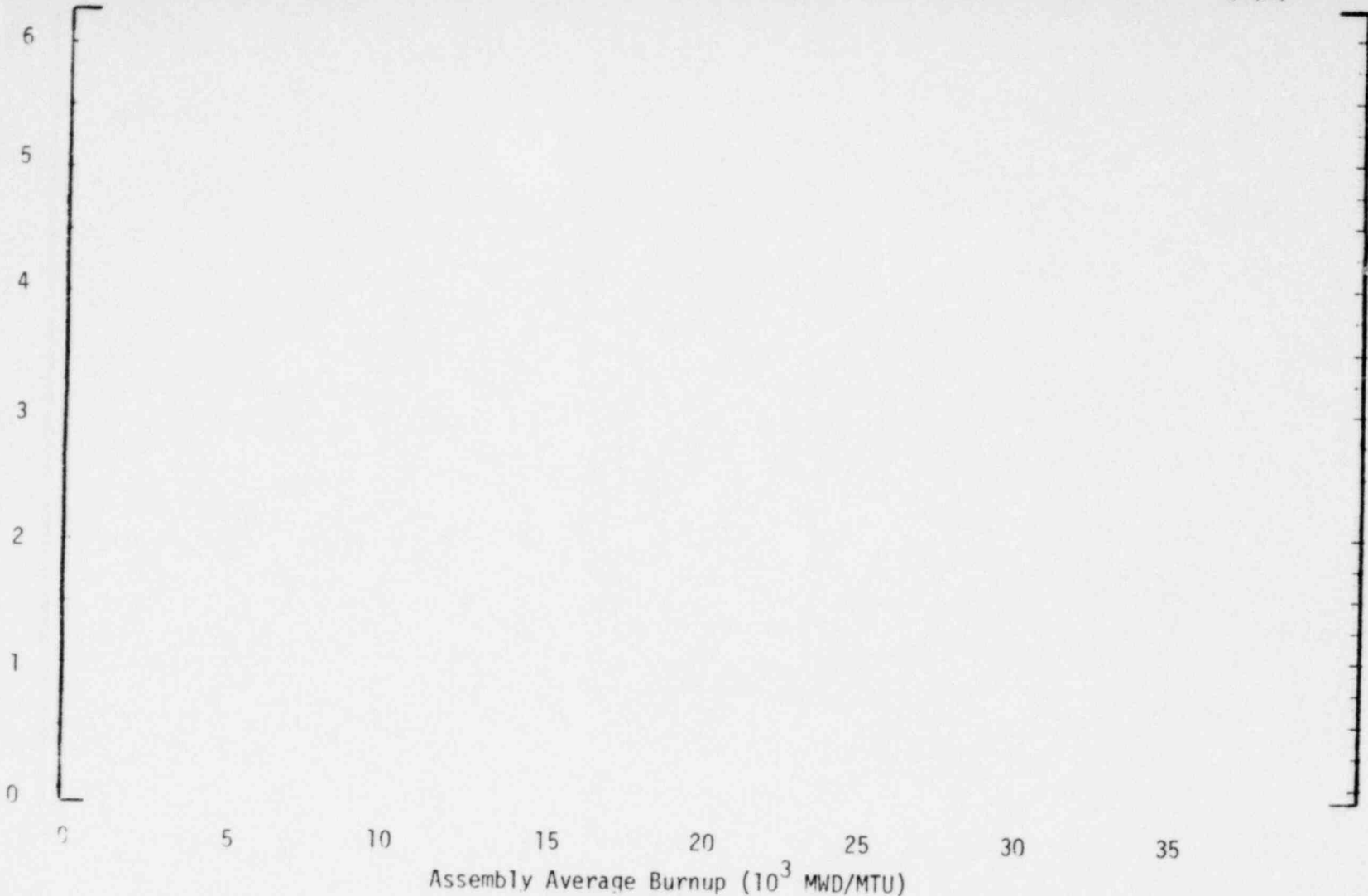4

3

2

1

0

0    5    10    15    20    25    30    35

Assembly Average Burnup ($10^3$ MWD/MTU)

Figure 6-3  Rod Bow DNBR Reduction as a Function of Fuel Assembly Average Burnup
(0.374 Rod, R-Grid)

+(a,c)

DNBR Penalty (Percent)

6

5

4

3

2

1

0

0    5    10    15    20    25    30    35

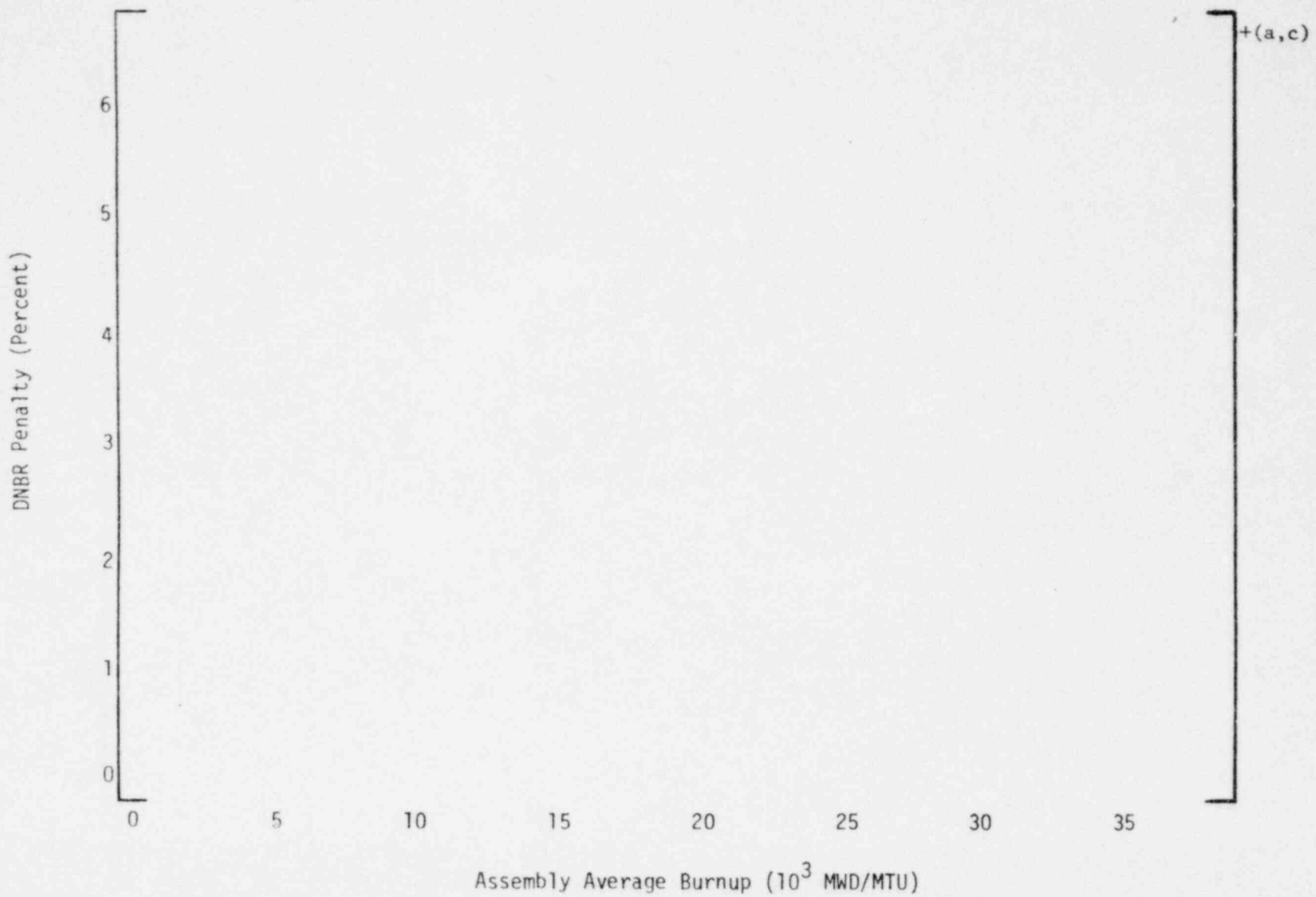Assembly Average Burnup ($10^3$ MWD/MTU)

Figure 6-4   Rod Bow DNBR Reduction as a Function of Fuel Assembly Average Burnup
(0.422 Rod, L-Grid)

## 6.4  ROD BOWING CONSIDERATIONS AT HIGH BURNUPS

The amount of fuel rod bowing has been observed to increase with burnup. The resultant rod bow correlations reflect this trend and consequently the magnitudes of the rod bow DNBR effect, and the rod bow power peaking factors also increase with burnup. However, by the time the fuel attains a burnup of 33,000 MWD/MTU, it is not capable of achieving limiting peaking factors due to the decrease in fissionable isotopes and the buildup of fission product inventory. This physical burndown effect is greater than the rod bowing effects which would be calculated based on the amount of bow predicted at those burnups. Therefore, for the purpose of evaluating effects of rod bow, 33,000 MWD/MTU represents the maximum burnup of concern.

1035 116

# SECTION 7

## CONCLUSIONS

Sufficient rod bow data exist to make conservative predictions on the extent and effect of rod bow in Westinghouse LOPAR fuel assembly designs.

Analyses of this extensive data show the following:

1. Rod bow gap closures are determined as a function of fuel assembly average burnup. The amount of bow accounted for in DNBR effects and power peaking factor uncertainties represents an upper tolerance limit on the standard deviation of channel closure. Using this upper bound gap closure and the conservative cold-to-hot multiplier of 1.2 for all burnups, the rod bow correlations for plant applications are defined in Table 6-1.

2. The rod bow DNBR effect as a function of rod bow closure is defined for design application (Figure 5-1). This function considers no DNBR effect for less than 50% closure and the DNBR effect determined from DNB tests at 85% closure and contact.

3. The rod bow DNBR effect for use in plant safety analysis is defined in Figures 6-2, 6-3 and 6-4 as a function of assembly average burnup. This effect is the result of the statistical combination of DNB and rod bow test data. If this effect is offset in a particular application by the use of DNBR margins, no resultant $F_{\Delta H}$ penalty would be required.

4. Based on 17x17 (8 grid) and 17x17 (7 grid) fuel rod bowing data, an $L^2$ rod bow sealing factor is justified for a different grid span length (L), as shown in Appendix D.

5. The rod bow power peaking factor uncertainty ($F_Q^B$) is accommo-
   dated within the total design peaking factor uncertainty ($F_Q^U$)
   by the approved statistical combination approach. Figure 6-1 shows
   the minimum $F_Q^U$ that must be accounted for as a function of
   assembly average burnup.

6. The results of the analyses show a rod bow DNBR effect of less than
   5% at 33,000 MWD/MTU assembly average burnup. This represents the
   maximum burnup of concern, due to the physical peaking factor burn-
   down effect of the fuel. Likewise, the maximum required total
   peaking factor uncertainty ($F_Q^U$), including the effects of rod
   bow, is 1.069.

7. Conservative analysis for vibratory wear or fretting for rods bowed
   to contact predicts an insignificant amount of clad wear.

# SECTION 8

# REFERENCES

1. "Interim Safety Evaluation Report on Westinghouse Fuel Rod Bowing," USNRC, April 1976.

2. Letter, C. Eicheldinger (Westinghouse) to D. F. Ross (NRC), NS-CE-1161, August 13, 1976.

3. "Interim Safety Evaluation Report on Effects of Fuel Rod Bowing on Thermal Margin Calculations for Light Water Reactors," Revision 1, USNRC, February 16, 1977.

4. RESAR-3S, Reference Safety Analysis Report for 3425 MWt NSSS, Volume II (Section 4.2, Mechanical Design), Westinghouse Electric Corporation, July 1975.

5. P. G. Hoel, "Introduction to Mathematical Statistics", John Wiley, p. 58ff (1971).

6. American National Standards Institute, "American National Standards Assessment of the Assumption of Normality," ANSI N15.15 (1974)

7. USNRC Regulatory Guide 5.22, Assessment of the Assumption of Normality, April 1974.

8. P. G. Hoel, "Introduction to Mathematical Statistics," John Wiley, p. 269ff (1971).

9. J. F. Archard, "Contact and Rubbing of Flat Surfaces," Journal of Applied Physics, August 1953, p. 981.

10. Markowski, E. M., Lee, L., Biderman, R., Casterline, J. E., "Effect of Rod Bowing on CHF in PWR Fuel Assemblies," ASME 77-HT-91.

1035 119

11. Letter, C. Eicheldinger (Westinghouse Nuclear Safety) to D. F. Ross (NRC), NS-CE-1580, October 24, 1977.

12. D. B. Owen, "Factors for One-Sided Tolerance Limits and for Variable Sampling Plans", SCR-607, March 1963.

13. Motley, F. E., Hill, K. W., Cadek, F. F. and Shefcheck, J., "New Westinghouse Correlation WRB-1 for Predicting Critical Heat Flux in Rod Bundles with Mixing Vane Grids," WCAP-8762 (Westinghouse Proprietary) and WCAP-8763 (Non-proprietary), July 1976.

14. Motley, F. E., Wenzel, A. H. and Cadek, F. F., "Critical Heat Flux Testing of 17x17 Fuel Assembly Geometry with 22-Inch Grid Spacing," WCAP-8536, (Westinghouse Proprietary) and WCAP-8537 (Non-proprietary), May 1975.

15. Motley, F. E. and Cadek, F. F., "Application of Modified Spacer Factor to L-Grid Typical and Cold Wall Cell DNB," WCAP-7988 (Westinghouse Proprietary) and WCAP-8030 (Non-proprietary), October 1972.

16. Letter, T. M. Anderson (Westinghouse) to J. F. Stolz (NRC), NS-TMA-2053, dated March 16, 1979.

17. Letter, J. F. Stolz (NRC) to T. M. Anderson (Westinghouse); Subject: Staff Review of WCAP-8691, April 5, 1979.

# APPENDIX A
# FUEL ROD FRETTING

The Archard wear equation derived for unlubricated sliding surfaces due to fretting relates the worn volume to the normal force and the sliding distance as follows:

$$V = \frac{S F L}{4260 H} \qquad (A-1)$$

where:

$V$ = wear volume ( cu in)

$S$ = wear coefficient

$F$ = normal force on contacting surfaces (lb)

$H$ = hardness (kg/sq mm)

$L$ = total sliding distance (in.)

The constant 4260 contains the shape factor and conversion constants.

This equation has been applied to rod to grid fretting and has been shown to be conservative from both out-of-pile hydraulic tests (D-loop) and reactor experience.

## A-1.  WEAR COEFFICIENT

As shown above, wear is directly related to the wear coefficient, S, which must be experimentally determined.

Since no wear coefficient data were available on Zircaloy-4 pairs at the small normal forces typical of vibrating bowed rods, a wear test program was recently conducted. A schematic diagram of the vibratory wear test apparatus is illustrated in figure A-1. The first phase of the testing employed loads of 0.1 and 0.5 pounds with no resultant measurable wear depth as shown in table A-1. The second phase was then performed with higher loads of 1 and 2 pounds in order to achieve measurable wear depths. For the 0.5 pound test and a wear depth of 0.001 in., the limit of measurement capability and upper limit wear coefficient of [          ]$^{+(b,c)}$ was determined from the Archard equation. A comparable value was
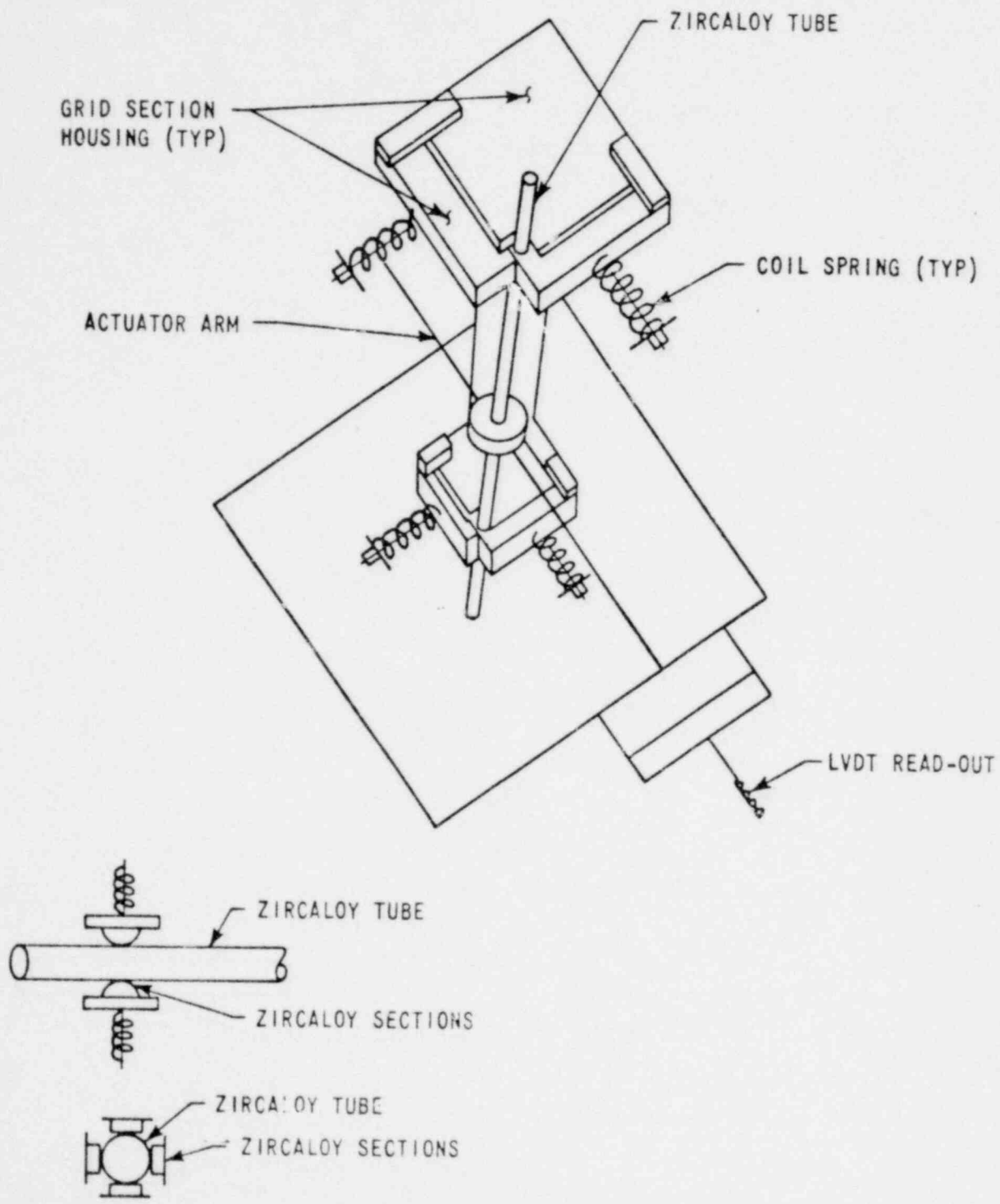
ZIRCALOY TUBE

GRID SECTION
HOUSING (TYP)

COIL SPRING (TYP)

ACTUATOR ARM

LVDT READ-OUT

ZIRCALOY TUBE

ZIRCALOY SECTIONS

ZIRCALOY TUBE

ZIRCALOY SECTIONS

Figure A1. Vibratory Wear Test Apparatus

A-2

1035 122

obtained for the 2 pound test (a load much greater than forces experienced in contacting bowed rods). Therefore, the use of [          ]$^{+(b,c)}$ is judged conservative.

## A-2.    WEAR DEPTH AND LENGTH

Next, the relationship among wear depth, length, and volume will be established. It is assumed that the worn section is a circular segment, as shown in figure A-2.

where:

    c = scar width
    h = wear depth of scar
    $\ell$ = wear length

Segment area = $1/2 \ [r^2 \ \theta - (r-h) \ c]$

$$\sin \frac{\theta}{2} = \frac{c}{2r}$$

For small wear depths:

$$\theta = \frac{c}{r}$$
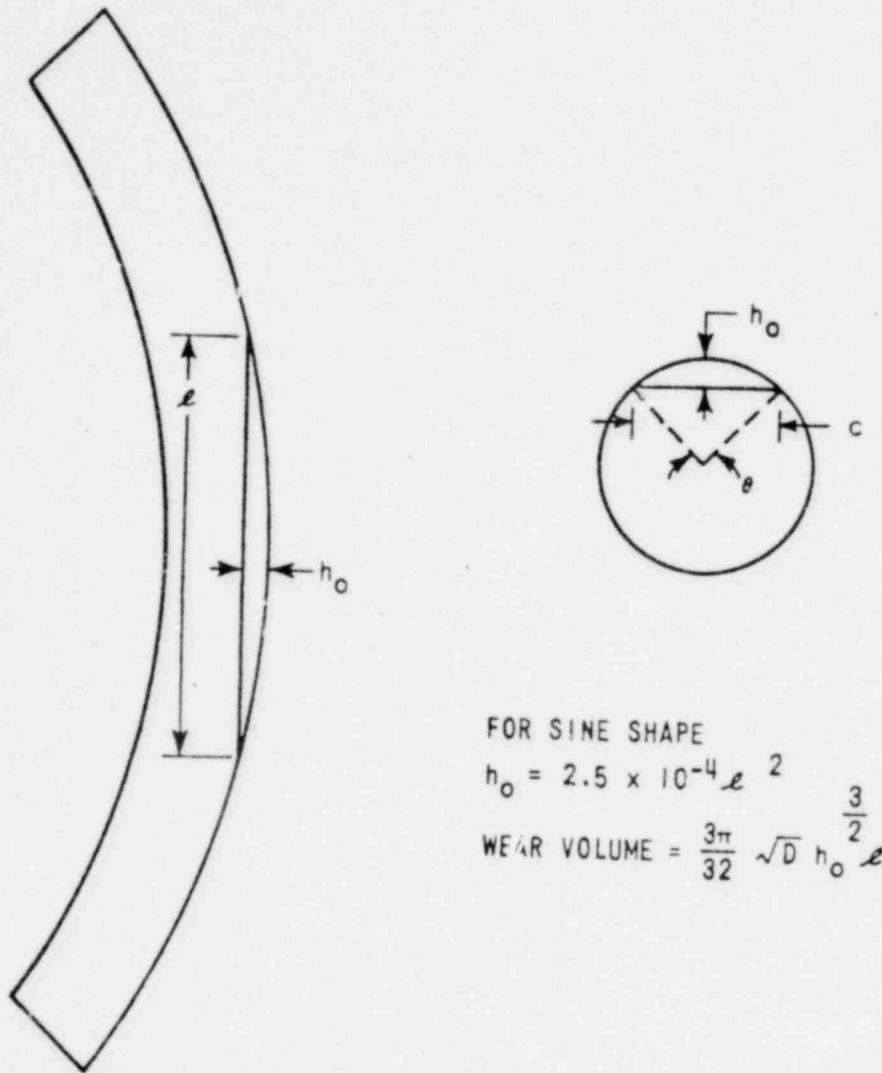
Simplifying,

$$\text{Segment area} = (1/2) \ c \ h$$

1035 123

FOR SINE SHAPE

$$h_o = 2.5 \times 10^{-4} \ell^2$$

$$\text{WEAR VOLUME} = \frac{3\pi}{32} \sqrt{D} \, h_o^{\frac{3}{2}} \ell$$

Figure A 2.  Definition of Wear Depth

1035 124

But from trigonometric relationship:

$$c/2 = \sqrt{h\,(d\text{-}h)}$$

Segment area $= h\sqrt{h\,(d\text{-}h)}$ (A-2)

The shape of the bowed rod is described as:

$$\frac{y}{y_0} = 1 - \cos\frac{\pi x}{L}$$ (A-3)

where:

$y$ = rod deflection at coordinate $x$

$y_0$ = mid span deflection

$x$ = axial position from mid span

$L$ = span length

The wear depth varies along the length of the rod in the scar area as:

$$y + h = h_0$$ (A-4)

where, $h_0$ = maximum wear depth at $x = 0$

The volume of the wear scar is determined by summing up the incremental segment areas along the scar length, or:

$$\text{volume} = \int_{-\frac{\ell}{2}}^{\frac{\ell}{2}} (\text{segment area})\ dx$$

$$= 2\int_{0}^{\frac{\ell}{2}} h\sqrt{h\,(D\text{-}h)}\ dx$$

A-5

1035 125

Since h is small relative to D, simplification results:

$$\text{volume} = 2 \int_{0}^{\frac{\ell}{2}} h \left( \sqrt{h \cdot D} \right) dx \qquad \text{(A-5)}$$

By substitution of Equations A-3 and A-4 into Equation (A-5), the resulting volume is obtained:

$$\text{volume} = \frac{3\pi}{32} \sqrt{D} \, h_0^{\frac{3}{2}} \, \ell \qquad \text{(A-6)}$$

When wear occurs on a bowed rod, the relationship between the depth and length of the wear scar is dependent on the bow shape. If the shape is sinusoidal as in Equation (A-3) the length of the scar is uniquely determined for any given wear depth. As can be seen in figure A-3, the clearance and relative geometry are the same for a single rod bowing full channel width into a straight rod or for two rods bowing toward each other a half channel width. This depth-length relationship can be graphically plotted and curve fit to be analytically described as:

$$h_o = K \, \ell^m \qquad \text{(A-7)}$$

where:

$m = 2.0$

$K = 2.5 \times 10^{-4}$

## A-3  IMPACTING AND WEAR MODEL

Vibration data have been obtained from strain gage instrumented fuel rods operated in a hydraulic test loop at reference conditions of temperature and flow rate. Spectrum analysis of results show that fuel rod vibration is random with a fundamental frequency of

WHICH MORE LIMITING
(1) ONE ROD BOWING FULL CHANNEL
(2) TWO RODS BOWING HALF CHANNEL

CLEARANCE = 0.140 $(1 - \cos \frac{\pi x}{L})$

CLEARANCE = 2 $[0.070 (1 - \cos \frac{\pi x}{L})]$
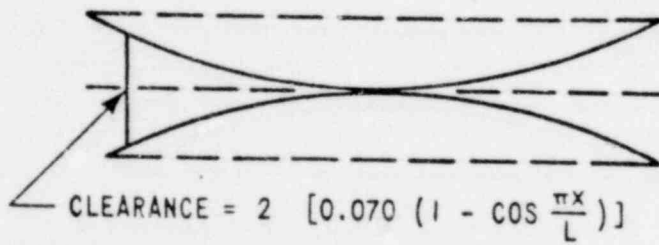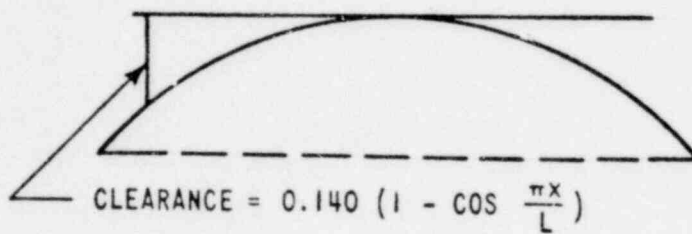
BOW VELOCITY = 1/2 (AMPLITUDE/TIME)

CONCLUSION: NO DIFFERENCE

Figure A 3.  Rod Deflection Definition

A 7

1035 129

of [ ]$^{+(b,c)}$ Hz, a single peak RMS amplitude of [ ]$^{+(b,c)}$ mil and single peak maximum amplitude of [ ]$^{+(b,c)}$ mil. While the [ ]$^{+(b,c)}$ mil amplitude occurs infrequently, it is conservative to calculate wear assuming a [ ]$^{+(b,c)}$ mil vibration amplitude at a frequency of [ ]$^{+(b,c)}$ Hz. The assumption of [ ]$^{+(b,c)}$ mil amplitude provides higher energy for wear and keeps the rods in the wear regime a longer time interval. Figure A4 shows the various regimes the vibrating rods experience. When the rod surfaces are more than [ ]$^{+(b,c)}$ mils apart, no contact can occur. At [ ]$^{+(b,c)}$ mils separation the rods begin contact but at zero normal force. As bowing proceeds, the normal force increases and as the rods slide over each other wear results. As the rods bow into hard contact, the normal force increases greatly due to the high spring constant of the clad and motion at the contact point ceases. Analysis indicates that the fuel rods then vibrate in a mode consistent with a half span length and a frequency of [ ]$^{+(b,c)}$ Hz.

Conservation of energy is applied to determine the buildup of normal force which is then used in the Archard equation to determine the wear volume. The vibration energy of the fuel rod is dissipated by damping when no contact occurs. When rods are in the wear regime, some of the rod energy produces wear, but the amplitude is reduced. Therefore, the relationship between normal force and amplitude is required.

Equating excitation work and damping work, the following derivation for excitation force is made:

$$\text{Excitation work/cycle} = \text{damping work/cycle}$$

$$\text{Damping work/cycle} = 2\pi\,\omega^2\,A^2\,\zeta\,W/g \qquad\qquad (A\text{-}8)$$

where:

$\omega$  =  $2\pi f = 2\pi \times$ [    ]$^{+b,c}$ frequency, sec$^{-1}$

$A$  =  [    ]$^{+b,c}$ in., amplitude

$\zeta$  =  [    ]$^{+b,c}$ damping factor

$W$  =  1.02 lbf, weight/span

$g$  =  386 in/sec$^2$, gravitational acceleration

A-8
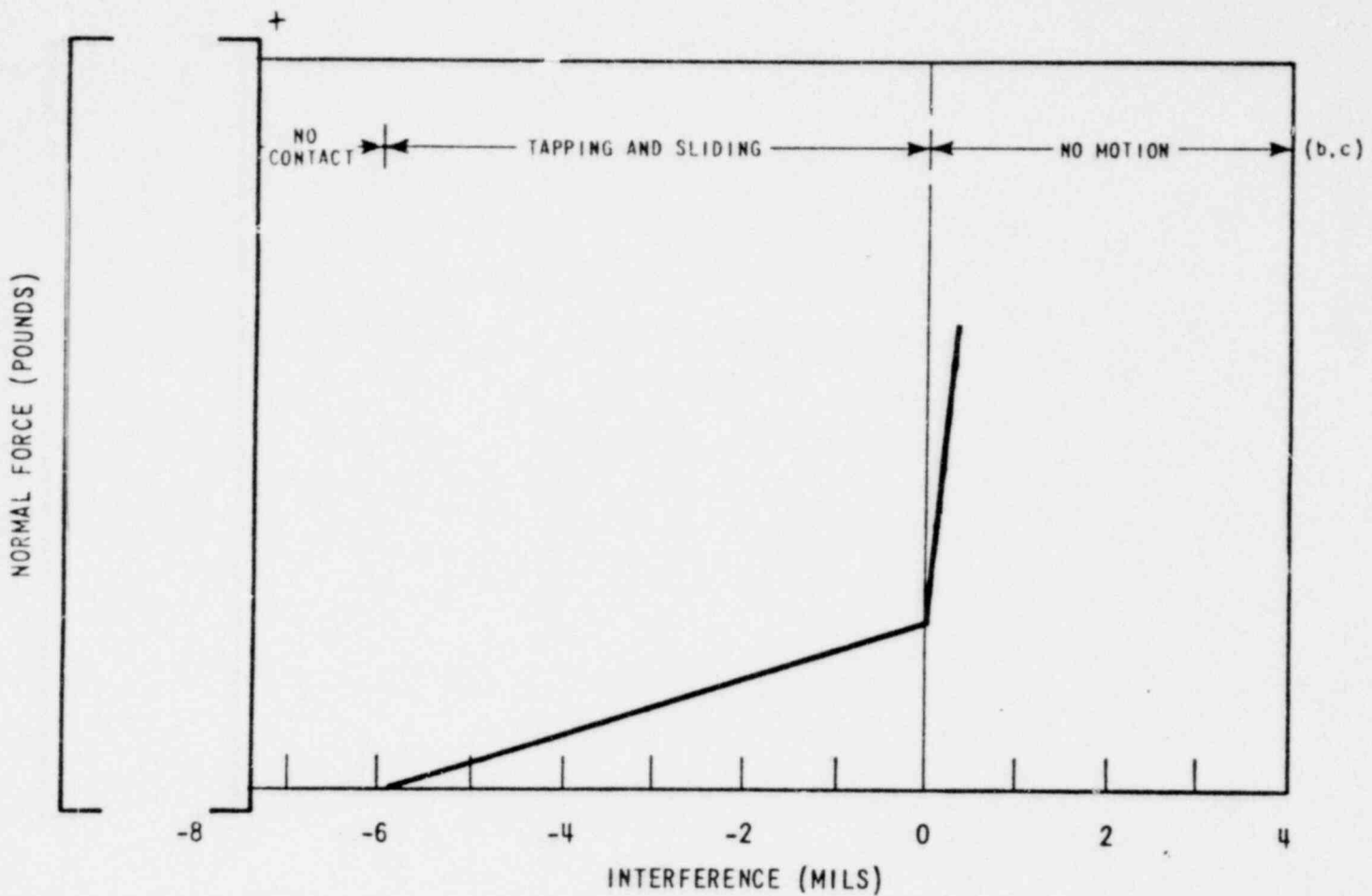
Figure A-4.  Normal Force vs Interference

Damping work/cycle = $5.4 \times 10^{-5}$

Excitation work/cycle = force x travel
$$= F^* A$$

Therefore, the force, $F^* = 0.018$ lb

In the wear regime, the excitation energy is partitioned between wear and damping:

Excitation work = wear work + damping work

$$F^*A = 4\mu \, \overline{N} \, A + 2\pi \, \omega^2 \, \zeta \, w/g \, A^2$$

where:

$\overline{N}$ = normal force, 1bf

$\mu$ = coefficient of friction

Then solving for amplitude:

$$A = (F^* - 4\mu \, \overline{N})/(2\pi \, \omega^2 \, \zeta \, w/g \qquad\qquad (A-9)$$

The graphical behavior of amplitude and normal force for $\mu = [\quad]^{+(b,c)}$ is shown in figure A-5. As expected, when normal force is zero (no contact or wear) the amplitude is the unimpeded value of $[\;]^{+(b,c)}$ mil. At the maximum value of normal force $\overline{N_0}$, the amplitude is zero and motion ceases.

As seen in figure A-4, the normal force is proportional to the separation distance or the so-called interference or:
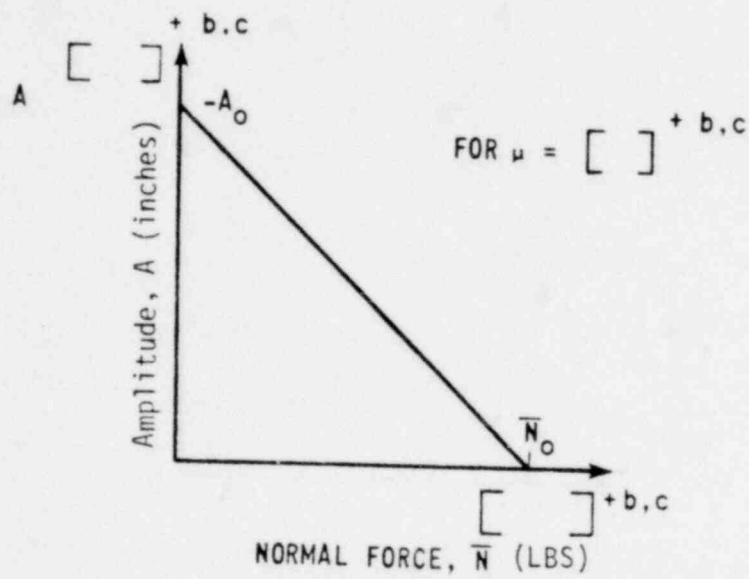
$$\overline{N} = KX$$

Figure A-5. Amplitude vs Normal Force

The separation distance can be described as:

$$X = Vt$$

where:

V = bow velocity

Then the normal force varies with time as follows:

$$\overline{N} = KVt$$
$$\overline{N}(t) = \dot{N}t$$

(A-10)

$$\dot{N} = \text{time rate of change for N}$$

From equation A-9 or figure A-5, it follows that amplitude varies linearly with normal force or:

$$A(t) = A_0 - \dot{A} t$$

(A-11)

The wear rate is proportional to the product of normal force and amplitude:

$$\text{Wear rate} = a \dot{\omega} = a \overline{N} A$$

then:

$$\dot{\omega} = A \overline{N}$$

$$= A_0 \dot{N}t - \dot{A} \dot{N} t^2$$

(A-12)

The behavior of amplitude, normal force, and wear rate are shown graphically in figure A-6. It is seen that wear rate builds-up from zero, goes through a maximum, and then returns to zero.

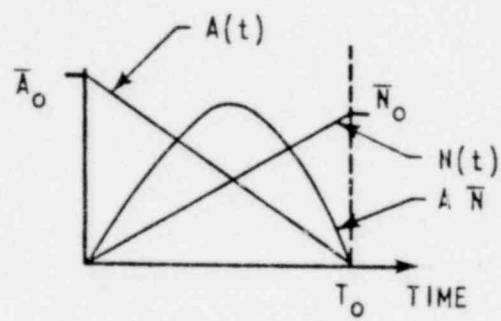The total wear can be determined by integration of the wear rate over the time interval that wear occurs, $T_0$.

Figure A-6. Fretting Parameters vs Function of Time

1035 133

$$\text{Total wear} = a \int_0^{T_0} \dot{\omega} \, dt$$

$$= a \left( \frac{A_0 \dot{N} T_0^2}{2} - \frac{\dot{A} \dot{N} T_0^3}{3} \right) \qquad \text{(A-13)}$$

$$= a \, A_0 \, T_0 \, \frac{\overline{N}_0}{6}$$

Equation (A-13) can be interpreted as meaning that in calculating wear as is done by the Archard equation, the effective normal force to be used with peak amplitude $A_0$, over the total wear time interval $T_0$, is one sixth of the peak normal force $N_0$.

In the NRC SER* it was accepted that channel closure varies with the square root of burnup with a zero burnup offset. For individual rods, however, the most likely value for initial bow in those rods which contact at end of life is zero. It can be shown for parabolic functions that the slope or bow velocity is 1/2 of the bow displacement divided by total time. For purposes of wear calculations, however, it would be conservative to use linear burnup dependence. The time interval of concern for wear calculations is the time to traverse the interference range of [ ]$^{+(b,c)}$ mils. The wear time is then maximum when bow rate is minimum. This occurs when channel closure is reached at the end of three cycles. The time required to traverse the interference range for various bow rates is shown in figure A-7. The maximum time is seen to be about [ ]$^{+(b,c)}$ hours.

Table A-2 summarizes the parameters used in the Archard equation to determine the wear depth of 0.044 mil.

---

* "Interim Safety Evaluation Report on Effects of Fuel Rod Bowing on Thermal Margin Calculations for Light Water Reactors," Revision 1, USNRC, February 16, 1977.
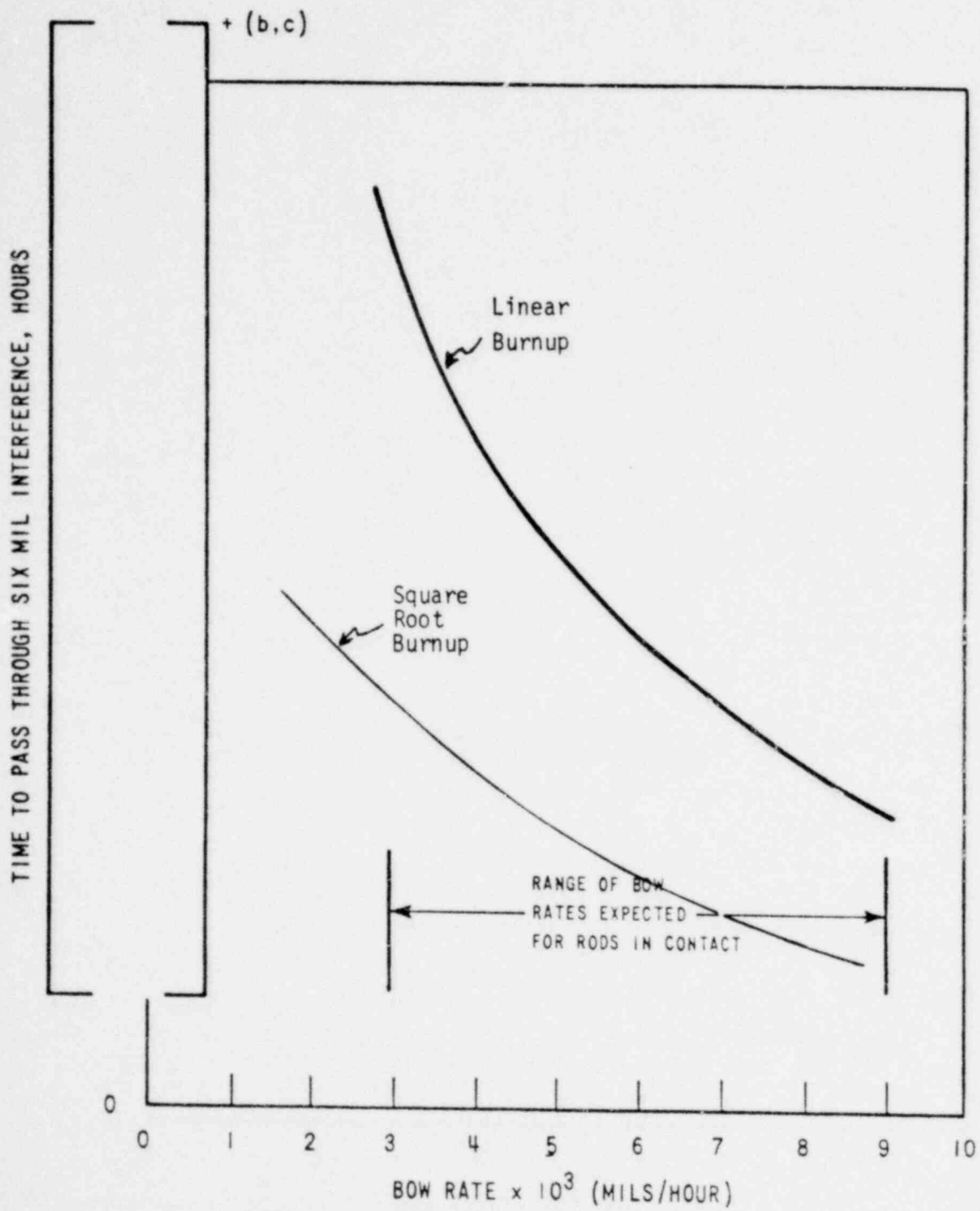
1035 134

Figure A-7. Fretting Time vs Bow Rate

1035 135

## TABLE A-1

### CURRENT TEST PROGRAM FOR ZR/ZR
### WEAR COEFFICIENT

| Test | Load (lb) | Amp (in.) | Cycles | Measured Wear Depth (in.) |
|------|-----------|-----------|--------|---------------------------|
| 1 | 0.1 | 0.010 | $7.7 \times 10^6$ | |
| 2 | 0.5 | 0.010 | $7.7 \times 10^6$ | [ ] +(b,c) |
| 3 | 1.0 | 0.010 | $7.6 \times 10^6$ | |
| 4 | 2.0 | 0.010 | $7.6 \times 10^6$ | |

## TABLE A-2

### FRETTING ANALYSIS

Use force = $\dfrac{\overline{N}_o}{6}$ = 0.0015 lb

$S$ = [ ] +(b,c)

$H$ = [ ] +(b,c)

Freq = [ ] +(b,c) Hz

Amp = [ ] +(b,c) in.

Time = [ ] +(b,c) hr

Wear volume = $2.42 \times 10^{-8}$

Wear Dept = 0.044 mil

1035 136

A-16

# APPENDIX B
# COLD TO HOT INCREMENTAL INCREASES
# IN ROD BOW

The correlation described in section 4 is based on bow measurements made with assemblies removed from the core. A correction is next presented for estimating the changes in bow from those measured to those existing at power.

The rods are assumed to have zero axial force during bow measurements. This is because of shaking and movement during fuel shuffling prior to measurements.

After replacement in the core, application of coolant external pressure causes the clad to shrink diametrally and axially due to the anisotropic strain properties of Zircaloy. The axial strain is greatest in the thinnest part of the clad wall. This gradient in axial strain across the clad diameter causes the clad to bow, the amount of bow being proportional to the average axial strain and the amount of wall eccentricity. Wall eccentricity is defined as the quotient of the difference between the maximum and minimum wall thickness with the average thickness. The first part of table B-1 lists the amount of mid-span bow in inches, taking into account the straightening effects of the grid, due to 100 percent axial strain in a clad with 100 percent wall eccentricity. In 15X15 for example, 8.7 mils of bow would occur in span 2 if the clad were strained 0.56 mils/inch and had a wall eccentricity of 0.18 (87 x 0.56 x 0.18). Part 2 of table B-1 lists the calculation of axial strain due to 2250 psi external pressure. Part 3 tabulates the results of using parts 1 and 2 for a clad wall eccentricity of 8 percent. It has been found that [ ]$^{+b,c}$ percent of Westinghouse clad has wall eccentricity less than 8 percent. For example, the 17 x 17 eight grid design will experience 3 mils of bow in span 3 due to 8 percent wall eccentricity and 2250 psi external pressure.

As the core is brought to temperature at zero power, the clad and thimbles remain at comparable temperatures. No differential axial expansion between fuel rods and thimbles occurs. Therefore, the axial force in the fuel rod remains zero. No change in bow occurs because of no change in the axial force acting on existing bow.

1035 137

## TABLE B-1

### CHANGE IN BOW DUE TO 2250 PSI PRESSURE
### AND 8% WALL ECCENTRICITY AT OPTIMUM PITCH

#### Bow/Unit Strain/Unit Eccentricity

| Array | Bottom | Bow/Strain/Eccentricity in Span | | | | | |
|---|---|---|---|---|---|---|---|
| | | 2 | 3 | 4 | 5 | 6 | 7 |
| 15 x 15 (14 x 14) | 74 | 87 | 89 | 88 | 83 | 15 | --- |
| 17 x 17 (7) | 80 | 94 | 96 | 95 | 91 | 16 | --- |
| 17 x 17 (8) | 91 | 67 | 66 | 65 | 64 | 59 | 19 |

#### Axial Strain

$$\text{Axial Strain} = 2.5 \times 10^{-7} \times \text{Pressure}$$
$$= (2.5 \times 10^{-7})\ (-2250)$$
$$= -0.56 \text{ mils/inch}$$

#### Mils of Bow Due to 2250 psi and 8% Eccentricity

| Array | 15 x 15 (14 x 14) | 17 x 17 (7) | 17 x 17 (8) |
|---|---|---|---|
| Span 7 | --- | --- | 0.9 |
| 6 | 0.7 | 0.7 | 2.6 |
| 5 | 3.7 | 4.1 | 2.9 |
| 4 | 3.9 | 4.3 | 2.9 |
| 3 | 4.0 | 4.3 | 3.0 |
| 2 | 3.9 | 4.2 | 3.0 |
| Bottom | 3.3 | 3.6 | 4.1 |

During the period the core is brought to 100 percent power, the clad temperature rises faster than the thimble temperature until the clad is approximately 100°F hotter than the thimbles. Differential thermal expansion between clad and thimbles results in 12 pounds compression loading on each fuel rod in 15x15 and 10 pounds in 17 x 17. Reacting tension loads in the thimbles are higher in the ratio of number of fuel rods per thimble. The axial strains in clad and thimble together equal the magnitude of differential expansion between clad and thimble.

The bow increment resulting from this 12 pound loading is proportional to load, span length squared, initial bow and inversely proportional to flexural rigidity. The proportionality constant is determined from an analysis which accounts for the effects of grid stiffness and support from adjacent spans.

During an overpower incident, the differential thermal expansion between clad and thimbles will increase the loading and bow a proportional amount. The loading increments due to changes in power, however, can never exceed the current value of grid slip force. On the other hand, if the increment of rod loading due to power changes are less than the current grid/rod slip load, subsequent differential expansion between rod and thimble due to greater rod growth than thimble growth may be expected to result in further load increases. The rod compression loads will then rise until they equal the current grid/rod slip loads and increase no further. For these reasons, cold to hot changes in bow are based on current values of grid slip load rather than magnitude of power change. This will result in maximum possible estimates for cold to hot increments in rod bow. Table B-2 summarizes the parameters used to calculate the cold to hot bow increments in table B-3.

The rod bow correlations are corrected for temperature and pressure effects prior to performing the DNB and power peaking analyses. The cold to hot correction is a direct multiplier on the magnitude of bow. The standard deviation at hot conditions, $\sigma_{HOT}$, is obtained by multiplying the standard deviation at cold conditions, $\sigma_{COLD}$, by the cold to hot correction factors, $f_{CH}/100$, given in table B-3.

1035 139

## TABLE B-2
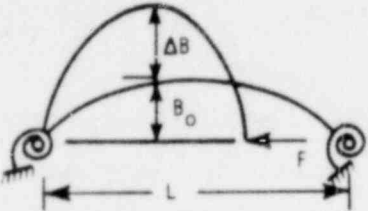## CHANGE IN BOW, COLD TO HOT, DUE TO GRID FORCE

$$\frac{\Delta B}{B_O} = \frac{K\,F L^2}{EI}$$

$$K = 0.0475$$

| No. Grids | Span Length, L | |
|---|---|---|
| | Middle | End |
| 7 | 26.2 | 24.6 |
| 8 | 20.6 | 24.4 |

$E = 13 \times 10^6$

| Array | 15 x 15 (14 x 14) | 17 x 17 |
|---|---|---|
| I, Moment of Inertia | $6.02 \times 10^{-4}$ | $3.85 \times 10^{-4}$ |

$F_O$, BOL Maximum Span Load — Rods Off Bottom

| Array | Span | | | | | | |
|---|---|---|---|---|---|---|---|
| | Bottom | 2 | 3 | 4 | 5 | 6 | 7 |
| 15 x 15 (14 x 14) | 16 | 30 | 43 | 43 | 30 | 16 | --- |
| 17 x 17 (7) | 12 | 22 | 32 | 32 | 22 | 12 | --- |
| 17 x 17 (8) | 12 | 22 | 32 | 42 | 32 | 22 | 12 |

f, Span Load Fraction vs. Time

| Time | BOL | EOC-1 | EOC-2 | EOC-3 |
|---|---|---|---|---|
| $f = F/F_O$ | 1.0 | 0.35 | 0.10 | 0.03 |

$$\frac{\Delta B}{B_O} = K\,f\,F_O\,L^2/EI$$

1035 170

## TABLE B-3

### $f_{CH}$, % CHANGE IN BOW, COLD TO HOT, DUE TO GRID FORCE (RODS OFF-BOTTOM)

| Span | 15x15 (14x14) | | | |
|------|-----|-------|-------|-------|
|      | BOL | EOC-1 | EOC-2 | EOC-3 |
| T | 5.9 | 2.1 | 0.6 | 0.2 |
| 5 | 12.6 | 4.4 | 1.3 | 0.4 |
| 4 | 18.1 | 6.3 | 1.8 | 0.6 |
| 3 | 18.1 | 6.3 | 1.8 | 0.6 |
| 2 | 12.6 | 4.4 | 1.3 | 0.4 |
| B | 5.9 | 2.1 | 0.6 | 0.2 |
| | 17 x 17 (7) | | | |
| T | 6.8 | 2.4 | 0.7 | 0.2 |
|   | 14.3 | 5.0 | 1.4 | 0.5 |
|   | 20.8 | 7.3 | 2.1 | 0.7 |
|   | 20.8 | 7.3 | 2.1 | 0.7 |
|   | 14.3 | 5.0 | 1.4 | 0.5 |
|   | 6.8 | 2.4 | 0.7 | 0.2 |
| | 17 x 17 (8) | | | |
| T | 6.7 | 2.4 | 0.7 | 0.2 |
|   | 8.8 | 3.1 | 0.9 | 0.3 |
|   | 12.8 | 4.5 | 1.3 | 0.4 |
|   | 16.8 | 5.9 | 1.7 | 0.6 |
|   | 12.8 | 4.5 | 1.3 | 0.4 |
|   | 8.8 | 3.1 | 0.9 | 0.3 |
|   | 6.7 | 2.4 | 0.7 | 0.2 |

The bows due to the application of system pressure to an eccentric rod, given in table B-1, are independent of bowing direction and magnitude. The bow due to application of pressure, $\delta_p$, is a fixed amount, for a given pressure and eccentricity, and the direction of bow is random. Thus, the variance of bow due to pressure effects is equal to:

$$\frac{\delta_p^2}{2} \tag{B-1}$$

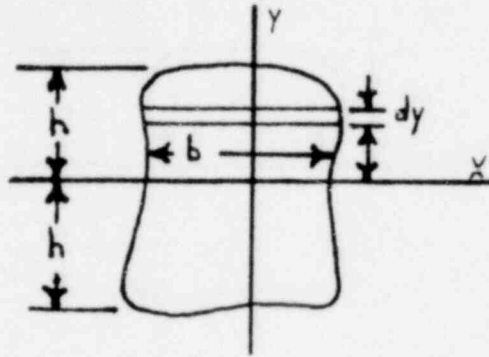The variance of rod bow with cold to hot and pressure corrections is:

$$\sigma_{HOT}^2 = [\sigma_{COLD} \cdot (1 + f_{CH}/100)]^2 + \frac{\delta_p^2}{2} \tag{B-2}$$

APPENDIX C

## ROD BOW SCALING FACTORS

In this appendix, bending deflection of a creep sensitive rod is derived following the methods of Rabotnov[*].

Consider a rod with a cross section shown below:



The height of the section is 2h, and the section width is b, which is a function of y. If a creep law of the form $\sigma = \sigma(\epsilon)$ is postulated, rod sections remain plane on deformation and $\dot{\epsilon} = Ky$ where K is the time rate of change of curvature of the center line of the rod. If the properties of the material are the same in tension and compression, the bending moment M is:

$$M = \int_{0}^{A} y\sigma dA \qquad \text{(C-1)}$$

where A is cross-sectional area of the rod.

Introducing a power creep law:

$$\sigma = \sigma_m \left(\frac{\dot{\epsilon}}{\dot{\epsilon}_m}\right)^{\frac{1}{m}} = \sigma_m \left(\frac{Ky}{\dot{\epsilon}_m}\right)^{\frac{1}{m}} \qquad \text{(C-2)}$$

---

[*]  Y. N. Rabotnov, "Creep Problems in Structural Members", North-Holland Publishing Co., Amsterdam, Holland, 1969.

then

$$M = \int_{0}^{A} y\ \sigma_m \left(\frac{Ky}{\epsilon_m}\right)^{\frac{1}{m}} d A \tag{C-3}$$

where $\sigma_m$ and $\epsilon_m$ are constants.

Solving C-3 for curvature:

$$K = \left[ \frac{M}{\int_{0}^{A} \sigma_m \left(\frac{1}{\epsilon_m}\right)^{\frac{1}{m}} y^{1+\frac{1}{m}} d A} \right]^{m} \tag{C-4}$$

Knowing the relationship between the bending moment and the rate of change of curvature, the rate of rod displacement can be found by integrating

$$\frac{d^2 \dot{y}}{d t^2} = \left[ \frac{M}{\int_{0}^{A} \sigma_m \left(\frac{1}{\epsilon_m}\right)^{\frac{1}{m}} y^{1+\frac{1}{m}} d A} \right]^{m} \tag{C-5}$$

The length effect can be determined by non-dimensionalizing this length variable as follows:

$$\text{Let } s = \frac{z}{L} \tag{C-6}$$

where L is the distance between grids, span length.

Then

$$\frac{d^2 \dot{y}}{ds^2} = L^2 \left[ \frac{M}{\int_{0}^{A} \sigma_m \left(\frac{1}{\epsilon_m}\right)^{\frac{1}{m}} y^{1+\frac{1}{m}} d A} \right]^{m} \tag{C-7}$$

The rate of deflection is obtained by double integration and can be symbolically shown as

$$\dot{y} = L^2 \int_{o}^{s=1} ds \int_{o}^{s} \left[ \frac{M}{\int_{o}^{A} \sigma_m \left(\frac{1}{\dot{\varepsilon}_m}\right)^{\frac{1}{m}} y^{1+\frac{1}{m}} dA} \right]^m ds \qquad (C-8)$$

Equation C-8 shows that creep deflection varies with the square of the span length L. In order to obtain further simplifications, the nature of the creep law must be explored.

It can be shown for Westinghouse clad material that n-1 i.e. $\dot{\varepsilon} \backsim \sigma$. The equation C-8 becomes

$$\dot{y} = L^2 \int_{o}^{s=1} ds \int_{o}^{s} \left[ \frac{M}{\int_{o}^{A} \sigma_m \left(\frac{1}{\dot{\varepsilon}_m}\right) y^2 dA} \right] ds \qquad (C-9)$$

Making use of the following definitions:

$$\frac{\sigma_m}{\dot{\varepsilon}_m} = \overset{\backsim}{E} \quad \text{(the creep modules)}$$

$$\int_{o}^{A} y^2 dA = I \quad \text{(the moment of inertia)}$$

equation C-9 becomes

$$\dot{y} = \frac{L^2}{\overset{\backsim}{E} I} \int_{o}^{s=1} ds \int_{o}^{s} M \, ds$$

As mentioned earlier, the integration of M can only result in a pure number. Then for a given bending moment applied to two different fuel designs, the resultant bow varies as $L^2/I$.

## APPENDIX D

## ROD BOW SPAN LENGTH DEPENDENCE

The 17x17 demonstration assemblies irradiated in plant I* contain seven grids while those irradiated in 17x17 cores contain eight grids (Standard). Table D-1 compares span lengths for these two designs. Channel spacing probe measurements using a strain gage probe were taken in Plan. I demonstration assembly RD-1 at EOC-3 and in several Plant L* assemblies at EOC-1. These data were corrected for probe stiffness effects. Plant L assemblies A-64 and B-27 were selected from those probed since data are available in all spans as is the case for demonstration assembly RD-1. From Table D-1, it can be seen that (4) 26.2 inch span lengths exist in the seven grid assembly versus (5) 20.6 inch span lengths in the eight grid assemblies. The top span is considered non-typical because of the plenum. It is the purpose of this evaluation to determine the span length dependence on rod bow for these two span lengths.

If no rod bow were present, all channels would exhibit nominal dimensions. The deviation from nominal is a measure of rod bow and the standard deviation of the data set quantifies the bow or variability. Table D-2 presents the standard deviation for outer and inner channels ($\sigma_o$ and $\sigma_i$), the number of outer and inner channels ($N_o$ and $N_i$) and the standard deviation for the combined set of inner and outer channels ($\sigma_T$). It can be seen from Table D-2 that the axial distribution of standard deviation differs for plant I and L assemblies. This is believed to be caused by the different burnup levels of the assemblies.

The three assemblies under study achieved different burnup levels so that normalization to a common burnup is necessary. The burnup levels were 16,300, 18,100 and 19,200 MWD/MTU for RD-1, A-64 and B-27, respectively. A linear burnup correction relationship, based on the best fit equation (4-5), is employed as follows:

---

* Plant designations I and L follow the nomenclature given in Table 3-1.

1035 141

TABLE D-1

## COMPARISON OF SPAN LENGTHS

|  | Span Length in Inches | |
| Span | Seven Grid+ | Eight Grid* |
|------|-------------|-------------|
| 1 | 24.4 | 24.4 |
| 2 | 26.2 | 20.6 |
| 3 | 26.2 | 20.6 |
| 4 | 26.2 | 20.6 |
| 5 | 26.2 | 20.6 |
| 6 | 18.6 | 20.6 |
| 7 |  | 20.6 |

+ Plant I 17x17 Demonstration Assembly, RD-1.

* Plant L 17x17 Assemblies, A-67 and B-27.

## CHANNEL SPACING STANDARD DEVIATION

| | A-64, F-1 | | | | | B-27, F-1 | | | | | RD-1, F-1 | | | | | RD-1, F-2 | | | | |
|---|---|---|---|---|---|---|---|---|---|---|---|---|---|---|---|---|---|---|---|---|
| Span | $N_6$ | $\sigma_o$ | $N_i$ | $\sigma_i$ | $\sigma_T$ | $N_6$ | $\sigma_o$ | $N_i$ | $\sigma_i$ | $\sigma_T$ | $N_6$ | $\sigma_o$ | $N_i$ | $\sigma_i$ | $\sigma_T$ | $N_6$ | $\sigma_o$ | $N_1$ | $\sigma_i$ | $\sigma_T$ |
| 2 | | | | | | | | | | | | | | | | | | | | $^{4}$(b,c) |
| 3 | | | | | | | | | | | | | | | | | | | | |
| 4 | | | | | | | | | | | | | | | | | | | | |
| 5 | | | | | | | | | | | | | | | | | | | | |
| 6 | | | | | | | | | | | | | | | | | | | | |

A-64, F-1:  Plant L Fuel Assembly, Face 1

B-27, F-1:  Plant L Fuel Assembly, Face 1

RD-1, F-1:  Plant I Demo Assembly, Faces 1, 2

      F-2

      $\sigma$:  Standard deviation for channel closure

      N:  Number of channels measured

Subscripts:

      o - outer channel

      i - inner channel

      T - combined inner and outer channel

$$\sigma = \sigma_N \cdot \frac{3.65 + 0.649 \cdot BU}{3.65 + 0.649 \cdot N} \qquad (D-1)$$

where: $\sigma$ = standard deviation at burnup BU

$\sigma_N$ = standard deviation at burnup N

In order to proceed, the following functional relationship between standard deviation and span length is postulated:

$$\sigma_m = AL^m \qquad (D-2)$$

where: $\sigma_m$ = best fit standard deviation

A = constant for best fit

L = span length

m = exponent on span length

For purposes of determining the exponent m, the above equation can be linearized to the form:

$$\log \sigma_m = \log A + m \log L \qquad (D-3)$$

When a linear regression analysis is performed on the natural logarithms of the corrected standard deviations and corresponding span lengths, a value of [      ]$^+$ is obtained for m and [      ]$^+$ for log A with a correlation coefficient of .8. Hence: $\qquad$ (a,c)

$$\sigma_m = [\quad\quad]^+ (L)^{[\quad\quad]^+} \qquad (D-4) \quad (a,c)$$

As a value very near 2 was obtained with a high correlation coefficient, it is concluded that the channel spacing data supports a second power span dependence.

APPENDIX E

ROD BOW EFFECT ON DNB CORRELATION DISTRIBUTION

The DNB correlation parameters for unbowed and bowed configurations are designated (M/P) and $(M/P)_B$ respectively. The rod bow penalty function $\delta$ relating these two parameters is defined by the relation

$$\delta = 1 - \frac{(\overline{M/P})_B}{(\overline{M/P})} \qquad (E-1)$$

Solving for $(M/P)_B$ gives

$$(\overline{M/P})_B = (M/P)(1-\delta) \qquad (E-2)$$

The mean and variance of the $(M/P)_B$ distribution are determined from the mean and variance of the (M/P) and $\delta$ distributions using relationships given in Reference E-1. The resulting equations are:

$$(\overline{M/P})_B = (\overline{M/P})\ (1-\overline{\delta}) \qquad (E-3)$$

$$\hat{\sigma}_B^2 = (1-\overline{\delta})^2\left[\hat{\sigma}\ (M/P)\right]^2 + (\overline{M/P})^2\ \hat{\sigma}_\delta^2 \qquad (E-4)$$

where the sample mean and variance of the $(M/P)_B$ distribution are $(\overline{M/P})_B$ and $\hat{\sigma}_B^2$, of the (M/P) distribution are $(\overline{M/P})$ and $\left[\hat{\sigma}(M/P)\right]^2$ and of the $\delta$ distribution are $\overline{\delta}$ and $\hat{\sigma}_\delta^2$, respectively. The carat is used over the variances to indicate that they are estimates based on sampling data.

In order to determine an upper tolerance limit on $\hat{\sigma}_B$, the effective degrees of freedom associated with the value of $\hat{\sigma}_B^2$ given by the following equation (Ref. E-1) is used.

E-1

$$n_B - 1 = \frac{\hat{\sigma}_B^4}{\dfrac{(1-\bar{\delta})^4 \left[\hat{\sigma}(M/P)\right]^4}{n-1} + \dfrac{(\overline{M/P})^4 \hat{\sigma}_\delta^4}{n_\delta - 1}} \tag{E-5}$$

where $n$ and $n_\delta$ are the number of measurements used in determining
the DNB correlation and channel closure distributions, respectively.
Equations (E-3), (E-4) and (E-5) are indicated as Equations (5-4), (5-5)
and (5-6), respectively, in Section 5.2.2.

Reference E-1:   J. L. Jaech, "Statistical Methods in Nuclear Material
Control," TID-26298, USAEC, 1973, p. 158.

# APPENDIX F

## ROD BOW POWER PEAKING FACTOR UNCERTAINTY
$$(F_Q^B)$$

### F-1    Local Power Increase

Local changes in the fuel rod pitch caused by fuel rod bowing create small local power changes (both positive and negative) in the surrounding fuel rods. A positive power increase results from improved local neutron moderation for an increase in the local pitch, for example, for the rod adjacent to a bowed rod with the bow away from it. Conversely, the power in the rod adjacent to the bowed rod in the direction of the bow decreases due to the reduced local moderation.

### F-2    Calculational Method

Two dimensional transport theory calculations for a 9 x 9 array of discrete fuel rods were used to determine the local power changes due to a single displaced fuel rod in a typical Westinghouse 15x15+ fuel assembly lattice. The effects of nearby water filled thimble tubes on the local power changes were also investigated. The conditions used in this study, a burnup of 22,000 MWD/MTU with zero boron concentration in the coolant provide conservatively higher power changes than would be calculated during most of a normal operating cycle. Power perturbations for various magnitudes and directions of rod displacement are shown in figures F-1, F2 and F3.        Details of the calculations are given in Appendix G.

Power changes due to a single displaced rod were also computed for a 17 x 17 lattice and found to be somewhat smaller than those shown in figures F-1, F-2 & F-3.    The more conservative power changes shown in the figures were also used for 17 x 17 and 16 x 16 bowing power change calculations. Power changes due to a single displaced rod were determined for a one-eighth symmetric 37 rod array. The power change on the center rod of the array due to its own displacement and the individual displacements of the 36 surrounding rods in each of eight directions were computed.

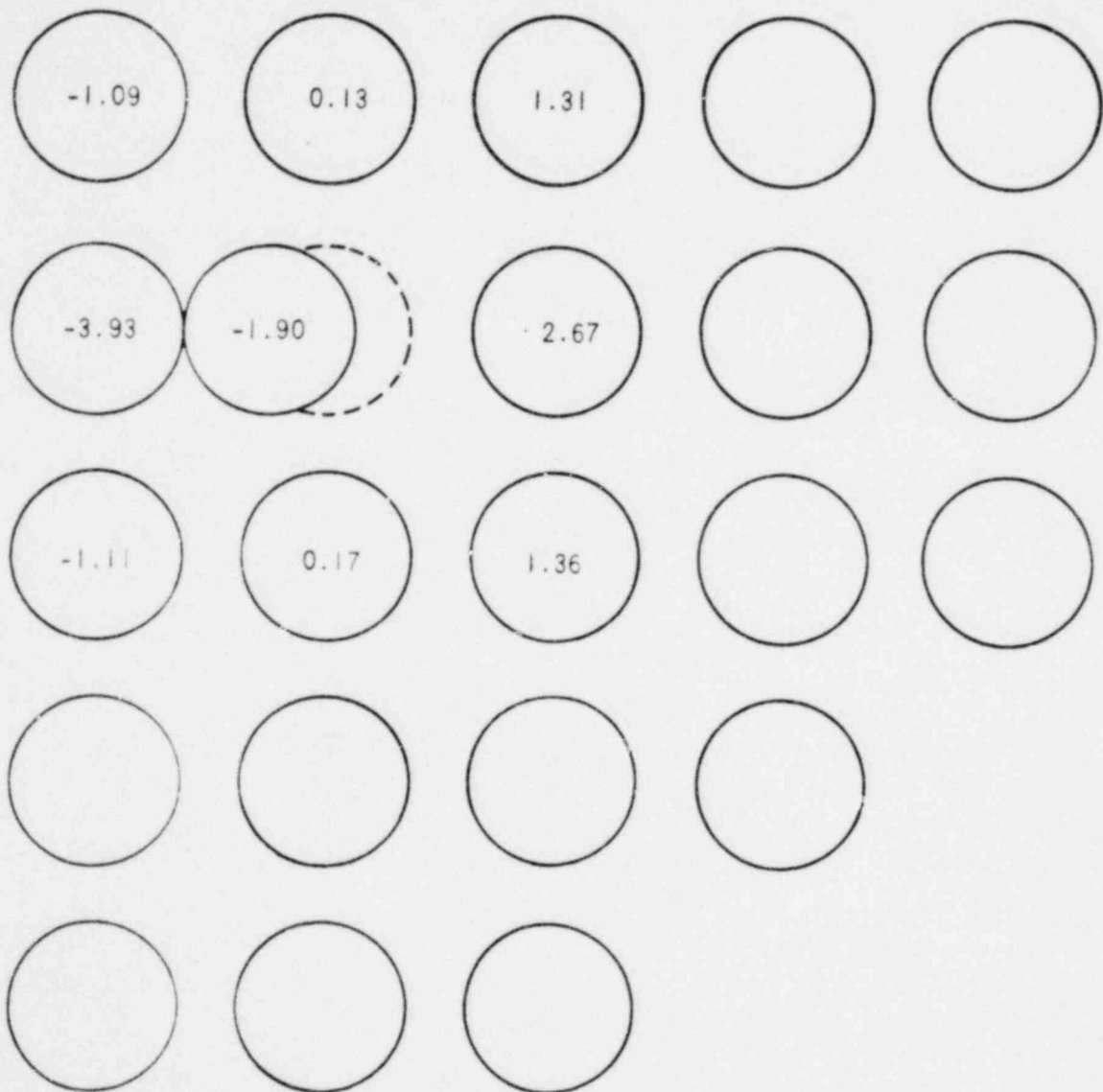+Also applies to a 14x14 fuel assembly lattice.

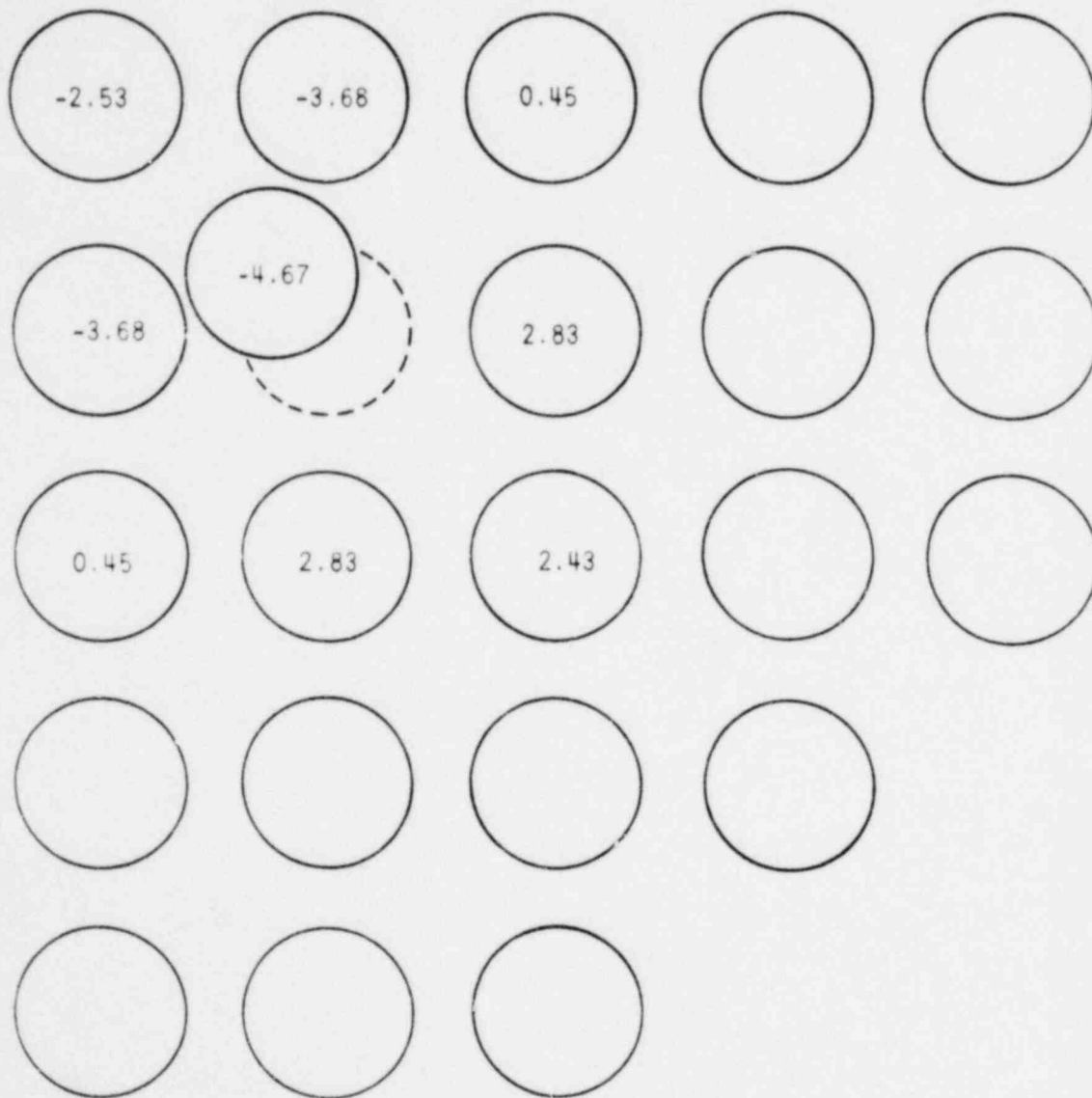Figure F-1   Percent Power Change for Lateral Rod Displacement = $C_O$

1035 154

Figure F-2    Percent Power Change for Diagonal
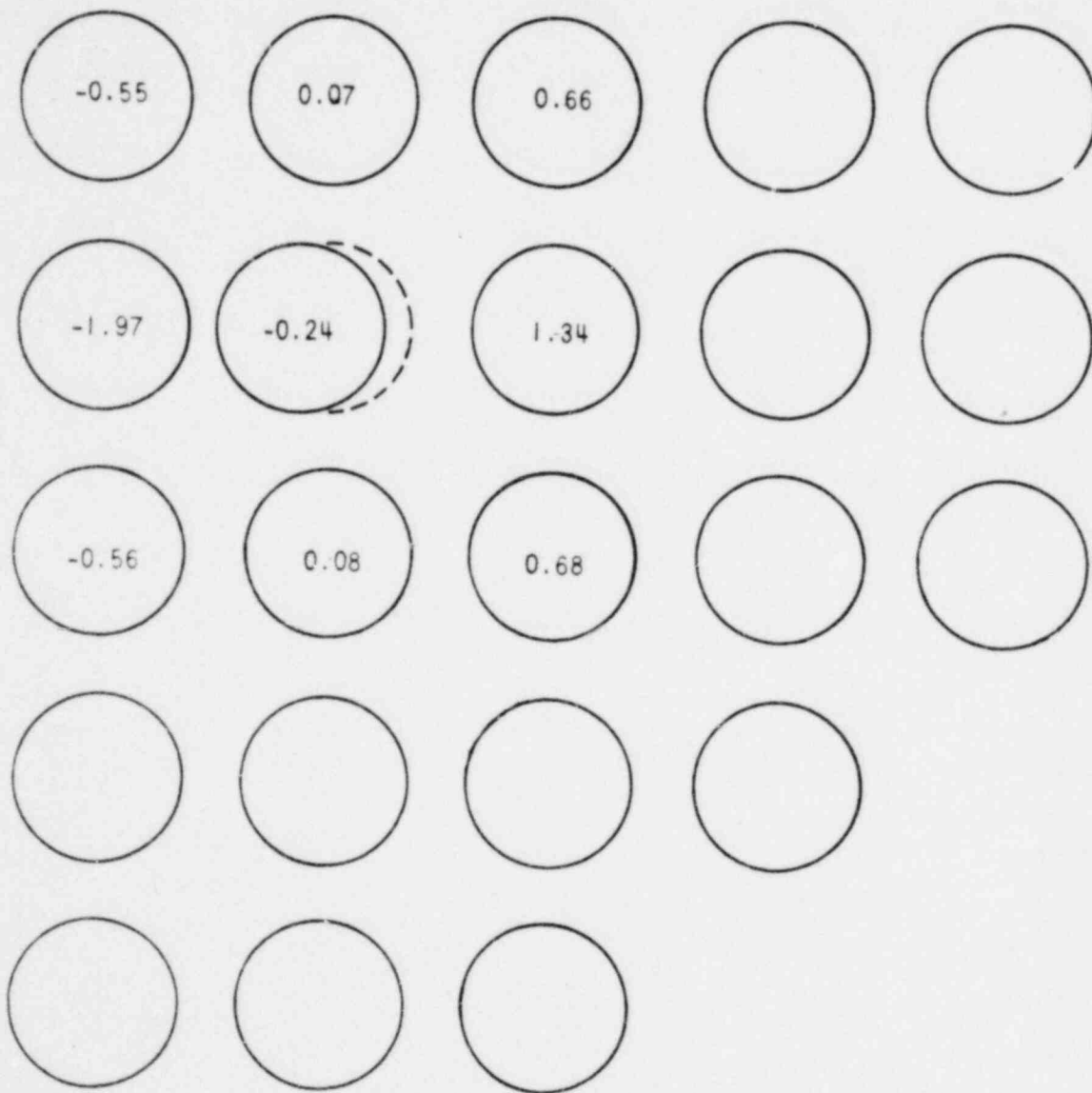Rod Displacement = $C_o \sqrt{2}$

1035 155

Figure F-3    Percent Power Change for Lateral
Rod Displacement = $C_o/2$

Single event power changes were calculated as a function of rod displacement of a single rod, but the empirical predictions for rod bow presented in table 6-1 are in terms of the projected gap closure. Gap closures result from the simultaneous bow of two rods. However, it may be shown that the standard deviation of bowing displacement is equal to the standard deviation of projected gap closure. The geometric relation between rod displacements, $\delta$, and projected gap closure, C, is shown in figure F-4. The mean value of clearance is $C_o$ and the variance of C is the expected value of $(C \cdot C_o)^2$.

$$\sigma_c^2 = E\left[C \cdot C_o\right]^2 = E\left[\delta_1^2 \cos\theta_1^2 + \delta_2^2 \cos\theta_2^2 - 2\delta_1\delta_2\cos\theta_1\cos\theta_2\right] \qquad (F-1)$$

or

$$\sigma_c^2 = \int_{-\infty}^{+\infty} \delta_1^2\, P(\delta_1)\, d\delta_1 \cdot \int_0^\pi \cos\theta_1^2 P\,(\cos\theta_1)d\theta_1 \qquad (F-2)$$

$$+ \int_{-\infty}^{\infty} \delta_2^2\, P(\delta_2)\, d\delta_2 \cdot \int_0^\pi \cos\theta_2^2 P\,(\cos\theta_2)d\theta_2$$

$$- 2E\left[\delta_1\,\delta_2\,\cos\theta_1\,\cos\theta_2\right]$$
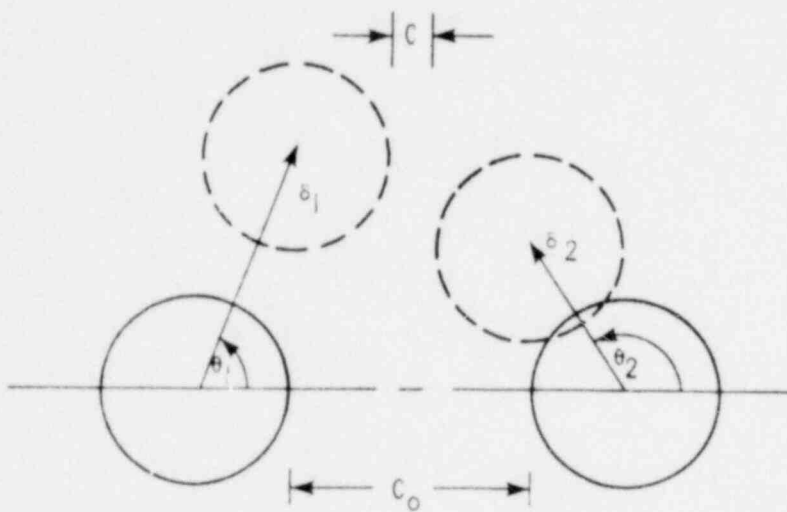
where:

P = probability density functions

Therefore, the variance of gap closure may be written as:

$$\sigma_c^2 = \frac{\sigma_{\delta_1}^2}{2} + \frac{\sigma_{\delta_2}^2}{2} - 2E\left[\delta_1\,\delta_2\,\cos\theta_1\,\cos\theta_2\right] \qquad (F-3)$$

The expected value of the last term in the above equation is zero if the rods bow independently, and since $\sigma_{\delta_1} = \sigma_{\delta_2} = \sigma_\delta$.

$$\sigma_c = \sigma_\delta \qquad (F-4)$$

1035 157

$$C = C_O - \delta_1 \cos \theta_1 + \delta_2 \cos \theta_2$$

$-\infty \leq \delta \leq +\infty$    NORMALLY DISTRIBUTED WITH MEAN = 0 AND VARIANCE = $\sigma^2$

$0 \leq \theta \leq \pi$    UNIFORMLY DISTRIBUTED

Figure F-4   Relation Between Rod Bow and Gap Closure

1035 158

The power change on the center rod due to its own bow was determined for several values of rod displacement. The individual power changes were (conservatively) fit to the curve.

$$S_{1j} = -0.02 \left(\frac{\delta_{1j}}{C_o}\right)^2 - 1.88 \left(\frac{\delta_{1j}}{C_o}\right)^3, \quad -C_o \leqslant \delta_{1j} \leqslant C_o \qquad (F-5)$$

where:

$S_{1j}$ = power change in the center rod due to its own bow in direction j

$\delta_{1j}$ = bow in direction j

$C_o$ = initial gap clearance

This function applies to all bowing directions.

The power changes on the center rod due to the bows of the surrounding rods were calculated to be linear functions of bowing displacement. The power changes can be represented by the expression

$$S_{ij} = A_{ij} \, S_o \, \frac{\delta_{ij}}{C_o} \qquad (F-6)$$

where:

$S_{ij}$ = power change on the center rod in the array due to the bow of rod i in direction j

$A_{ij}$ = attenuation factor of rod i in direction j

$S_o$ = reference power change

The computed attenuation factors, $A_{ij}$, for the 37 rod array with eight possible bowing directions, for $S_o$ = 2.83 percent and $\delta_{ij}$ = $C_o$ are shown in figure F-5 This set of attenuation factors was used for bowing power change calculations for all assemblies.

Individual power changes on a rod due to its own bow and the bow of the 36 surrounding rods were determined with Monte Carlo techniques. The computer code used for these calculations was similar to the DRAW code used to compute densification power spikes. The sequence of calculations is shown in the flow diagram given in figure F-6. Input to the calculation consists of the probability distribution of bowing displacement for a given value of $\sigma_\delta$, the power change versus rod displacement function for the center rod, the reference power
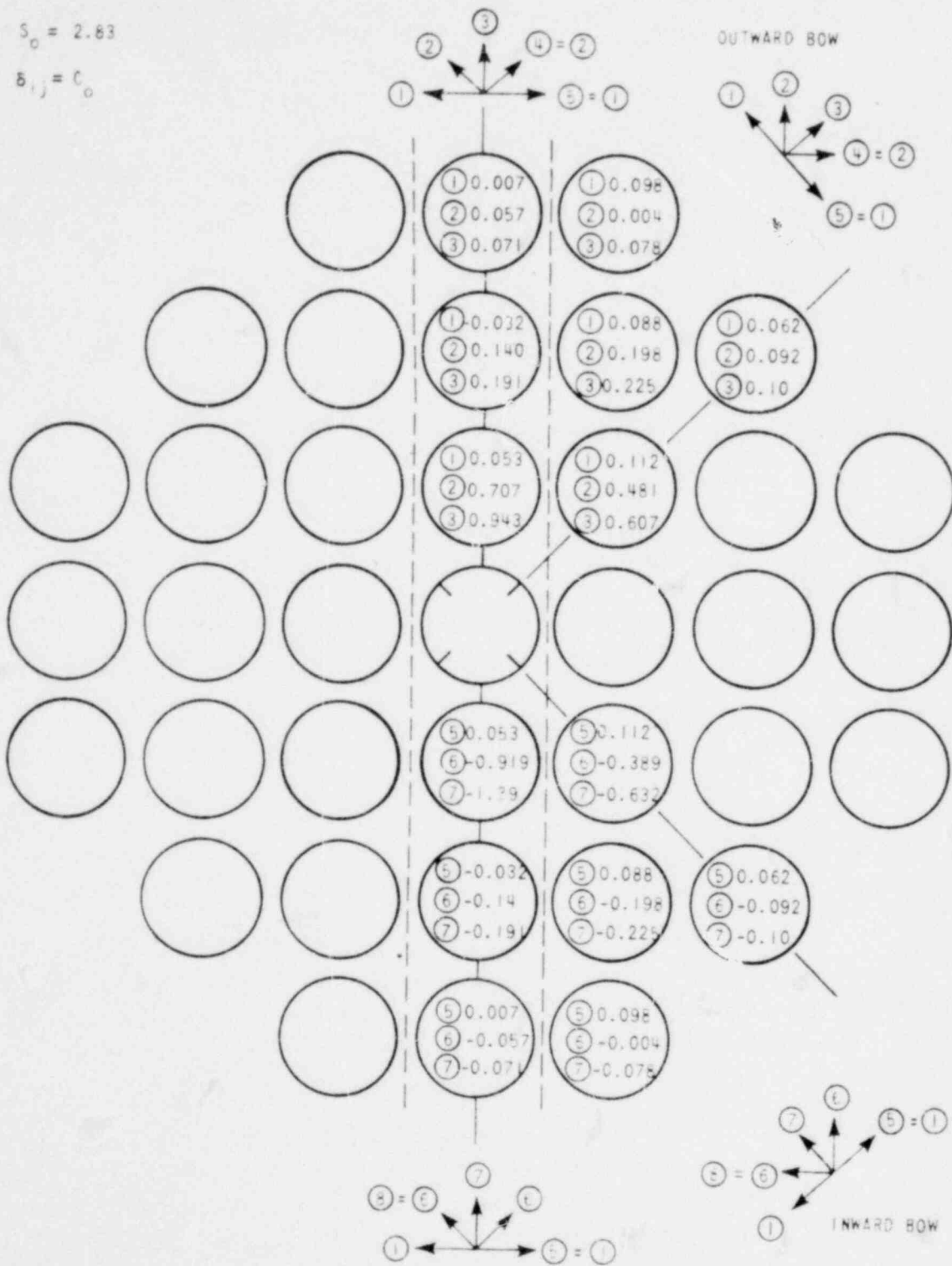
F-7

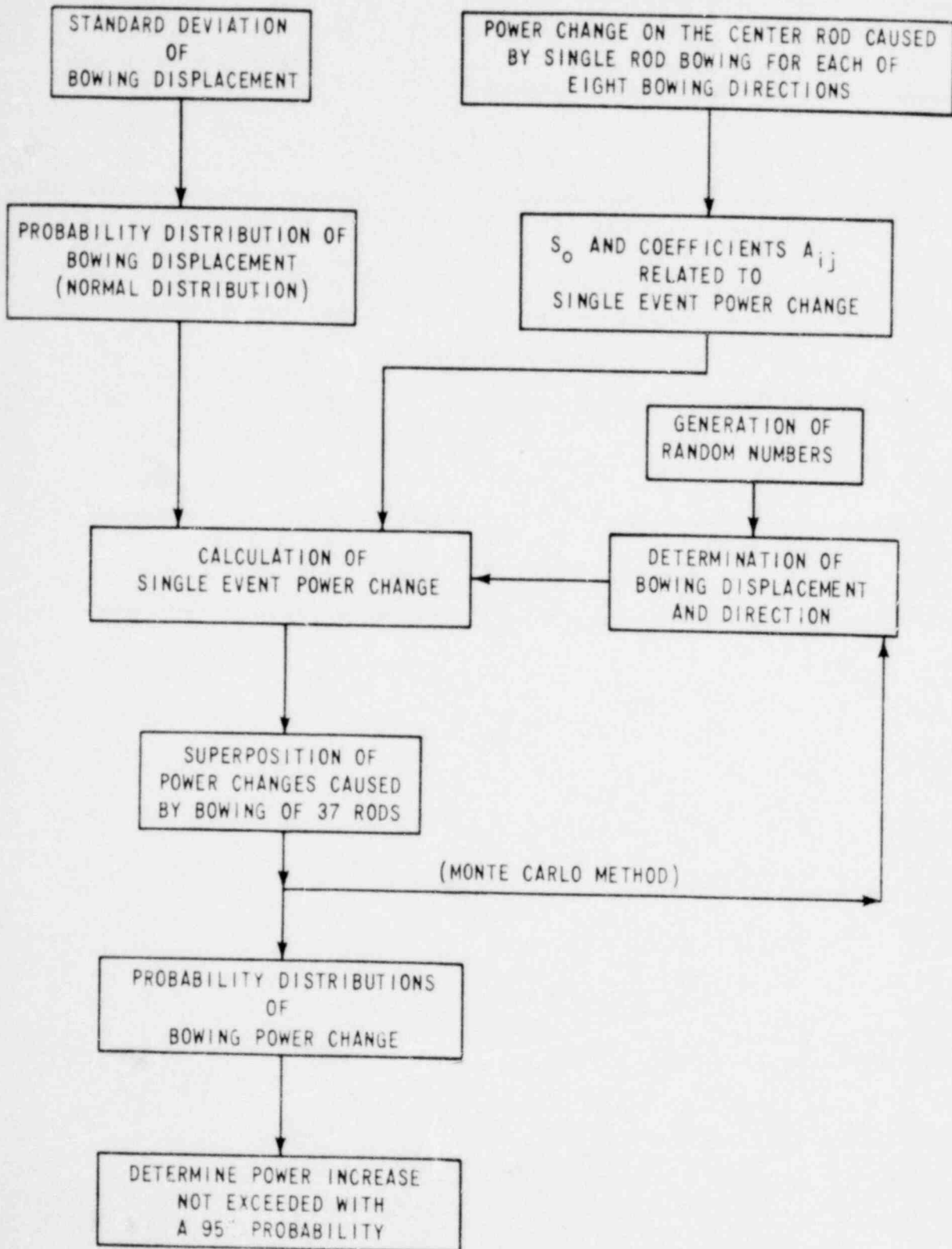Figure F-5 Array Geometry and Bow Attenuation Factors

1035 160

Figure F-6 Flow Chart for Evaluating Bowing Power Change

1035 16█

change $S_0$, and the array of attenuation factors $A_{ij}$. Random numbers are used to determine one of the eight bowing directions and a displacement for one rod in the array. The power change on the center rod due to the bow of this rod is computed. The same procedure is applied to all rods in the array, giving 37 individual power changes on the center rod. The total power change on the center rod is determined by superposition of the 37 individual power changes. This represents a power change on the center rod for one set of randomly chosen conditions. The procedure is repeated until power changes on the center rod have been computed for 50,000 sets of randomly chosen conditions.

The results of the calculations are the probability distributions of bowing power change for the given values of $\sigma_\delta$. Results of typical calculations are shown in figure F-7 where the probability distributions for bowing power change are shown for several values of $\sigma_\delta/C_0$, which is the normalized standard deviation of rod displacement. The bowing power increase not exceeded with a 95 percent probability, $F_Q^B$, can be determined as a function of $\sigma_\delta/C_0$ from this family of probability distributions for bowing power change. The value of $F_Q^B$ is plotted versus $\sigma_\delta/C_0$ in figure F-8.

F.3   Verification of Monte Carlo Method — The Monte Carlo method of solution was verified by comparison with an exact solution. The 37 rod array was analyzed for the case where there were two bowing directions. The attenuation factors were the same for each direction of bow and the center rod in the array did not bow. The attenuation factors, $A_i$, used for the example are shown in figure F-9.

The power change on the center rod due to the bow of any rod i is given by:

$$S_i = S_0 \, A_i \, \frac{\delta_i}{C_0} \qquad\qquad -\infty \leqslant \delta_i \leqslant +\infty \qquad\qquad (F-7)$$

The mean value of the change is zero and the variance of $S_i$ is given by :

$$\sigma_{S_i}^2 = S_0^2 \, A_i^2 \, \frac{\sigma_\delta^2}{C_0^2} \qquad\qquad (F-8)$$

The variance of the power change due to the bow of N rods surrounding the center rod is:

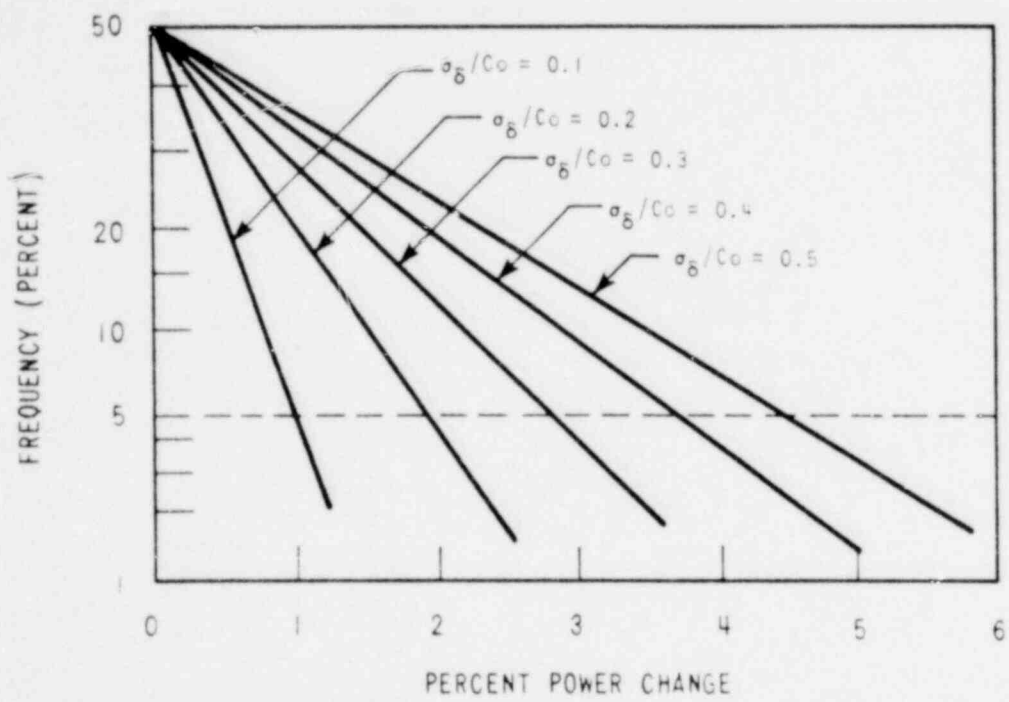$$\sigma_S^2 = \sum_{i=1}^{N} S_0^2 \, A_i^2 \, \frac{\sigma_\delta^2}{C_0^2} \qquad\qquad (F-9)$$

F-10

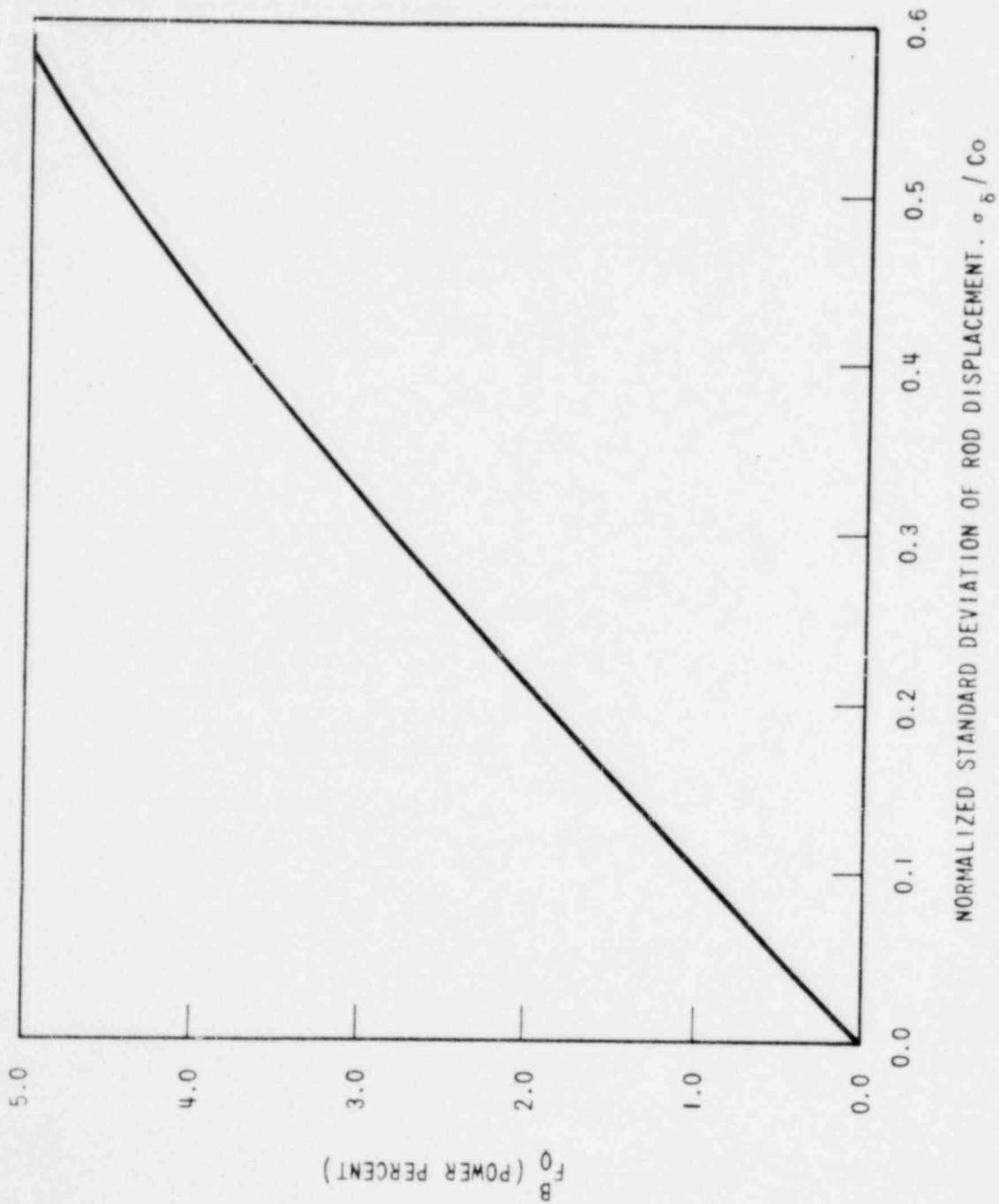Figure F-7  Probability Distribution of Bowing Power Increase as a Function of $\sigma_\delta/C_o$

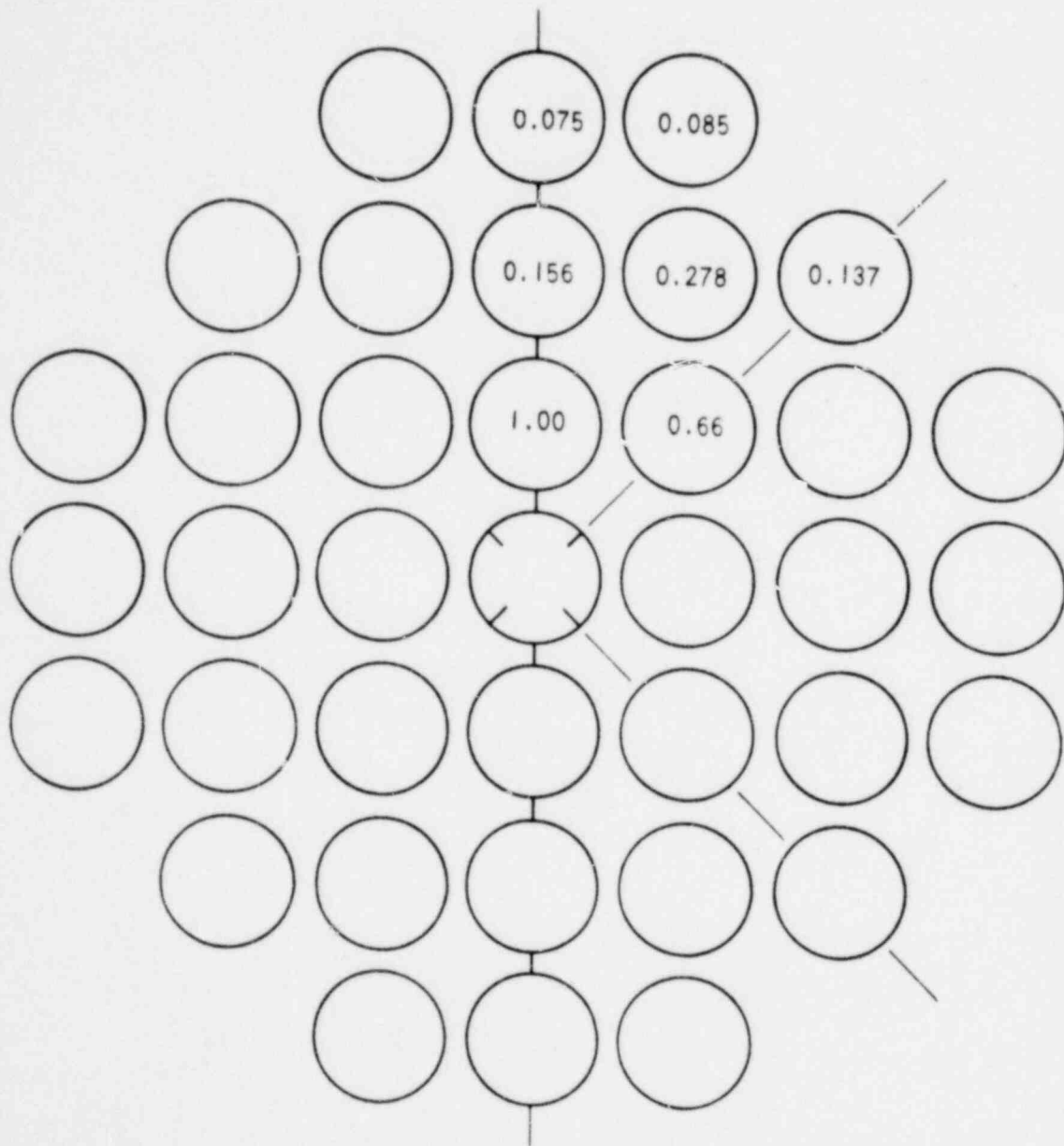Figure F-8   $F_Q^B$ as a Function of $\sigma_\delta/C_o$

1035 165

F-12

Figure F-9 Array Geometry and Bow Attenuation Factors Used
For Monte Carlo Verification

Results were computed for $\sigma_0 = 2.83$ and the attentuation array shown in figure F-9

$$\sigma_S^2 = (2.83)^2 \, (4+4 \,(0.66)^2 + 4(0.156)^2 + 8(0.278)^2 + 4(0.137)^2$$

$$+ \, 4(0.075)^2 + 8(0.085)^2) \, (\frac{\sigma_\delta}{C_o})^2 \qquad\qquad (F\text{-}10)$$

from which:

$$\sigma_S = 7.27 \frac{\sigma_\delta}{C_o} \qquad\qquad (F\text{-}11)$$

The power spike not exceeded with a 95 percent probability is:

$$S_{95} = 1.645 \, \sigma_S = 11.972 \frac{\sigma_\delta}{C_o} \qquad\qquad (F\text{-}12)$$

The above equation is plotted in figure F-10 along with the results of the Monte Carlo method for the same problem. The Monte Carlo solution is in good agreement with, and slightly more conservative than the exact solution.

## F.4    Effect of Gap Closure Distribution on Bowing Power Spikes

The distribution of bowing displacements in a span was assumed to be normal. The assumption of a normal distribution is conservative for predicting the magnitude of at least 99.5 percent of the bows. It is also conservative for predicting the frequency of bows with magnitudes of $\delta/C_o < 1$.

The contributions of bows within discrete displacement intervals to the total power change were computed assuming a normal distribution. The percent of the contribution to the power change not exceeded with a 95 percent probability, $F_Q^B$, is plotted versus bow magnitude in figure F-11 for several values of $\sigma_\delta/C_o$. It can be seen that the greatest contribution to $F_Q^B$ comes from the large number of bows with small bowing displacements. For example, when $\sigma_\delta/C_o = 0.5$, over 60 percent of the value of $F_Q^B$ is contributed by bows with displacements of $\delta/C_o$ less than 0.5 and 96 percent of $F_Q^B$ results from bows with $\delta/C_o < 1$. The use of a normal distribution for this limiting example overestimates the frequency of the bows which contribute 96 percent of the power increase and may underestimate the frequency of the bows which contribute only 4 percent of the power increase. Therefore, the use of a normal distribution is conservative for performing power change calculations.
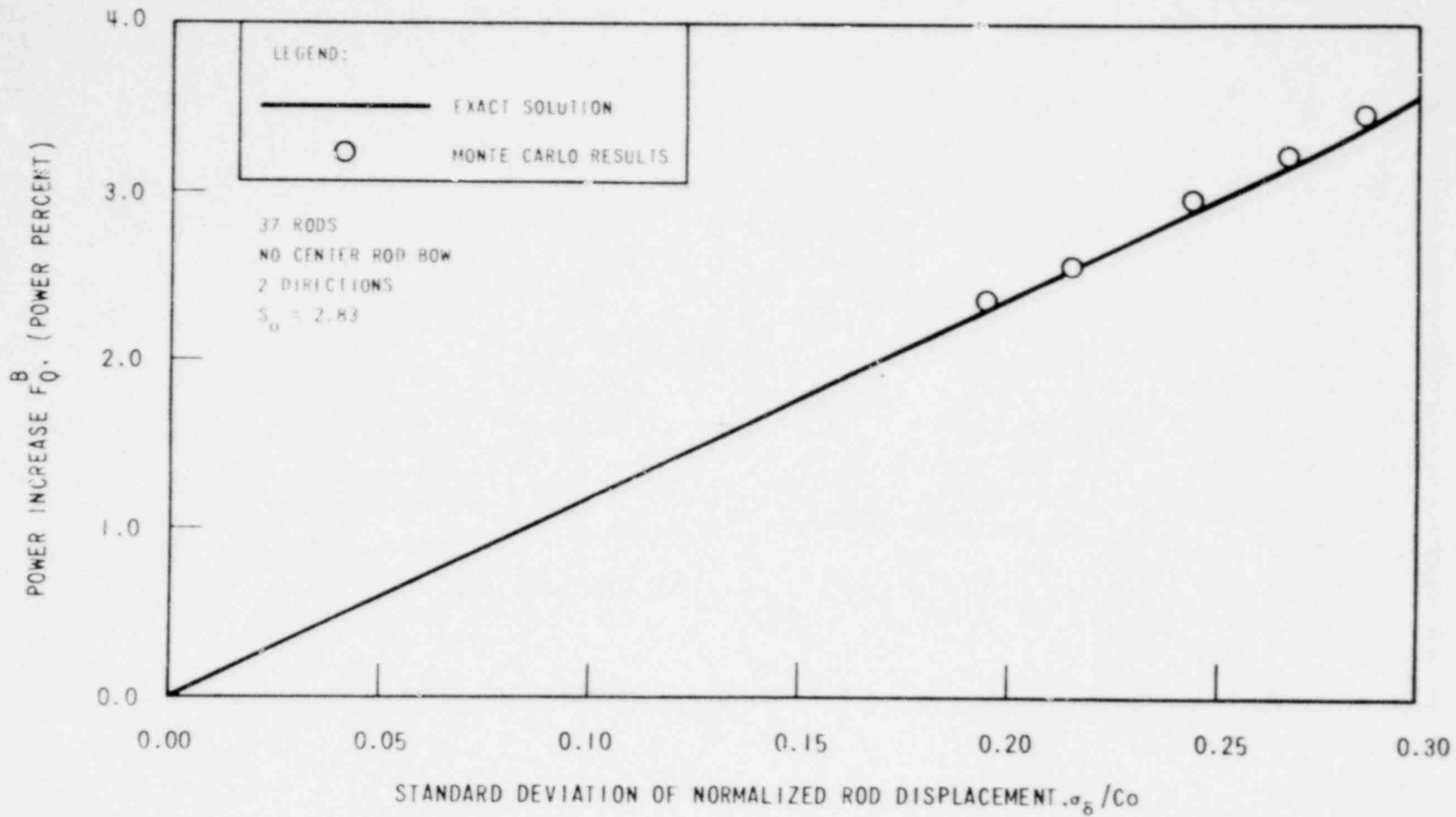
Figure F-10 Comparison of Monte Carlo Evaluation and Exact Solution for Bowing Power Increase

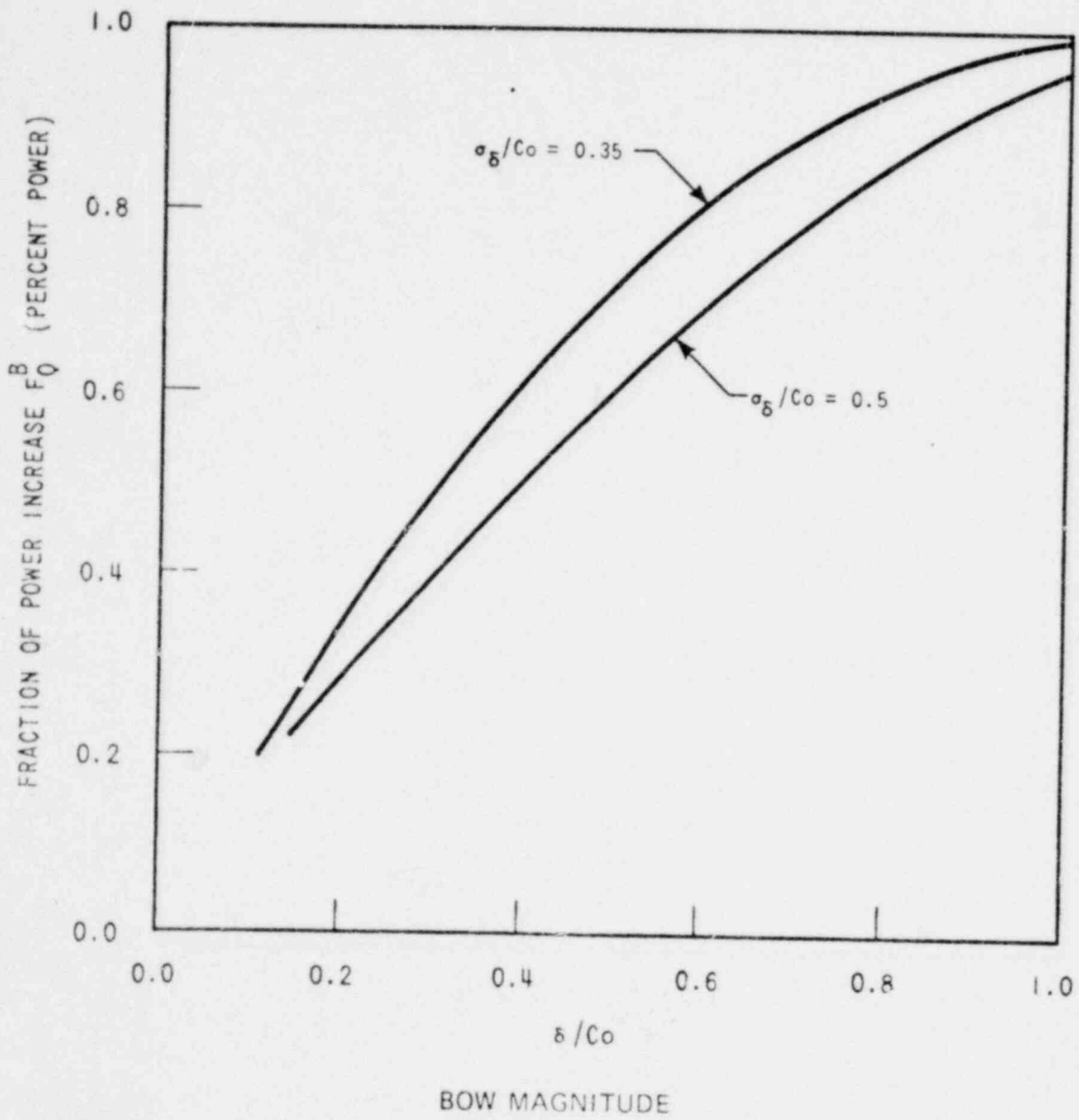Figure F-11 Fraction of Contribution to $F_Q^B$ vs $\delta/C_o$

1035 168

## F.5 Thimble Cell Rods

The bowing power changes for thimble cell rods were also computed. Single event changes are shown in figures F-12 & F-13. The single event power change on a rod near a thimble rod, due to the bow of surrounding rods, is slightly greater than on a rod completely surrounded by fuel rods. However, the power change on a rod near a thimble rod due to its own bow is more negative than for a rod completely surrounded by fuel rods. Also, for a thimble cell rod, there is one less rod near the center rod that can contribute to the total power change. As a result, the net power increases on rods near thimble rods are less than on rods completely surrounded by fuel rods.

## F.6 Peaking Factor Uncertainty Basis

In order to protect the reactor against the consequences of accidents, Westinghouse PWR's operate within a specified upper boundary on the value of local power density or linear heat generation rate (kw/ft). This is expressed in terms of $F_Q$, which is the ratio of the peak local power on the most limiting fuel rod in the core at a fixed time to the average linear power for the core at that time. The "limiting fuel rod" (or rods) is defined as that rod which is calculated to have the highest peak local power without uncertainties. To date, uncertainties have been applied to the "limiting fuel rod" by considering the deviations in fuel density and enrichment combined statistically into an engineering hot channel factor, 1.03, and the uncertainty in the nuclear power distribution calculation, 1.05. These were multiplied to conservatively give the total uncertainty factor, ($F_Q^U$) of $1.05 \times 1.03 = 1.0815$. The two components of this uncertainty factor are individually specified so that both conservatively bound 95 percent of the population, resulting in the total uncertainty factor being stated at a probability level greater than 95 percent.

An appropriate basis for design for $F_Q$ with rod bow is that there must be at least a 95 percent probability that the power peaking factor for the limiting fuel rod is less than or equal to the design power peaking factor, that is, the value assumed for the initial condition for accident analyses.

## F.7 Treatment of Uncertainties

In the evaluation of $F_Q$ the uncertainties in various parameters are considered. All probability distribution parameters used in the $F_Q$ design basis which are based on the evaluation of data are determined at the 95 percent confidence level.

Uncertainties considered in the establishment of the uncertainty factor, $F_Q^U$ include those due to uncertainty in calculation of the power distribution, those due to distributions about the nominal in local fuel density and local fuel enrichment, and local power changes due to geometry changes from the nominal, rod bow.
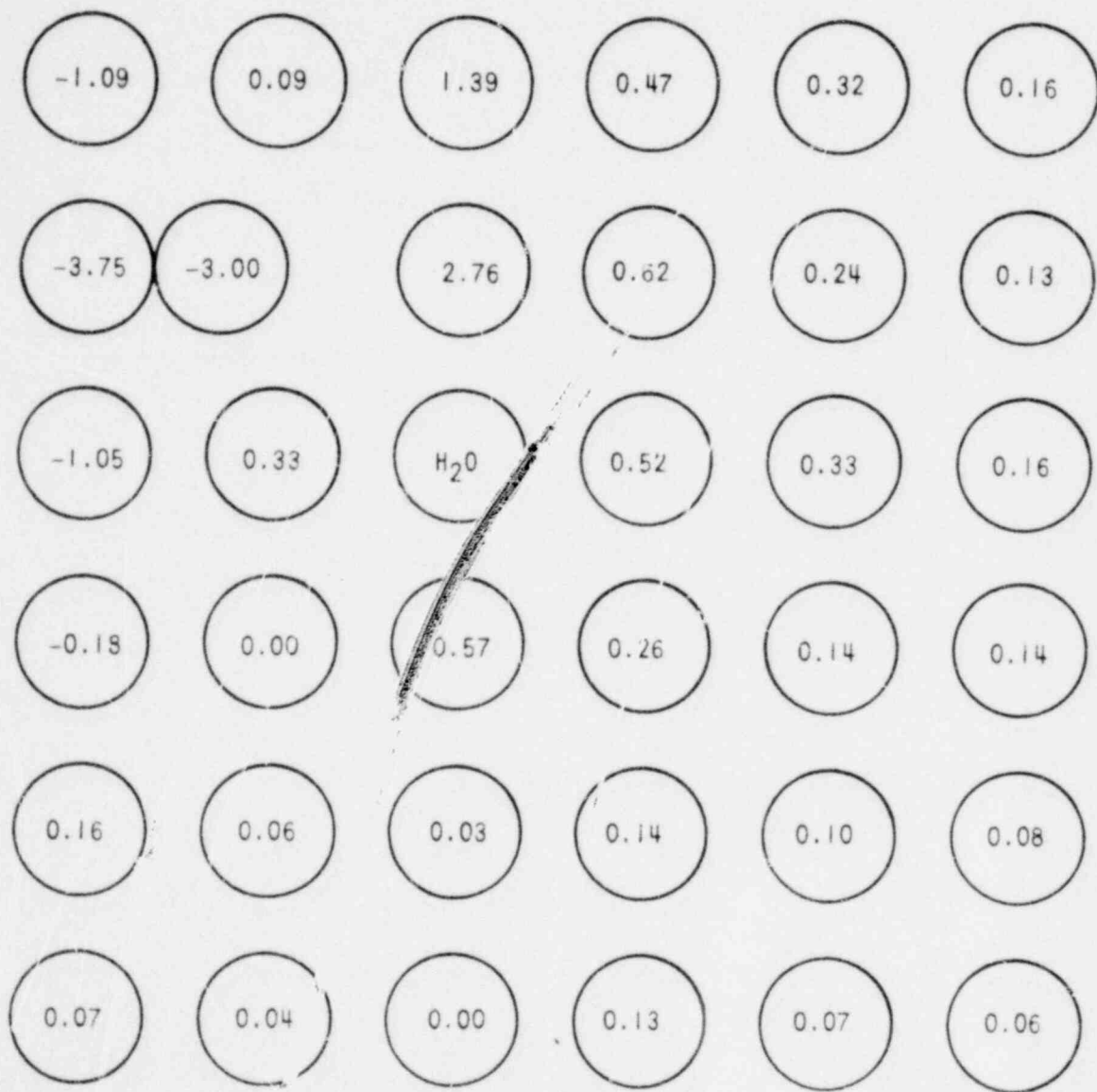
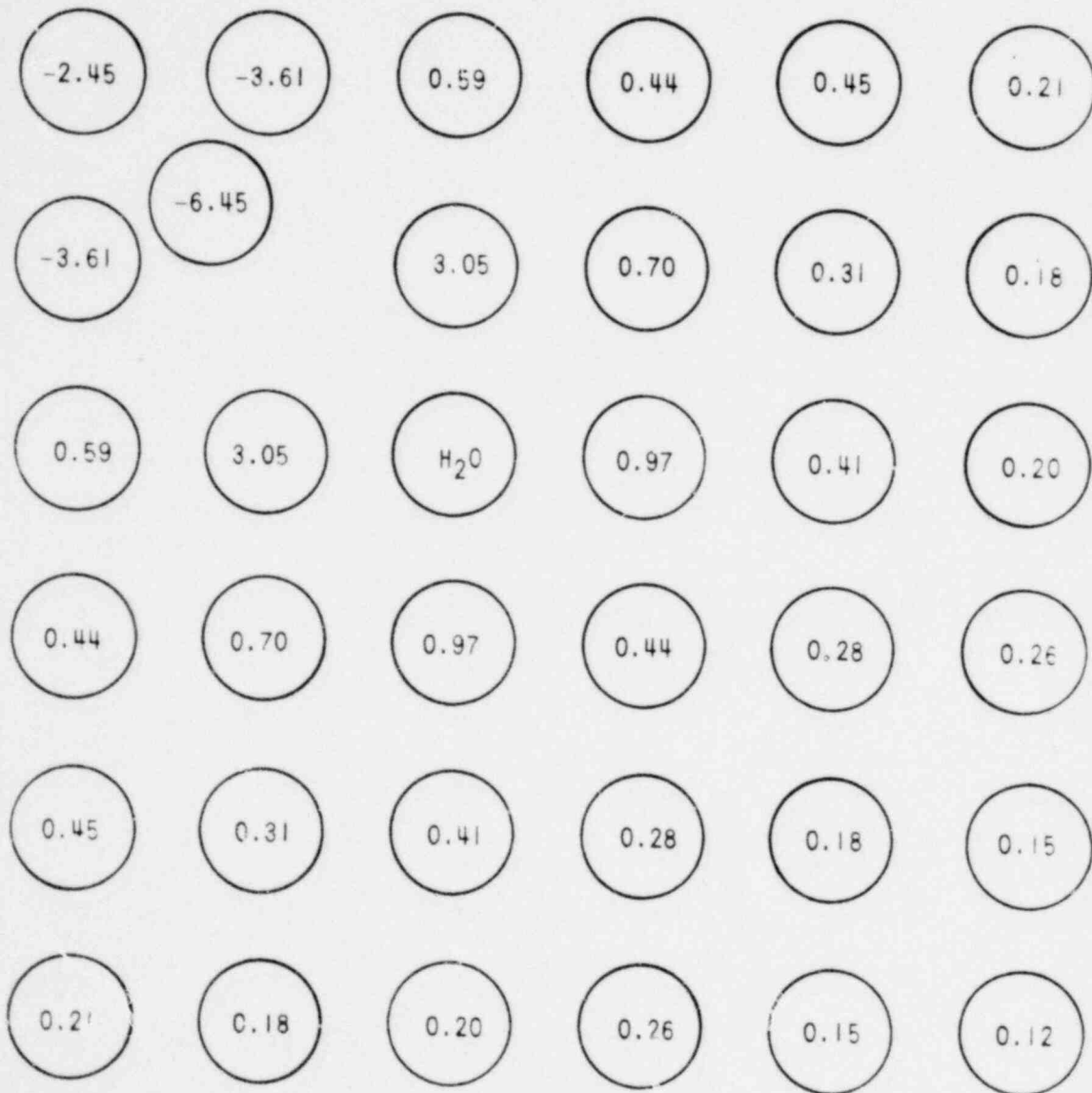Figure F-12  Percent Power Change Near a Thimble Rod

Figure F-13  Percent Power Change Near a Thimble Rod

### F-8    Local Fuel Density Variations

Density variations arise from variations that occur during the manufacturing process. The green pellet press pressure, pellet sintering temperature, pellet sintering time, and powder character-istics, for example, can affect the pellet final density. Variations in fuel density directly lead to variations in quantity of fissile material, and therefore, heat generation rate. The manufac-turing processes are performed on selected quantities or batch sizes of fuel or pellets. Therefore, although a random distribution of fuel density exists within a region, the random variation between adjacent pellets in a given fuel rod is small.

Pellet density variations within approximately a span length are typically on the order of one tenth of the density variation allowed by the specification range for the fuel region. Typical as-built density data on a regionwide basis have been previously provided[1] and show that the great majority of the pellets are near the middle of the specification range.

### F-9    Local Fuel Enrichment Variations

Fuel enrichment variations arise from variations from the nominal enrichment in the bottles of $UF_6$ gas received from the fuel enrichment facility. Additional variation arises during the manufacturing process as gas from different bottles, each containing ~4000 pounds, is intermixed to allow for recycle of scrap, and continuity of operation. Variations in fuel enrichment cause variations in heat generation rate. Although a random distribution of fuel enrichment exists within a region, the random variation between adjacent pellets in a given fuel rod is small. Typical as-built enrichment data on a regionwide basis have been previously provided[1].

Fuel density and enrichment variations are statistically combined into $F_Q^E$, an engineering hot channel factor for kw/ft. The value of $F_Q^E$ used in design is 1.03, and is stated at the design probability level. Typical as-built values of $F_Q^E$ for fuel regions are less than this design value. The infrequently occurring causes of change in pellet density and enrichment, and the contin-uous pellet manufacture and rod loading process allow a single value of $F_Q^E$ to adequately characterize the pellets within a given gridspan. The design value of $F_Q^E$, 1.03, is sufficiently large to conservatively account for pellet-to-pellet and grid span-to-grid span variation in fuel enrichment and density.

---

1    Letter-Eicheldinger to Stello NS-CE-676. June 16. 1975.

## F.10 The Nuclear Power Distribution Uncertainty, $F_N^U$

Since the design peaking factor is a result of calculations for specified core conditions, calculational uncertainties must be considered and allowed for in a total uncertainty allowance. The appropriate values of $F_N^U$ for this purpose are determined by examination of potential errors in the calculation introduced by input data describing the reactor, and by basic neutron cross-section data, by geometry approximations and by deficiencies in the neutron transport model used. These have been quantified by comparison with accurate experimental results obtained from critical experiments, isotopic post-irradiation analysis, and power reactor reactivity and flux distribution measurements. An examination of these uncertainties has been made[2,3] Power distribution experiments are described in which differences between measured and predicted values of $F_Q$ were quantified. Based upon these comparisons, it has been concluded that fewer than 5 percent of actual peaking factors will exceed the calculated values by more than 4.58 percent. This number was rounded up to 5 percent for conservatism. Later experiments of a similar nature have been analyzed and these confirm the adequacy of the 5 percent calculational uncertainty allowance[4].

The calculational model uses nominal dimensions of fuel rods, and average density and enrichments of the fuel regions. Therefore, no account has been taken in the usual calculations of fuel rod power distributions for the effects considered in $F_Q^E$ or rod bow.

Conservatism accrues from the design use of the power distribution calculated during an extreme load follow transient. A more realistic treatment would consider operating time weighted peaking factors, which for Westinghouse PWR's are much lower than those currently used for design, such as 1.9 versus 2.15. Correspondingly, a larger deviation would then be applied.

## F.11 INDEPENDENCE OF $F_Q^E$, $F_N^U$, AND ROD BOW

The correct manner of calculating the effect of variations in fuel enrichment fuel density, rod bow effects, and nuclear calculational uncertainties can be determined by an examination of the uncertainties' independence.

2. Langford, F. L. Jr., and Nath, R. J., "Evaluation of Nuclear Hot Channel Factor Uncertainties", WCAP-7308-L, April 1969, (Westinghouse Proprietary).

3. Nodvik, R. J., "Evaluation of Mass Spectrometric and Radiochemical Analysis of YanKee Core I Spent Fuel", WCAP-6068, March 1966, (Westinghouse Proprietary).

4. McFarlane, A. F., and Langford, F. L., Jr., "Power Peaking Factors Supplement 1, "WCAP-7912-S1-P-A, January 1975, (Westinghouse Proprietary).

In the preceeding discussion, the mechanism by which each of these deviations influence the local power level have been described. At this point, it can be noted that enrichment variations arise because of different causes than density variations, such as changing the green pellet press pressure which changes the fuel density but not its enrichment. Likewise, these deviations from nominal have a local effect confined to the space of a small number of pellets and do not affect the base calculation of $F_Q$ or local power density when expressed as the nominal value of local power divided by the core average power. None of the effects allowed for in $F_Q^E$ or rod bow has any bearing on the routinely performed calculation of $F_Q$ with nominal or average dimensions. Therefore, $F_N^U$ is independent of $F_Q^E$ and rod bow.

Rod bow has been observed to be independent of density and enrichment. The frequency and magnitude of rod bow has not been correlatable from region to region with the differences in density and/or enrichment from region to region. A comparison of $F_Q^E$ determined from as-built manufacturing data with observed rod bow likewise shows no correlation. Independence is also inferred from the observation that $F_Q^E$ is random in the radial and axial directions, whereas bow occurs preferentially in the bottom spans of the core.

## F.12    Evaluation of $F_Q^U$

The independence of the various individual uncertainties constituting the uncertainty factor on $F_Q$ enables $F_Q^U$ to be calculated by statistically combining the individual uncertainties on the limiting rod. The standard deviation of the resultant distribution of $F_Q^U$ is determined by taking the square root of the sum of the variances of each of the contributing distributions. By the central limit therorem, normality of the individual distributions is not a prerequisite for normality of the resultant distribution; however, the input uncertainties are close to normal.

The values for $F_Q^E$ and $F_N^U$ to be used in this evaluation are straight-forward; the 1.645 $\sigma$ (95 percent probability) values are 0.03 and 0.05, respectively.

Using the stated design values, $F_Q^U$ is evaluated as:

$$F_Q^U = 1 + \left[ (0.03)^2 + (0.05)^2 + (F_Q^B - 1)^2 \right]^{\frac{1}{2}}$$

Using the current maximum $F_Q^U$ design value of 1.0815, a maximum $F_Q^B$ of 0.057 is permitted without applying an additional rod bow penalty.

1035 174

# APPENDIX G
# LOCAL POWER VARIATIONS
# DUE TO SINGLE ROD BOW

The power perturbations caused by rod bow are due primarily to the local changes in neutron moderation. The rod away from a single bowed rod essentially has a larger effective lattice pitch and more surrounding moderating coolant, therefore, an increase in moderation, a higher thermal to fast flux ratio, and a higher power than at the normal slightly undermoderated pitch. For the rod near the bowed rod and the bowed rod itself, the converse occurs. Increased fuel and decreased moderator thermal absorption promote the power increase for a given bow displacement. Therefore high enrichment and high burnup fuel surrounded by soluble boron free coolant will give the largest power changes (both positive and negative). An average enrichment of 3.2 w/o at the average burnup of 16,000 MWD/MTU with the average boron concentration of about 450 to 500 ppm provides an appropriate power spike to apply to the peak rod at any time in any cycle with the present fuel management schemes where the peak power usually occurs in a once burned fuel assembly (~11,000 MWD/MTU) near BOL (~1000 ppm boron). No fuel rod with burnup greater than 22,000 MWD/MTU has been found to lead the core, especially at low boron concentration. Fuel with 22,000 MWD/MTU burnup and moderator with 0 ppm boron was conservatively used in this study. Although this analysis uses 3.04 w/o U-235 fuel, the high burnup and low boron more than compensates for the small difference between 3.04 w/o and 3.20 w/o U-235 fuel. Since both power penalties and benefits are obtained due to fuel rod bow and either is equally probable, the expected power spike penalty on any rod is zero. There is only a change in the expected deviation of each rod's power.

## G.1 METHOD

Two dimensional transport theory calculations of a 9 by 9 array of fuel rods with reflecting boundary conditions were used to determine the local power peaking due to a single bowed fuel rod in typical Westinghouse 15x15+ and 17 x 17 fuel assemblies. Two energy groups, $S_4$ symbolic angular quadrature, and isotropic scattering ($P_0$) were used in this study. Each fuel rod (homogenized fuel and clad) was treated in xy geometry as a discrete square explicitly surrounded by the moderating coolant. Cross sections were generated using a modified version

+Also 14x14 fuel assemblies

of the LEOPARD code.[1] Calculations were made for bows in the lateral directions with bowing displacements of $C_0/2$ and $C_0$, where $C_0$ is the nominal distance between adjacent rods (see figure 5-12). Power change calculations for bows in the diagonal direction were computed for a bowing displacement of $C_0\sqrt{2}$ for the 15x15 assembly and for displacements of $C_0\sqrt{2}/2$ and $C_0\sqrt{2}$ for the 17 x 17 assembly. The perturbation in local power due to a bowed rod was determined as the ratio of the perturbed (center rod bowed) to unperturbed (no bowed rods) power for each fuel rod.

### Results

In all cases the maximum local power increase occurred in a fuel rod directly adjacent to the bowed rod on the side away from the bow. The diagonally bowed rods caused larger power increases than the corresponding lateral bow cases. Both the bowed rod's power and the touched rod's power always decreased.

The various case configurations and percent power changes for the worst rod(s), the bowed rod, and the touched rod(s) are summarized in table G-1 for easy comparison.

This table shows that the 15x15 results are more conservative than the 17 x 17 results.

### G.2 SENSITIVITIES

The reference maximum rod bow power spikes given in table G-1 are relatively insensitive to changes in the cross sections due to spectrum effects of the pitch change in the rod directly affected by the maximum rod bow, or to enrichments higher than the reference 3.04 w/o U-235 enrichment.

A change of the enrichment from 3.04 w/o to 3.40 w/o U-235 increases the reference spike (2.83%) to about 2.9 percent.

Accounting for the harder spectrum on the rods closer together and the softer spectrum for the rods with more surrounding moderator as a result of a maximum bowing displacement increases the reference spike to about 3.0 percent.

The use of a more nearly correct linear anisotropic scattering ($P_1$) cross section set rather than the reference $P_0$ set, reduces the reference spike to about 2.0 percent.

Taken as a whole, these sensitivities show that the reference spike of 2.83 percent (So (see section 5)) is conservative by about 0.5 percent power for LOPAR assemblies at 3.4 w/o U-235, 22,000 MWD/MTU burnup and with 0 ppm soluble boron in the coolant.

---

1. Barry, R. F., "LEOPARD — A Spectrum Dependent Non-Spatial Depletion Code for the IBM-7094," WCAP-3269-26, September 1963.

   Barry, R. F., "The Revised LEOPARD Code — A Spectrum Dependent Non-Spatial Depletion Program," WCAP-2759, March 1965. (Westinghouse Proprietary).

1035 176

## TABLE G-1
### CONFIGURATIONS AND POWER CHANGES

| Case | Adjacent Water Hole Position | Bowed Rod | | Percent Power Change | | |
| --- | --- | --- | --- | --- | --- | --- |
| | | Displacement | Direction | Peak Rod(s) | Bowed Rod | Touched Rod(s) |
| 15x15 Assemblies | | | | | | |
| 1 | None | $C_0 \sqrt{2}$ | Diagonal | 2.83 | -4.67 | -3.68 |
| 2 | None | $C_0$ | Lateral | 2.67 | -1.90 | -3.93 |
| 3 | None | $C_0/2$ | Lateral | 1.34 | -0.24 | -1.97 |
| 4 | Diagonal | $C_0$ | Lateral | 2.76 | -3.00 | -3.75 |
| 5 | Diagonal | $C_0 \sqrt{2}$ | Diagonal | 3.05 | -6.45 | -3.61 |
| 17 x 17 Assemblies | | | | | | |
| 6 | None | $C_0/2$ | Lateral | 1.27 | -0.21 | -1.57 |
| 7 | None | $C_0$ | Lateral | 2.42 | -1.66 | -3.66 |
| 8 | None | $C_0 \sqrt{2}/2$ | Diagonal | 1.29 | -0.77 | -1.55 |
| 9 | None | $C_0 \sqrt{2}$ | Diagonal | 2.49 | -4.61 | -3.51 |

1035 177

EFFECT ON CHF OF A PARTIALLY BOWED
HEATED ROD IN A COLD WALL THIMBLE
CELL GEOMETRY

Correspondence with NRC:

1. NRC Acceptance Letter on Partial Rod Bow, April 5, 1979

2. Westinghouse Letter NS-TMA-2053, March 16, 1979

3. Westinghouse Letter NS-CE-1580, October 24, 1977

UNITED STATES
NUCLEAR REGULATORY COMMISSION
WASHINGTON, D. C. 20555

APR 5 1979

Mr. Thomas M. Anderson, Manager
Nuclear Safety Department
Westinghouse Electric Corporation
P. O. Box 355
Pittsburgh, Pennsylvania 15230

Dear Mr. Anderson:

SUBJECT: STAFF REVIEW OF WCAP-8691

Our review of certain aspects of WCAP-8691 (Proprietary) "Fuel Rod
Bowing" has been completed. Your letter NS-TMA-1924 dated September 1,
1978, advised us of your plan to submit a revised topical report on fuel
rod bowing to include new information requested in our June 19, 1978
letter. Subsequently you have submitted supplemental information
regarding the effect on critical heat flux of a partially bowed heated
rod in a cold wall thimble cell geometry.

We have reviewed the supplemental information regarding the effect on
critical heat flux of a partially bowed rod. We have concluded that
the supplemental information provides an acceptable basis for calculating
critical heat flux on bowed rods. Our evaluation is enclosed.

Please incorporate the supplemental information into the revision to
WCAP-8691.

Sincerely,

for John F. Stolz, Chief
Light Water Reactors Branch No. 1
Division of Project Management

Enclosure:
Evaluation of Westinghouse
Report

cc: Mr. D. Rawlins
Westinghouse Electric Corporation
P. O. Box 355
Pittsburgh, Pennsylvania 15230

1035 174

Evaluation of Westinghouse Report
on "Effect on CHF of A Partially
Bowed Heated Rod In A Cold Wall Thimble
Cell Geometry"

## Summary of Report

This report describes tests to determine the effects of a bowed rod on critical heat flux (CHF). The tests were done with a heated rod bowed to 85 percent of the maximum possible closure and the bowed rod was adjacent to a thimble tube. Figure 1 shows the position of the bowed rod relative to tne other rods in the bundle and Figure 2 shows the method of maintaining the bowed geometry throughout the test.

The test bundle consisted of 15 electrically heated rods and 1 unheated rod which simulated a control rod guide thimble. The bundle had a non-uniform radial power distribution with the 12 outer rods having less power than the 3 inner rods. The thimble was attached to the grid in the same manner as in a reactor core. The bowed heater rod had its point of maximum bow at the midpoint between the two topmost mixing vane grids, 136 inches above the beginning of the test section heated length. The axial heat flux distribution was, as shown in Figure 3, non-uniform with an approximate u sin u distribution.

The test method consisted of obtaining CHF data on the bowed geometry for inlet conditions which match inlet conditions for the tests in reference 1 (The tests of reference 1 had no intentional bow). The measured-to-predicted critical heat flux ratio ($^M/P$) was obtained for each test and a new parameter, $\delta_{pB}$, was defined such that

$$\delta_{PB} = \frac{\left(^M/P\right)_{no\ bow} - \left(^M/P\right)_{BOW}}{\left(^M/P\right)_{no\ bow}}$$

The parameter $\delta_{P8}$ is a measure of the effect of a partially bowed rod on CHF. $\delta_{P8}$ was found to scatter about zero for tests at 1500 and 1800 PSIA but was greater than zero for tests at 2100 and 2400 PSIA. The partial bow parameter was also found to be a function of the mass flux.

The value of the bow effect at a closure of 1.0 is the contact penalty as previously defined[4] at limiting conditions of heat flux and pressure. The bow penalty obtained from the 85% closure data yield values of 11.4% for all loops in service and 14% for the loss of flow accident and for one-loop-out-of-service analyses. Based on data reported by other investigators[3] a bow penalty of zero percent will be used for bow magnitude less than or equal to 50%. Linear interpolation will be used to calculate the bow penalty between 50% and 85% and between 85% and 100% gap closure. The resultant bow penalty as a function of gap closure is shown in Figure 4.

## Summary of Staff Evaluation

To obtain reliable CHF data on a partially bowed geometry is an extremely difficult task because of the possible influence of the restraints required to maintain the desired bowed geometry. For this reason, the supports and restraints used by Westinghouse to obtain 85% closure with a bowed rod were analyzed for possible influence on the CHF data.

The thermocouple us ! to detect CHF at the bow location was at the elevation of maximum bow. The special support grid used to maintain the desired bow was 1/2 inch downstream of the elevation of maximum bow. Simple finning analyses show that the possible finning effects of the support pins in the

grid did not extend more than approximately 1/4 inch from the pins. Therefore, there should be no increase in observed CHF due to the influence of the special support grids. There may be some hydrodynamic effects which extended as much as 1/2 inch below the grid but these effects would have resulted in a reduced value of the indicated CHF. Therefore, the Westinghouse method of maintaining the bowed geometry for the tests is acceptable.

The parameter which characterizes the effect of a partially bowed rod on CHF, $\delta_{PB}$, was found to be a function of pressure and mass flux. An attempt to correlate $\delta_{PB}$ in terms of the bow penalty for rods bowed to contact resulted in the relation

$$\delta_{PB} = F_{PB} \; (S_{BOW}) \; CORR$$

where $(\delta_{BOW})_{CORR}$ is the bow contact penalty obtained in reference 2. The $F_{PB}$ obtained from this correlation had a correlation coefficient of -0.5. Therefore the $F_{PB}$ correlation reported in the bow report is unacceptable.

The correlation of $\delta_{PB}$ with mass flux for the two high pressure data sets gives a much better fit than the $F_{PB}$ correlation. The partial bow correlation corrects all the high pressure data in such a manner that the data is distributed like a repeat set of non-bowed data. This is shown by testing for a significant difference between the corrected data and another, unbowed, data set. The t-statistic for comparing the two means is 0.1435 with 58 degrees of freedom; the probability of a deviation greater than t is between 0.8 and 0.9. Therefore, the partial bow correlation is acceptable.

The use of the data of reference 3 to justify no bow penalty for channel closure less than or equal to 50% is acceptable because the typical cell contact bow

results presented were the same as the results for tests conducted on
similar Westinghouse geometries. Thus, while critical heat flux is sensitive
to differences in test section geometry, the bow effect is not.

Staff Position

The letter report on CHF with partial rod bow provides an acceptable data
base for CHF on rods bowed to 85% of the bow necessary for contact. Further,
the relation for bow penalty as a function of gap closure, given in Figure 4 is
an acceptable bow penalty for use on Westinghouse fuel designs.

# References

1. Motley, F.E. and Codek, F.F., "DNB Test Results for R-Grid Thimble Cold Wall Cells", WCAP-7958-A1-A, January, 1975.

2. Nagino, Y., et.al., "Rod Bowed to Contact Departure from Nucleate Boiling Tests in Coldwall Thimble Cell Geometry", Jour. of Nuclear Science and Technology, 15 [8], pp. 568 - 573, August, 1978.

3. Markowski, E.S., et.al., "Effect of Rod Bowing on CHF in PWR Fuel Assemblies", ASME Paper 77-HT-91.
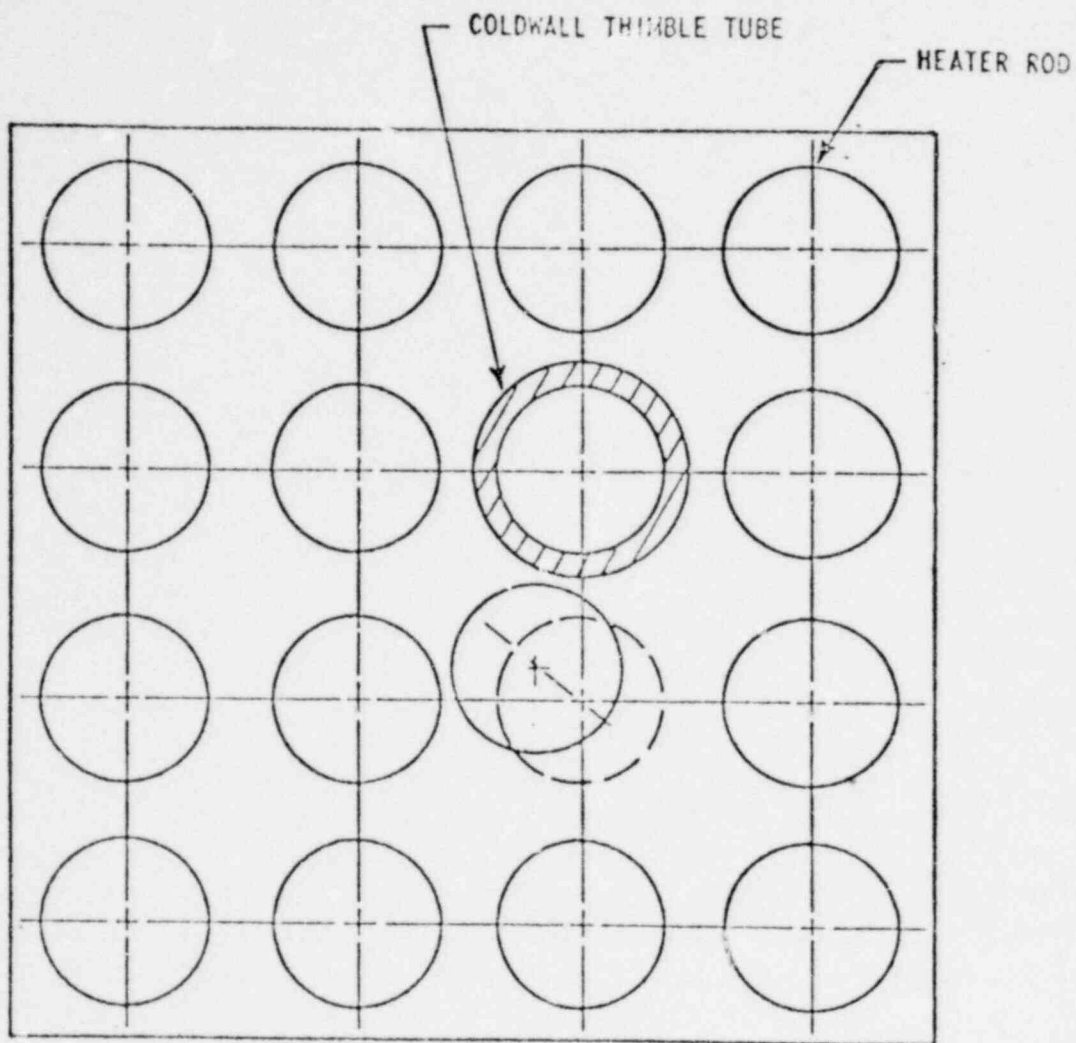
4. Letter, C. Eicheldinger to D.F. Ross, NS-CE-1161, August 13, 1976.

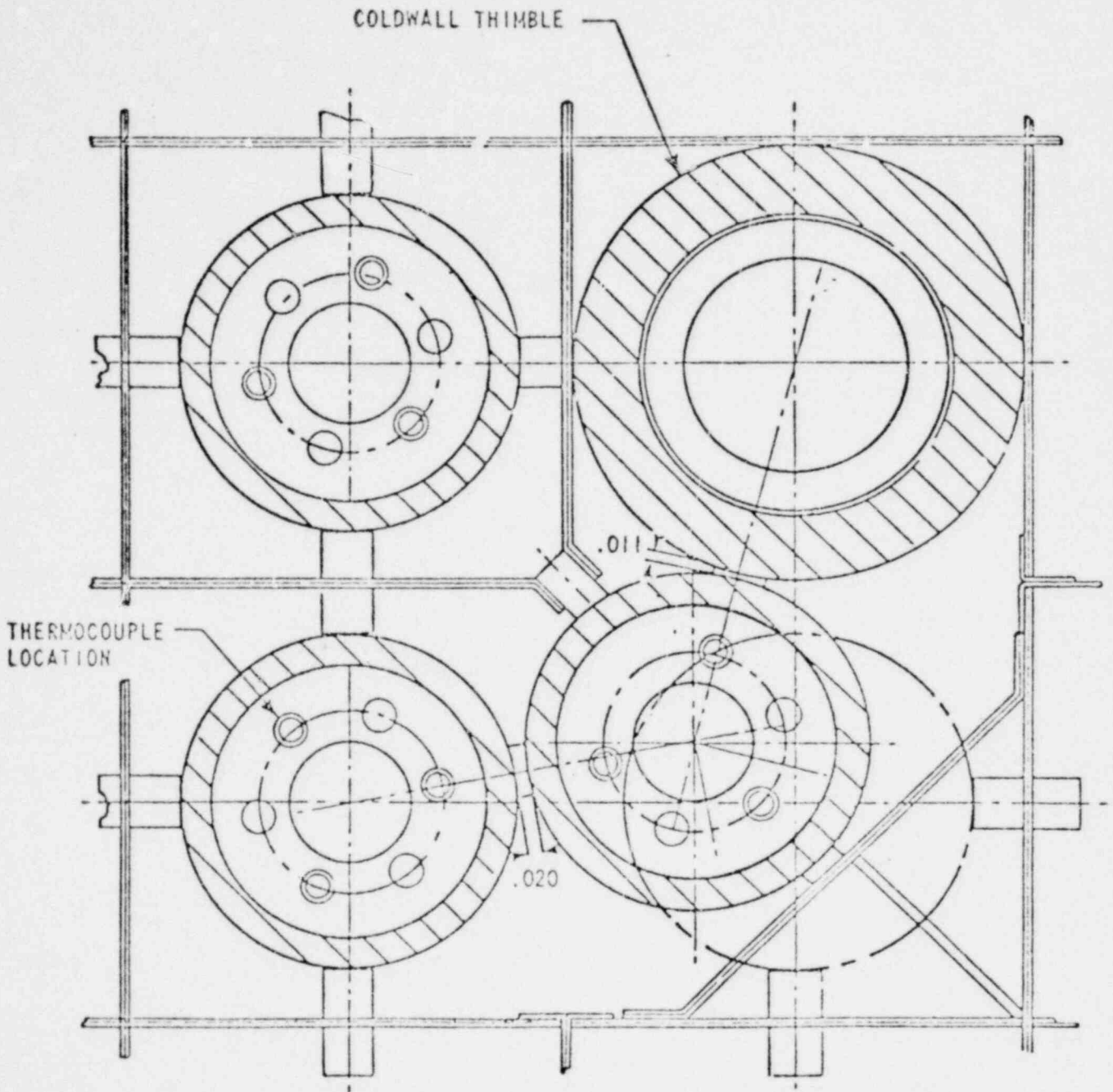Figure 1    Partial Rod Bow Test Section, 85 Percent Closure

COLDWALL THIMBLE

THERMOCOUPLE
LOCATION

.011 r

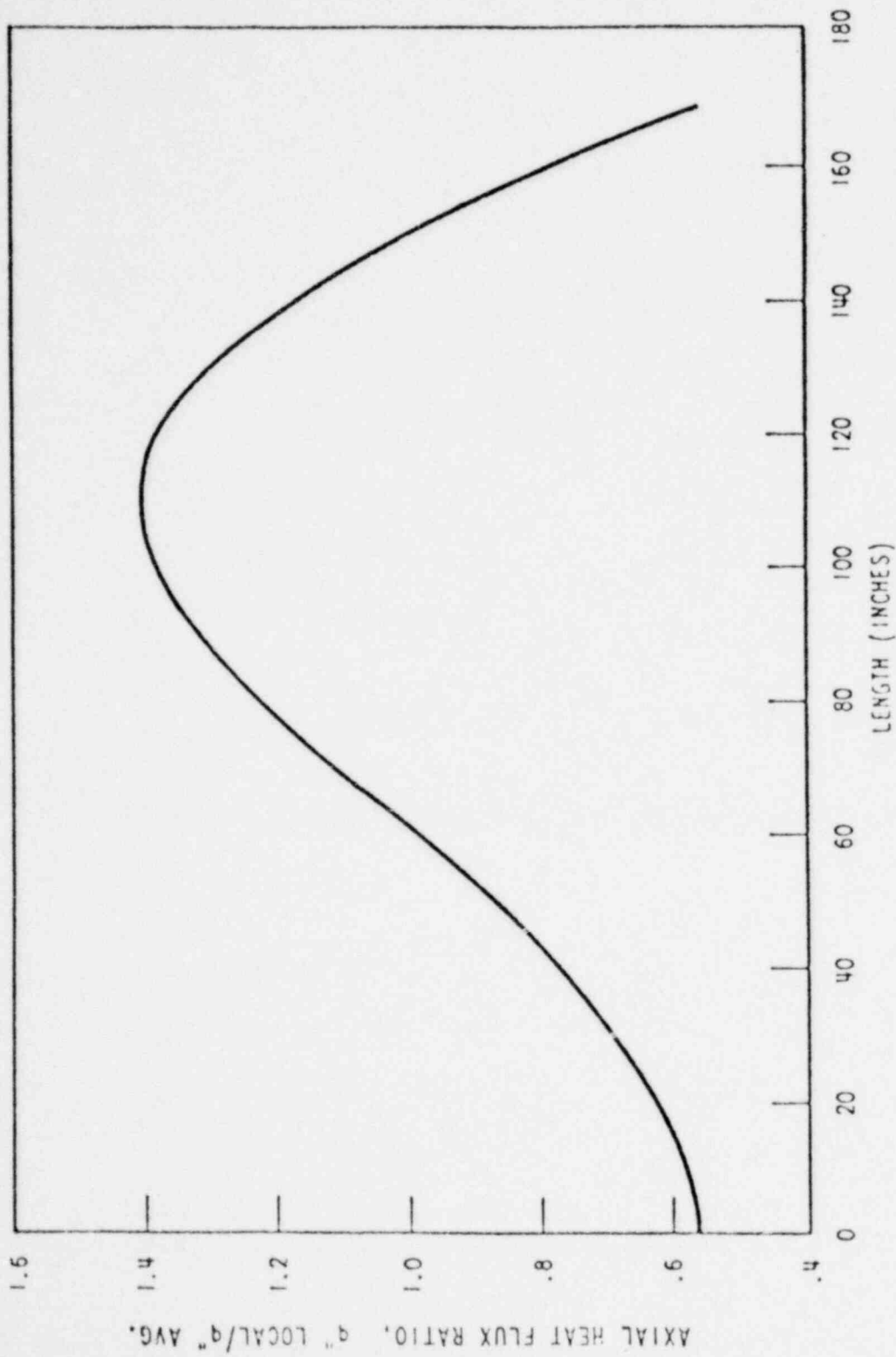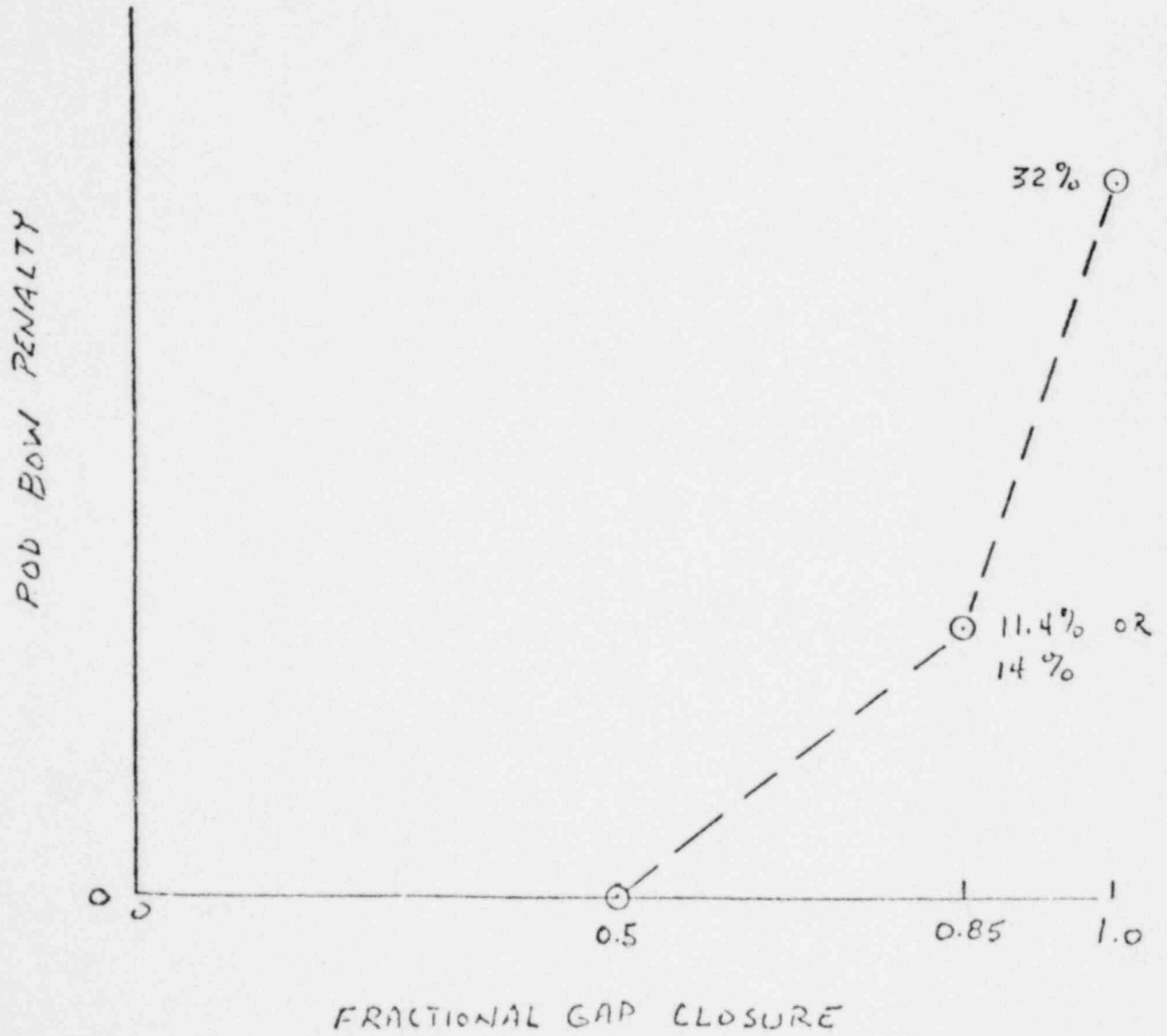.020

Figure 2    Special Support Grid, 85 Percent Closure

2-6

1035 186

Figure 3   Axial Heat Flux Distribution of 14-Foot Heater Rods

2-8

FIGURE 4

ROD BOW DNBR PENALTY VERSUS
FRACTIONAL CLOSURE

FRACTIONAL GAP CLOSURE

PWR Systems Division

Box 355
Pittsburgh Pennsylvania 15230

March 16, 1979

NS-TMA-2053

Mr. John F. Stolz, Chief
Operating Reactors Branch 1
Division of Project Management
Office of Nuclear Reactor Regulation
U. S. Nuclear Regulatory Commission
Washington, D.C.   20555

Dear Mr. Stolz:

Attached please find additional information on the "Effect on CHF of a
Partially Bowed Heated Rod in a Cold Wall Thimble Cell Geometry". A
recorrelation of the partial bow data and the method of application
of bow effect to reactor design are included.

This information has been discussed with Mr. Wayne Hodges.

Therefore, enclosed you will find the following:

1. Twenty-five (25) copies of the proprietary version of the above noted
   information.

2. Forty (40) copies of the non-proprietary version of the above noted
   information.

3. One (1) copy of Application for Withholding, (Non-proprietary).

4. One (1) copy of original Affidavit, (Non-proprietary).

This submittal contains proprietary information of Westinghouse Electric
Corporation. In conformance with the requirements of 10CFR2.790, as amended,
of the Commission's regulations, we are enclosing with the submittal, an
application for withholding from public disclosure and an affidavit. The
affidavit sets forth the basis on which the information may be withheld
from public disclosure by the Commission. Correspondence with respect to
the affidavit or application for withholding should reference AW-79-11
and should be addressed to R. A. Wiesemann, Manager of Regulatory and
Legislative Affairs, Westinghouse Electric Corporation, P. O. Box 355,
Pittsburgh, PA   15230.

Very truly yours,

T. M. Anderson, Manager
Nuclear Safety Department

cc: W. W. Hodges
BGC:pj
Enclosure

1035 189

## 1.0    SUMMARY

In the original submittal of partial rod bow CHF information[1] a method was presented for correlating the results which were dependent on the contact bow correlation. Subsequent evaluations have shown that the 85% closure partial rod bow data can be correlated as a function of [          ]$^{a,c}$ only considering the high pressure data (2100 and 2400 psia). The resulting correlation can be used to calculate the CHF effect for 85% closure. This result can be combined with the results of other available rod bow data to provide the effect of rod bow on CHF as a function of closure.

## 2.0    RE-CORRELATION OF THE 85 PERCENT CLOSURE PARTIAL BOW CHF DATA

The plots of $\delta_{PB}$ previously presented[1] show only a few data points which are outside the repeatability band. These points are at higher (2100 and 2400 psia) pressure and [                                    ]$^{a,c}$. There appears to be a linear function of decreasing bow effect with [                    ]$^{a,c}$. No bow effect is seen at low pressures, thus considering only the high pressure data, a linear function of [          ]$^{a,c}$ was determined.

$$(\delta_{PB})_{corr} = \left[ \hspace{6cm} \right]^{a,c}$$

## 3.0    EVALUATION OF PARTIAL ROD BOW CHF CORRELATION

The partial rod bow correlation should correct all the high pressure data in such a manner that the data will be distributed like a repeat data set. This is shown by plotting the residual -- the difference between the measured partial bow result and the correlation prediction ($\Delta_{PB}$ ' $\delta_{PB}$ - $(\delta_{PB})_{corr}$). Figures 1 and 2 show that the residuals do not exhibit any remaining trend with pressure, flow, quality, or heat flux. This indicates that the partial bow correlation has

---

(1)  NS-CE-1580, C. Eicheldinger to D. F. Ross, October 24, 1977.

# FIGURE 1

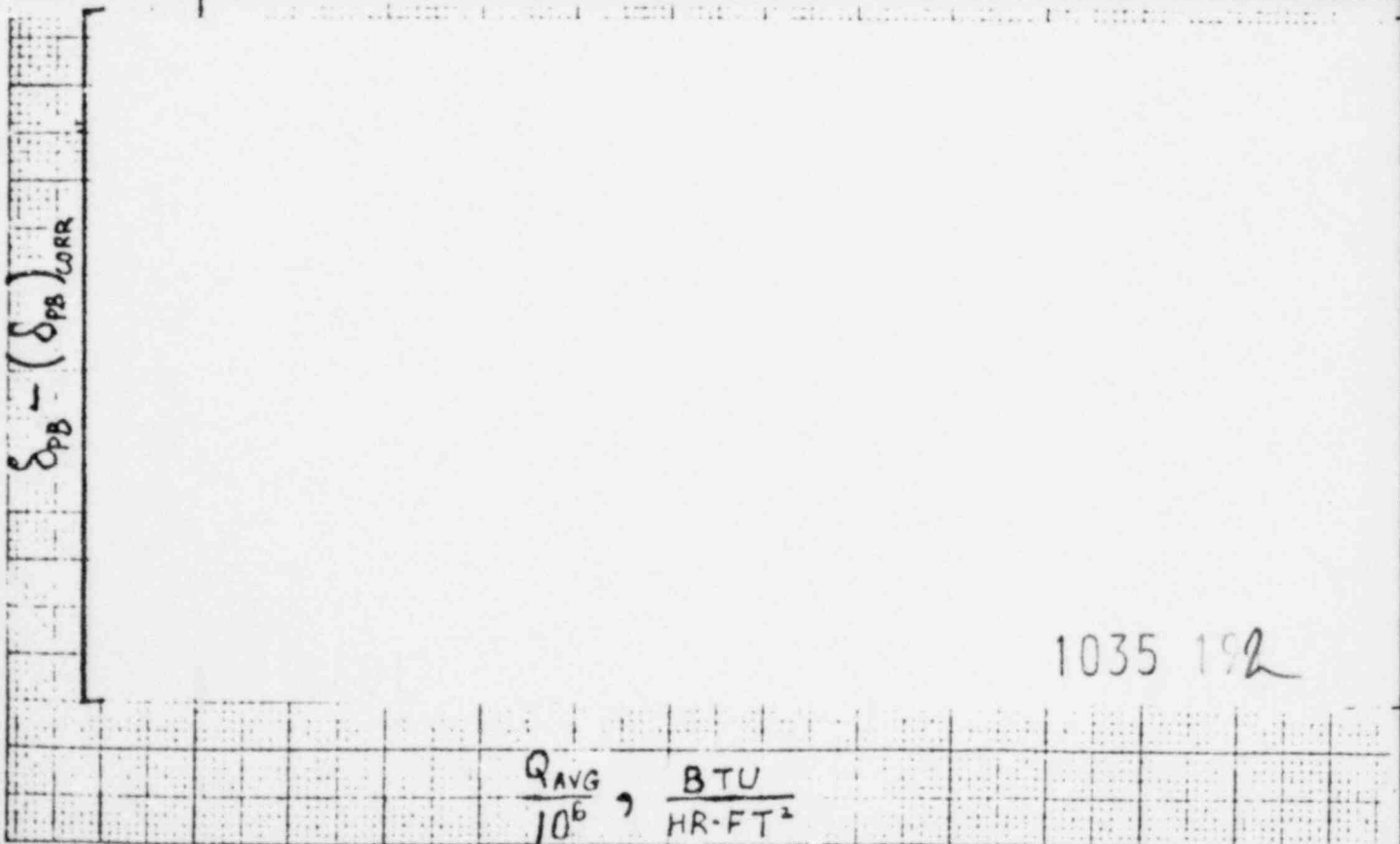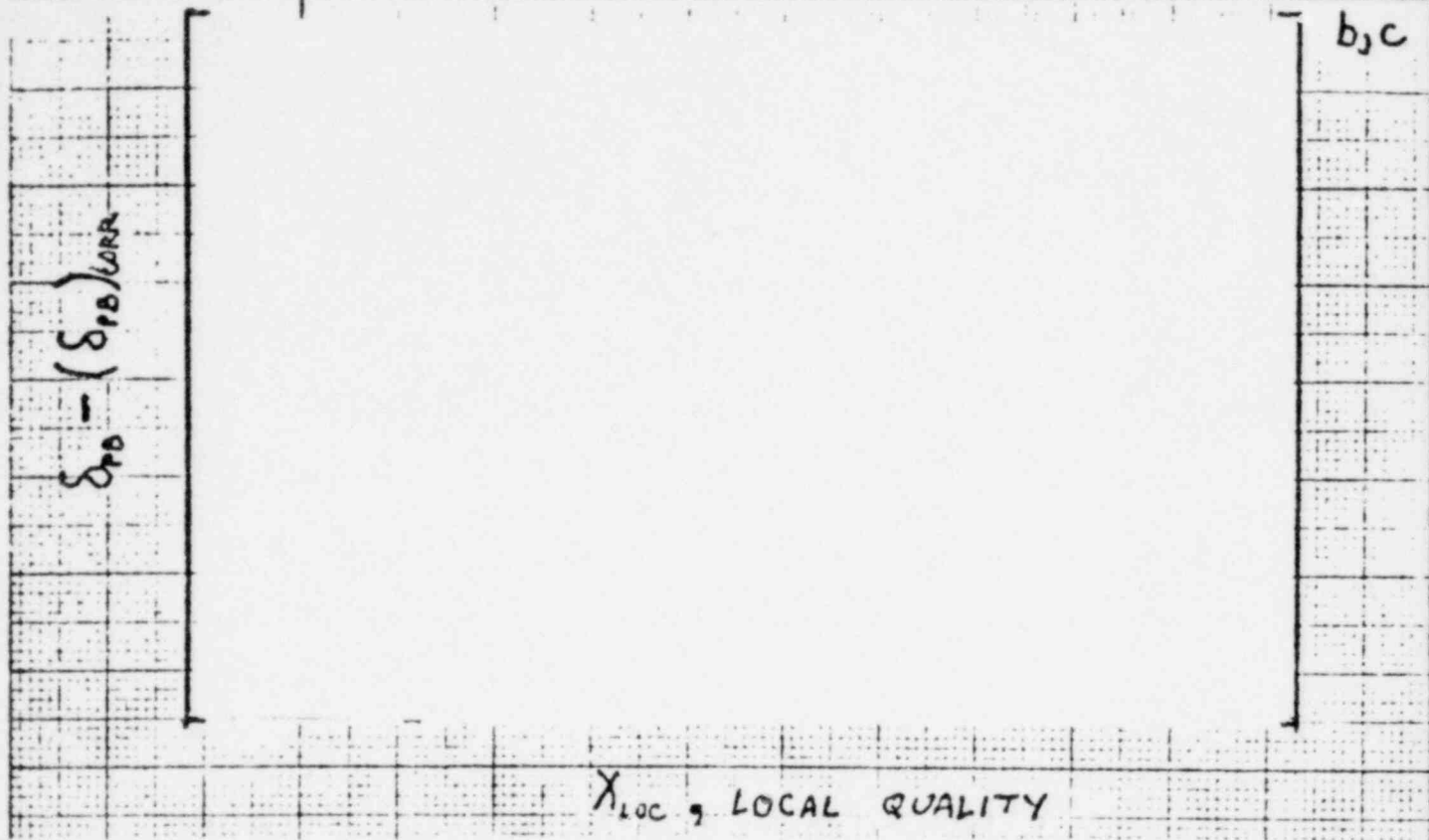## 85% PARTIAL ROD BOW CHF DATA, CORRECTED BY $(\delta_{PB})_{CORR}$

b,c

$P_{IN}$ , INLET PRESSURE, PSIA

b,c

1035 19

$\dfrac{G_{LOC}}{10^6}$ , $\dfrac{LB}{HR\text{-}FT^2}$

# FIGURE 2

## 85% PARTIAL ROD BOW CHF DATA, CORRECTED BY $(\delta_{PB})_{CORR}$

b,c

Y-axis: $\delta_{PB} - (\delta_{PB})_{CORR}$

X-axis: $X_{LOC}$, LOCAL QUALITY

Y-axis: $\delta_{PB} - (\delta_{PB})_{CORR}$

X-axis: $\dfrac{Q_{AVG}}{10^6}$, $\dfrac{BTU}{HR \cdot FT^2}$

1035 192

SIGNATURE ___ JWP ___ DATE ___ CURVE NO.

# POOR ORIGINAL

roperly taken into account all the important variables. The scatter of
he residuals is quite small and is within that expected from repeatability.

nother method of evaluating the partial rod bow correlation is to treat the
orrected partial rod bow data as a set of unbowed data and by statistical
valuation determine if there is a significant difference between the cor-
ected data and another, unbowed, data set. Table 1, attached, shows the
orrected partial bow data with the matching unbowed data and the difference
etween them. A "t" test on the difference, Table 2, shows that the hypothesis
s accepted that there is no difference between the data sets. The hypothesis
s accepted even if over 50% of the correct hypotheses are rejected.

.0 APPLICATION TO REACTOR CORE DESIGN

he bow effect on CHF is a strong function of closure. The partial bow test
hows that a large reduction in the bow penalty is obtained with only a small
ap. Data obtained by other investigators[1][2] indicate that at 50% closure
f the gap, there is no measurable CHF effect. This information has been com-
ined to provide the CHF effect of rod bow as a function of fractional closure
s shown in Figure 3. This linear interpolation is considered conservative and
ill be used in analysis of the rod bow effect.

he value of the bow effect at a closure of 1.0 is the contact penalty as pre-
iously defined[3] at limiting conditions of heat flux and pressure. The cor-
elation in this letter will be used to calculate the CHF effect at 85% closure.
or the analysis of all loops in service, a value of 11.4% will be used to account
or the effect of rod bow [

].a,c For the loss of flow accident and one-loop out-of-service analysis,
value of 14% will be used [

].a,c.

) Markowski, E.S., et.al., "Effect of Rod Bowing on CHF in PWR Fuel Assemblies,"
ASME paper 77-HT-91.

-) Letter, J. ''. Taylor to S. A. Varga, November 13, 1978, status report on R & D
programs described in Semiannual Topical Report BAW-10097A, Rev. 2.

) Letter, C. Eicheldinger to D. F. Ross, NS-CE-1161, August 13, 1976.

TABLE 1
85% PARTIAL ROD BOW CHF DATA. $\Delta\left(\frac{M}{P}\right) = \left(\frac{M}{P}\right)_{NO\,BOW} - \left(\frac{M}{P}\right)_{CORRECTED}$

| Row Nº | $\left(\frac{M}{P}\right)_{CORRECTED}$ | $\left(\frac{M}{P}\right)_{NO\,BOW}$ | $\Delta\left(\frac{M}{P}\right)$ |
|---|---|---|---|
| JC401 | 1.2178 | 1.0452 | -0.1726 |
| J0402 | 0.9837 | 0.9507 | -0.0330 |
| J0403 | 0.9642 | 1.0179 | 0.0537 |
| JC404 | 1.2027 | 1.1189 | -0.0838 |
| JC405 | 1.0962 | 1.0179 | -0.0783 |
| JC406 | 0.9920 | 0.9946 | 0.0026 |
| JC407 | 1.0011 | 1.0122 | 0.0111 |
| JC408 | 0.9322 | 0.8974 | -0.0352 |
| J0409 | 0.9829 | 1.0035 | 0.0206 |
| JC410 | 1.0683 | 1.0852 | 0.0169 |
| JC411 | 1.1353 | 1.0522 | -0.0831 |
| JC412 | 1.0250 | 1.0438 | 0.0188 |
| J0413 | 0.7917 | 1.0797 | 0.0870 |
| J0414 | 1.1626 | 1.0981 | -0.0645 |
| JC415 | 0.9001 | 0.9355 | 0.0354 |
| J0416 | 0.9287 | 0.9571 | 0.0284 |
| JC417 | 0.9982 | 1.0005 | 0.0023 |
| J0418 | 0.9711 | 0.9773 | 0.0062 |
| J0419 | 0.9437 | 1.0160 | 0.0723 |
| J0420 | 0.8098 | 0.8232 | 0.0134 |
| J0421 | 0.9755 | 0.9349 | -0.0406 |
| J0422 | 1.0322 | 0.9778 | -0.0544 |
| J0423 | 0.8598 | 0.8860 | 0.0262 |
| J0424 | 0.8819 | 0.8833 | 0.0014 |
| J0425 | 0.9376 | 0.9254 | -0.0122 |
| JC426 | 0.9277 | 0.8569 | -0.0708 |
| J0427 | 0.8800 | 0.9007 | 0.0207 |
| JC428 | 0.8760 | 0.9552 | 0.0792 |
| JC429 | 0.9420 | 0.9557 | 0.0137 |
| JC430 | 0.9695 | 0.9202 | -0.0493 |
| JC431 | 0.8388 | 0.8874 | 0.0486 |
| J0432 | 0.9378 | 0.8732 | -0.0632 |
| JC433 | 0.8631 | 0.9728 | 0.1097 |
| JC434 | 0.8338 | 0.8739 | 0.0401 |
| JC435 | 0.8642 | 0.9295 | 0.0653 |
| JC436 | 0.8780 | 0.9135 | 0.0355 |
| JC437 | 0.9280 | 0.9550 | 0.0270 |
| JC438 | 0.8029 | 0.8690 | 0.0661 |
| JC439 | 0.8567 | 0.8626 | 0.0059 |
| JC440 | 0.7824 | 0.8721 | -0.1033 |
| JC441 | 0.8516 | 0.9050 | 0.0534 |
| JC442 | 0.8110 | — | |
| JC443 | 0.8150 | 0.8690 | 0.0540 |
| J0444 | 0.9068 | 0.9295 | 0.0227 |
| JC445 | 0.9314 | 0.8569 | -0.0745 |
| JL446 | — | — | |
| JC447 | 1.0142 | 1.0148 | 0.0006 |
| JC448 | — | — | |

# TABLE 2

Hypothesis:  $\mu_d = 0$   $d_i = (M/P)_{PB \text{ corrected}} - (M/P)_{no \text{ bow}}$

test  $t = \dfrac{d-0}{S_d}$

**All Data**                    **Corrected Data Only**

$t = \dfrac{.00044}{.05814} = .00757$         $t = \dfrac{.0005}{.0581} = .0086$
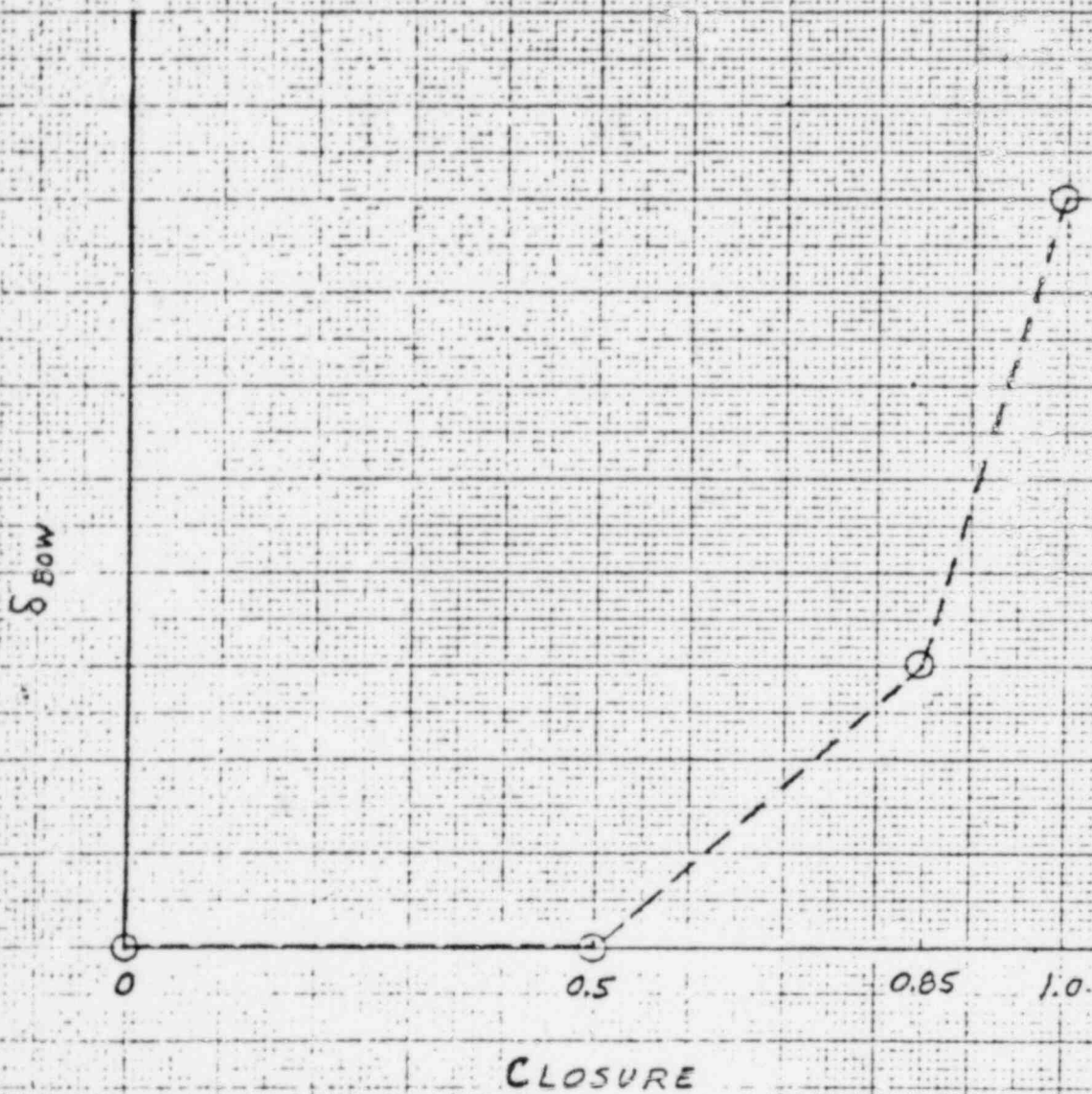
Critical value  $t_{45,.75} = .68$         $t_{30,.75} = .683$

∴ the hypothesis is accepted even if over 50% of the correct hypotheses are rejected.

Reference:  <u>Statistics and Experimental Design</u>

In Engineering and the Physical Sciences,
Vol. 1 p 227-229, John Wiley & Son, Inc.
New York, 1964.

ROD BOW DNBR PENALTY VS. FRACTIONAL CLOSURE

FIGURE 3

1035 196

POOR ORIGINAL

There is no effect on CHF from 0% to 50% closure. At zero closure no effect should be shown since this is the situation of normal spacing which is used in tests to develop the CHF correlations.

A series[1] of bowed rod CHF tests have been conducted which included a test in which a rod was bowed to about 50% of maximum closure and showed no measurable effect on CHF. Westinghouse considers the results of this 50% closure test to be applicable to Westinghouse fuel assemblies for the following reasons.

1) The typical cell contact bow results presented were the same as those conducted on similar Westinghouse geometries and were correlated in a similar manner.

2) Some of the typical cell runs presented were carried out with a large (80%) partial bow. These runs showed a much smaller bow effect than contact, a result entirely consistent with Westinghouse experience.

3) Accumulated experience with rod bow testing clearly shows that the bow effect is second order, i.e., is a relatively small effect which is superimposed on the underlying critical heat flux, and can be correlated with a few flow variables in a simple way. Thus, while critical heat flux is sensitive to differences in test section geometry, the bow effect is not. Hence, bow effects found with the above test sections are applicable to other test section geometries.

It is thus concluded that a Westinghouse 50% partially bowed test would produce the same result (no measurable effect) as did the published[1] test.

In addition, another source[2], with rod bow closures of up to 55% also concluded that no bow effect exists at these magnitudes of closures.

---

1) Markowski, E.S., et.al., "Effect of Rod Bowing on CHF in PWR Fuel Assemblies," ASME paper 77-HT-91.

2) Letter, J. H. Taylor to S. A. Varga, November 13, 1978, status report on R & D programs described in Semiannual Topical Report BAW-10097A, Rev. 2.

Westinghouse Electric Corporation     Power Systems

Box 355
Pittsburgh Pennsylvania 15230

October 24, 1977

NS-CE-1580

·Mr. Denwood F. Ross, Jr.
Assistant Director Reactor Safety
Division of Reactor Licensing
Office of Nuclear Reactor Regulation
U. S. Nuclear Regulatory Commission
7920 Norfolk Avenue
Bethesda, Maryland   20014

Dear Mr. Ross:

Enclosed are:

1.  Twenty-five (25) copies of Attachment on Fuel Rod Bow Penalties (Proprietary).
2.  Twenty (20) copies of Attachment on Fuel Rod Bow Pehalties (Non-Proprietary).

Also enclosed are:

1.  One (1) copy of Application for Withholding, AW-76-35, (Non-Proprietary).
2.  One (1) copy of Affidavit (Non-Proprietary).

This letter is intended to provide the basis for a near term revision of fuel rod bow penalties imposed on the current Westinghouse 15 x 15 and 17 x 17 designs.

The method currently in use for quantifying rod bow penalties is essentially a two-step process:

First, DNBR penalty as a function of channel closure is specified based upon critical heat flux rod bundle test results.  The bow penalty currently prescribed is basically a linear function of channel closure normalized to a measured DNBR penalty associated with rod contact in thimble cell geometry. This revision incorporates the results of recent partial bow thimble cell tests at 95% closure conducted by Westinghouse which demonstrate a significantly lower penalty at partial closure than indicated by the linear interpolation.

Secondly, rod bow magnitude, i.e. channel closure is specified as a function of fuel burnup based upon rod bow measurements of irradiated fuel assemblies. In the case of 15 x 15 LOPAR fuel, a statistical bound has been derived from a fit of twenty-seven regions of data.  In the case of 17 x 17, a conservative

bound had been specified based on a simplistic extrapolation of the 15 x 1 LOPAR data. This extrapolation was necessary due to a lack of actual 17 x 17 irradiated bow measurements. This revision establishes a 17 x 17 bow magni tude versus burnup projection in its own right based upon 17 x 17 bow measure- ments of demonstration assemblies irradiated in the VEPCO Surry plants. Poten- tial region to region variability is conservatively accommodated by augmentation of the Surry bow measurements by a factor of 1.5 as derived from the 15 x 15 LOPAR data. This data was additionally augmented by a factor of 1.2 to con- servatively account for potential cold to hot affects. We understand that this approach is consistent with current NRC recommendations on treatment of limited bow data sets.

The net result of these revisions is to reduce EOL design burnup DNBR bow penalties (before margins) to 11.7% for 15 x 15 LOPAR fuel and 10.6% for 17 x 17 fuel. By comparison the current EOL DNBR bow penalties for both designs is on the order of 30%.

Supporting information is provided in the attachments to this letter which provide an expanded discussion of the information discussed with the NRC Staff at an October 26, 1977 meeting.

We request that this revision be recognized as an interim position pending an expected statistical convolution of bow affect with DNB correlation statistics and/or, in the case of 17 x 17 fuel, the first full cores irrad- iated fuel examination. Convolution will require a definition of bow penalty as a function of closure rather than merely bounding the affect as done for the purpose of this interim position.

Westinghouse is recommending to its customers, both first core and reload, that they reference this submittal on their individual applications.

This submittal contains proprietary information of Westinghouse Electric Corporation. In conformance with the requirements of 10CFR Section 2.790, as amended, of the Commission's regulations, we are enclosing with this submittal an application for withholding from public disclosure and an affidavit. The affidavit sets forth the basis on which the information may be withheld from public disclosure by the Commission.

Correspondence with respect to the affidavit or application for withholding should reference AW-77-52 and should be addressed to R. A. Wiesemann, Manager of Licensing Programs, Westinghouse Electric Corporation, P. O. Box 355, Pittsburgh, Pa. 15230

Please feel free to contact us if you should have further questions on this matter.

Very truly yours,

C. Eicheldinger

C. Eicheldinger, Manager
Nuclear Safety Department

DWC:pj
Attachment

ATTACHMENT 1

# EFFECT ON CHF OF A PARTIALLY BOWED
# HEATED ROD IN A COLD WALL THIMBLE
# CELL GEOMETRY

# SECTION 1
# INTRODUCTION

The study of the effect of bowed rods on critical heat flux (CHF) has become of major interest recently in the design of pressurized water reactors. This report describes the concluding test in a program to determine the effects of a bowed heater rod in a reactor rod bundle thimble cell (that is, in a flow channel formed by three heated rods and an unheated control rod thimble tube). The test described in this report was done with a heated rod which was partially bowed to 85 percent, of the maximum possible closure.

Past efforts have investigated the effects of a heated rod bowed to contact[1] in a thimble cell. The results of those tests indicated that there is no effect at low pressures (1500, 1800 psia), but at high pressures (2100, 2400 psia) the contact caused a large decrease in CHF which varies linearly with the hot rod average heat flux.[2] Those trends are consistent with the findings of two other contact bow tests[3,4] carried out with a typical cell geometry.

Because heated rods bowed all the way to contact are rarely observed in irradiated reactor cores, it was decided to conduct a test more representative of the partial gap closures which are more often observed. It was expected that such a partially bowed heated rod would cause substantially less degradation of CHF than is seen at contact, because there is much less possibility that a partial bow geometry can induce stagnation or other strong localized effects around the point of maximum closure.

The bow geometry selected for this partial bow test was one in which a heater rod was bowed into a thimble cell toward another heater rod and the unheated thimble tube. This allows investigation of the effects of both types of gap reduction (that is, rod-to-rod and rod-to-thimble tube). A gap closure of 85 percent was tested and is shown in figure 1-1.

The results of this partial bow experiment are presented in this report.

---

1. Nagino, Y., et al., "Rod Bowed to Contact DNB Test Results from a Cold Wall Thimble Cell Geometry," to be published in the Journal of Nuclear Science and Technology.

2. The same results were found in two different thimble cell bow geometries with a heated rod bowed into contact with the two other heated rods of the thimble cell, and with a heated rod bowed into contact with a heated rod and the unheated thimble tube. [                                    ]a,c

3. Hill, K. W., et al., "Effect of a Rod Bowed to Contact on Critical Heat Flux in Pressurized Water Reactor Rod Bundles," ASME Paper 75-WA-HT-77.

4. Markowski, E. S., et al., "Effect of Rod Bowing on CHF in PWR Fuel Assemblies," ASME Paper 77-HT-91.
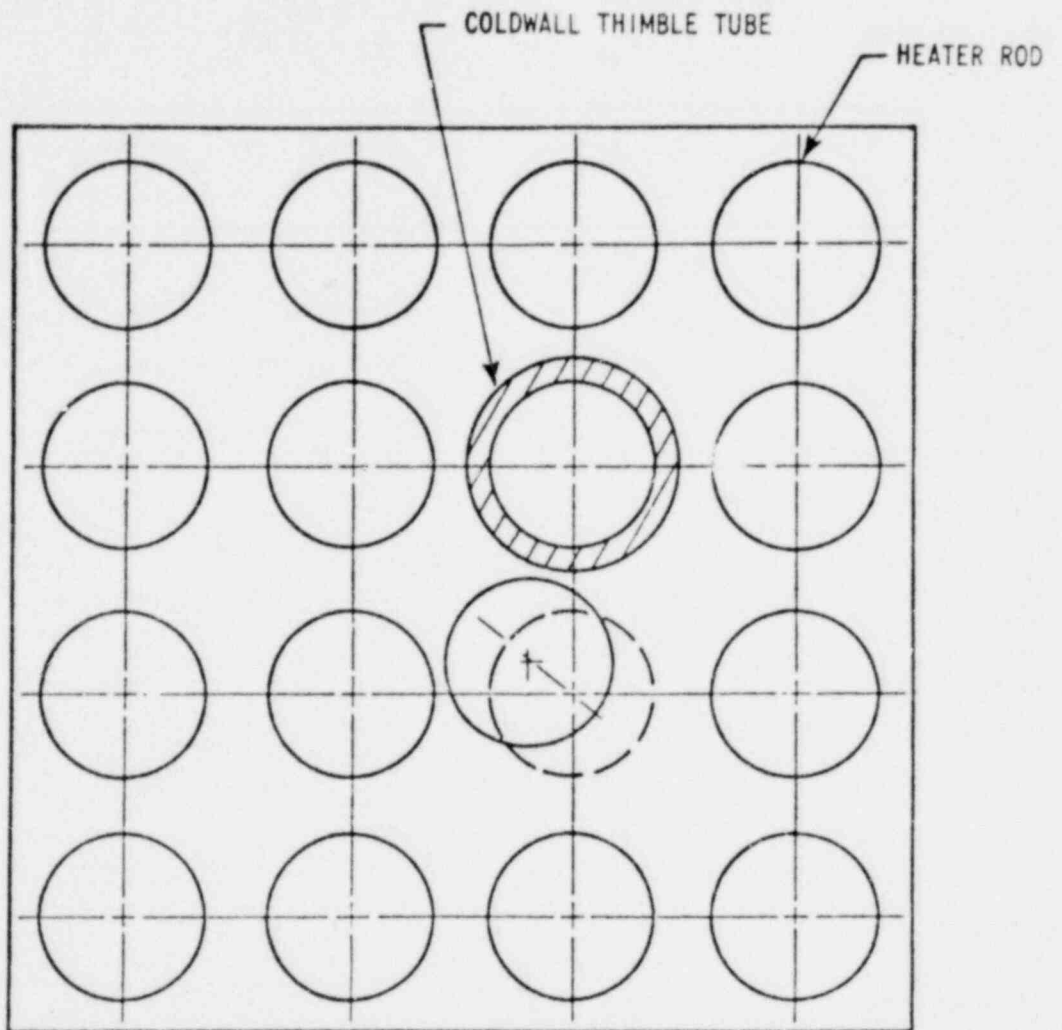
Figure 1-1. Partial Rod Bow Test Section, 85 Percent Closure

1035 202

# SECTION 2
# DESCRIPTION OF TEST FACILITIES
# AND TEST SECTIONS

## 2-1. FACILITY DESCRIPTION

The test was carried out in the heat transfer loop located in the Columbia University Chemical Engineering Laboratory. The test facilities consist of a 7.5 MW dc power supply, a main circulating loop, a side stream purification system, an auxiliary cooling system, and a control system. A layout of the facility is shown in figure 2-1. A flow diagram of the main circulating loop and auxiliary systems is illustrated schematically in figure 2-2. The main circulating loop components were designed according to section 1 of the ASME Boiler and Pressure Code and the following specifications:

| | |
|---|---|
| Loop flow rate, maximum | 400 gpm |
| Loop operating pressure,[1] maximum | 3500 psia |
| Loop operating temperature, maximum | 700° F |
| Main loop cooler heat removal capacity | 5 MW |

## 2-2. TEST SECTION DESCRIPTION

The test bundle consists of 15 heater rods and 1 unheated rod which simulates a control rod guide thimble, as shown in figure 2-3. The bundle has a nonuniform radial power distribution with the 12 outer rods having less power than the 3 inner rods. The simulated thimble guide tube occupies the fourth inner rod location. This thimble is made up of a thin steel rod over which ceramic cylindrical shells (with outer diameters equal to the thim'... outer diameter) are placed. These thimbles are attached to the grid in the same manner as in the reactor core, using a sleeve which is brazed into the grid and then bulged out above and below the grid to connect to the thimble. The dimensions of the test section shown in figure 2-3 are identical to those of the thimble cell test section employed in the previous Westinghouse test.[2]

---

1. Refers to all components except the pumps which were d   gned for 650°F inlet temperature and 2500 psia system pressure.

2. Motley  F  E  and Cade   F  F , "DNB Test Results for  4-Grid Thimble Cold Wall Cells," WCAP-7958-A1-A, January, 1975

Figure 2-1. Test Facility Layout
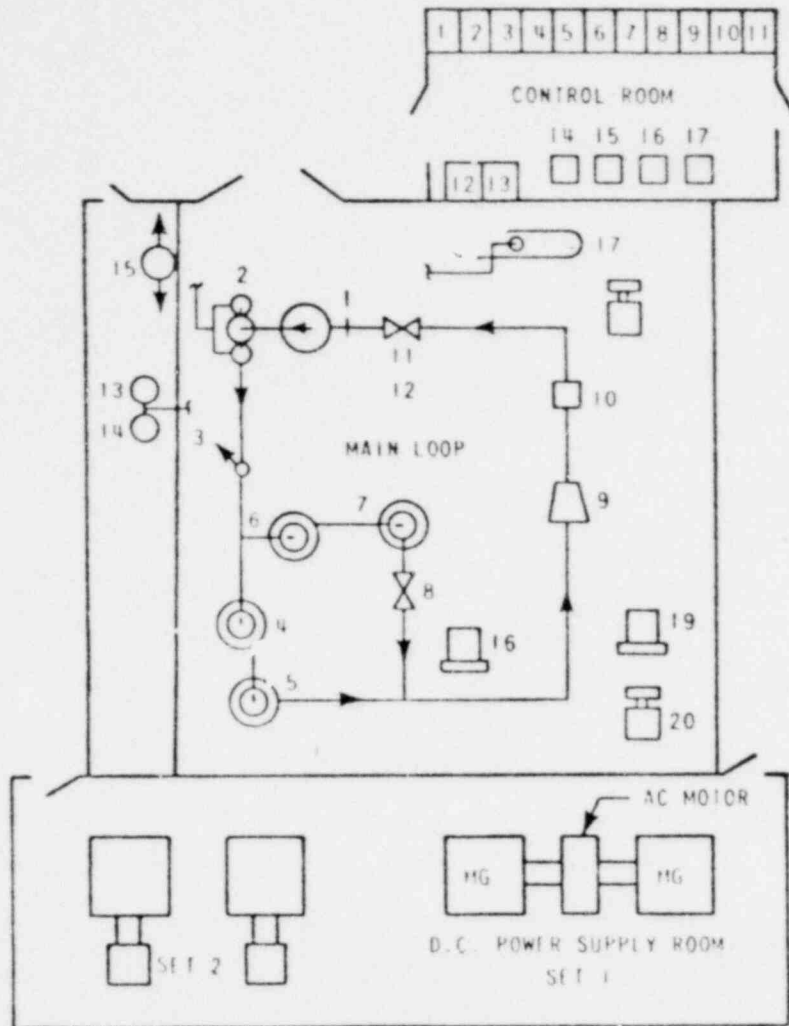
LEGEND

MAIN LOOP

| NO. | COMPONENT |
|---|---|
| 1. | TEST SECTION HOUSING |
| 2. | MAIN HEAT EXCHANGER |
| 3. | 4" LOOP PIPING |
| 4. | W MAIN CIRCULATING PUMP NO. 1 |
| 5. | W MAIN CIRCULATING PUMP NO. 2 |
| 6. | W MAIN CIRCULATING PUMP NO. 3 |
| 7. | W MAIN CIRCULATING PUMP NO. 4 |
| 8. | BYPASS VALVE |
| 9. | 4" VENTURI FLOW METER |
| 10. | 4" POTTER TURBINE METER |
| 11. | 4" FLOW CONTROL VALVE |
| 12. | 1" FLOW CONTROL VALVE |
| 13. | 6" DIA DEMINERALIZER |
| 14. | 6" DIA DEMINERALIZER |
| 15. | MAIN LOOP MAKEUP PUMP |
| 16. | PURIFICATION SYSTEM HEAT EXCHANGER |
| 17. | EVAP COOLER STEAM CONDENSER |
| 18. | EVAP COOLER RECIRCULATING PUMP |
| 19. | MAIN CIRCULATING PUMP COOLING WATER CIRC PUMP |
| 20. | MAIN CIRCULATING PUMP COOLING WATER HEAT EXCH. |

CONTROL ROOM

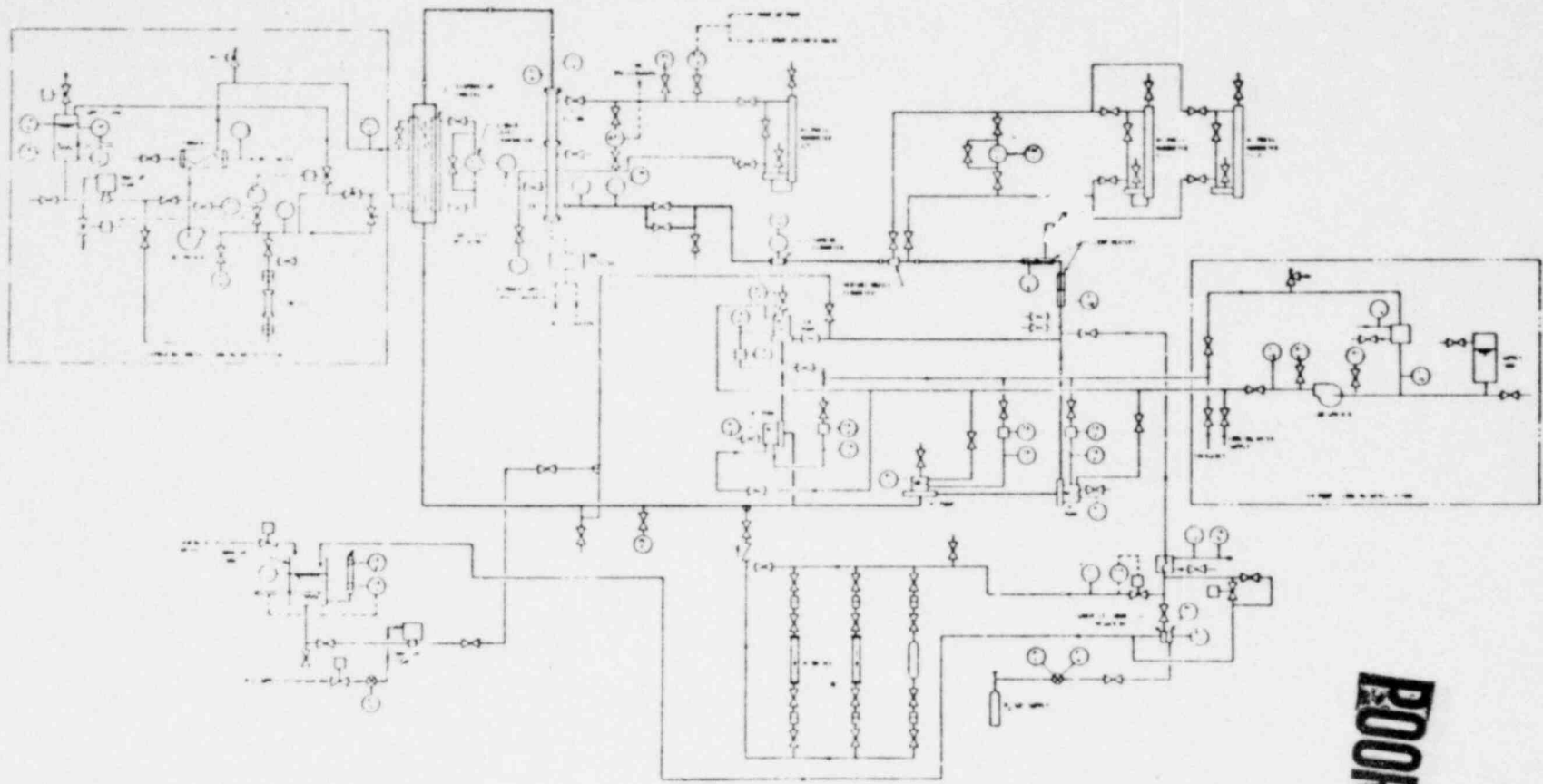| NO. | COMPONENT |
|---|---|
| 1-4. | INSTRUMENTATION AND CONTROLS |
| 5-8. | DNB DETECTORS - OFFNER RECORDERS |
| 9. | D.C. POWER CONTROL AND DATA ACQUISITION SYST. |
| 10. | THERMOCOUPLE HOT JUNCTION TERMINAL PANEL |
| 11. | THERMOCOUPLE TERMINAL PANEL |
| 12-14. | PRESSURE AND TEMP INSTRUMENTATION AND CONTROLS |
| 15. | TEST SECTION DELTA P MANOMETER |
| 16-17. | LOOP FLOW MANOMETER |

2-2

1035 204

11.146-4

Figure 2-2. Test Facility Instrumentation and Flow Schematic Diagram
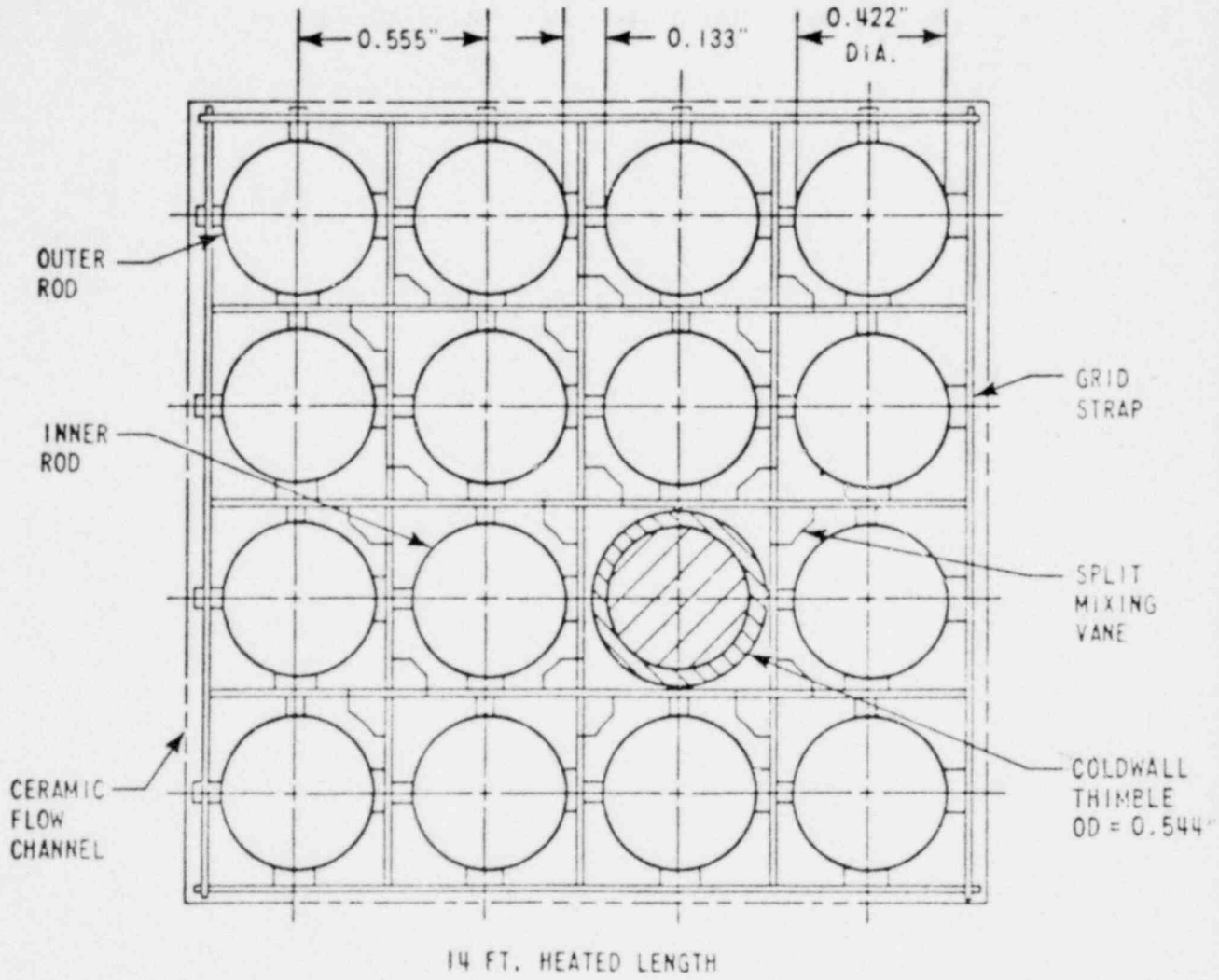
11,146-5

Figure 2-3.  Cross Section Schematic Diagram at a Grid
Location For Cold Wall Thimble Cell Bundle

1035 206

The bowed rod test section has a geometry identical to that of the unbowed test except that one of the heater rods has been bowed toward the thimble tube and an adjacent heater rod so that the gaps between the bowed rod and these nearby rods are partly closed (to 85 percent of full closure). The point of maximum closure is at the midpoint between the two topmost mixing vane grids, 136 inches above the beginning of the test section heated length. This location was chosen because both the original and repeat thimble cell tests showed that CHF almost always occurred at this location or at one of the two mixing vane grids above or below this elevation.

Prior to assembly, the rod to be bowed is permanently deformed to the desired closure. The rod bundle is then assembled using a special support grid located 1/2-inch above the midspan point to assure the proper closure. Figure 2-4 shows the configuration of the special support grid required to maintain the closure geometry shown in figure 1-1. The axial positions of the other mixing vane and support grids are shown in figure 2-5.

## 2-2.    HEATER ROD DESCRIPTION

The heater rods are constructed of two pieces of specially made tubing to provide a non-uniform axial shape. The special tubing has a constant outer diameter with a variable inner diameter. The thin wall thickness provides a high heat flux and the thick wall gives a low heat flux. By joining the thin ends of two tubes together, a heat flux peak is obtained. The position of the peak can be changed by varying the length of the two tubes. The axial heat flux shape used for this test is shown in figure 2-6.

A means of detecting the occurrence of critical heat flux (CHF) must be provided at several elevations along the rod beyond the peak heat flux. Thermocouples are located in the ceramic pieces which are fitted to the inside diameter of each heater tube. These thermocouples can detect the rapid and uncontrolled increase in temperature which occurs at CHF. At most elevations shown in figure 2-5, a thermocouple is installed as shown in figure 2-7. In this installation the thermocouple is connected to a copper ring to allow detection of CHF on all sides of the rod simultaneously. In those rods which are almost in contact, a special multiple thermocouple installation at the maximum closure elevation was developed to provide indications of any possible radial effects of gap closure on CHF. This special installation is used only at the maximum closure elevation (136 inches above the inlet). Figure 2-8 shows this installation.
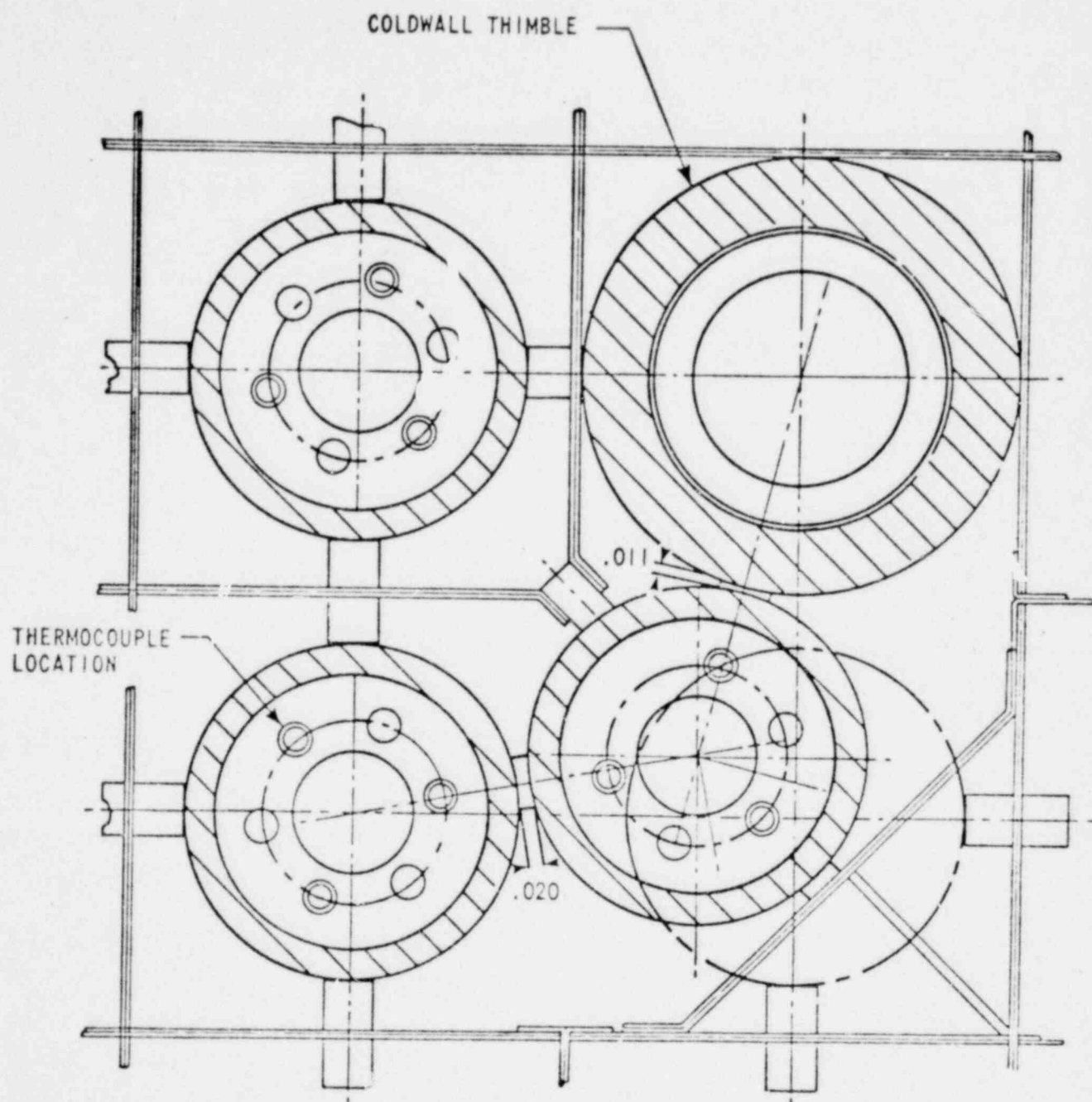
1035 209

COLDWALL THIMBLE

THERMOCOUPLE
LOCATION

.011

.020

Figure 2-4. Special Support Grid, 85 Percent Closure

2-6

1035 208

a,b,c

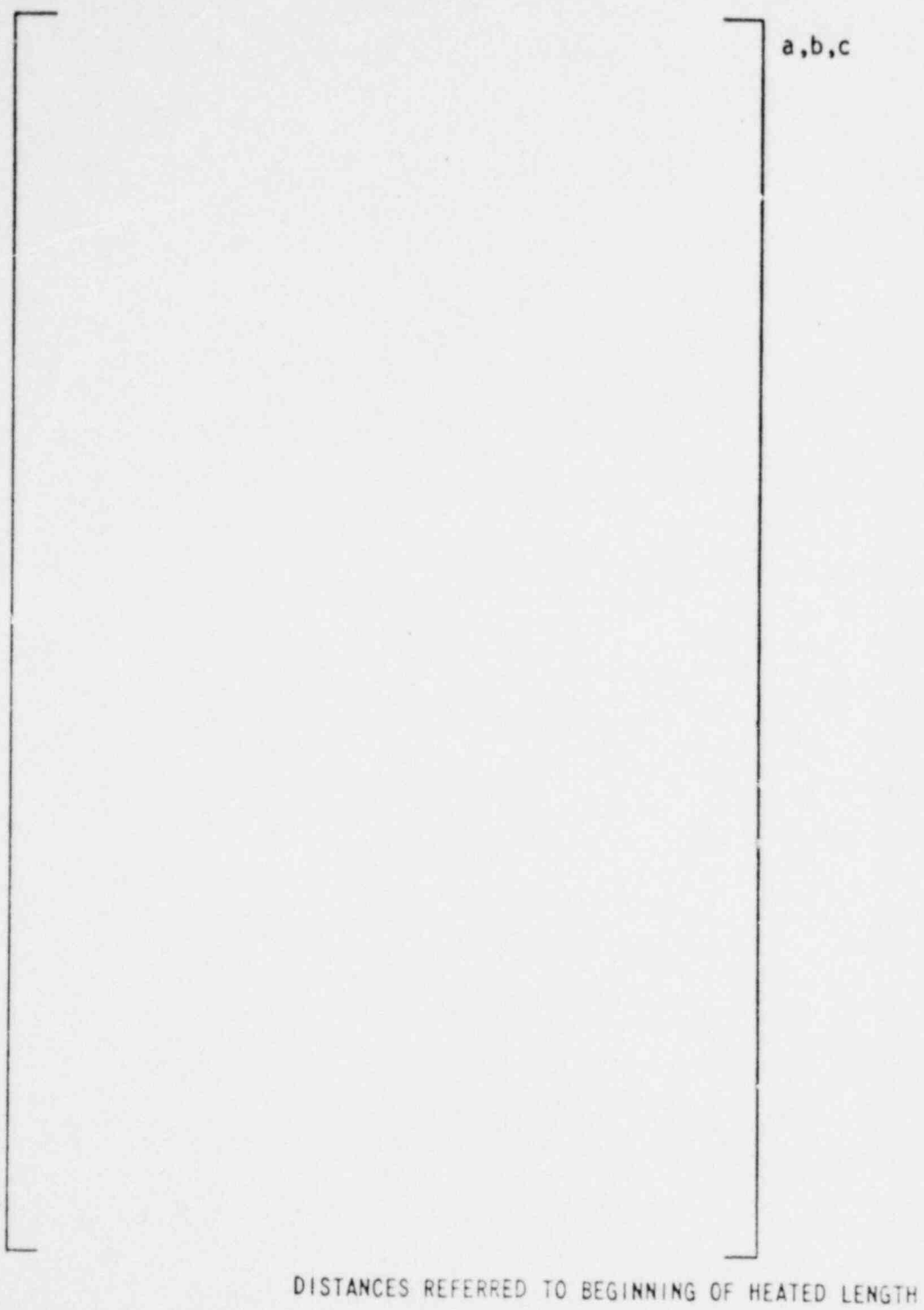DISTANCES REFERRED TO BEGINNING OF HEATED LENGTH

Figure 2-5. Axial Grid and CHF Detector Location
For 14-Foot Test Sections

1035 209
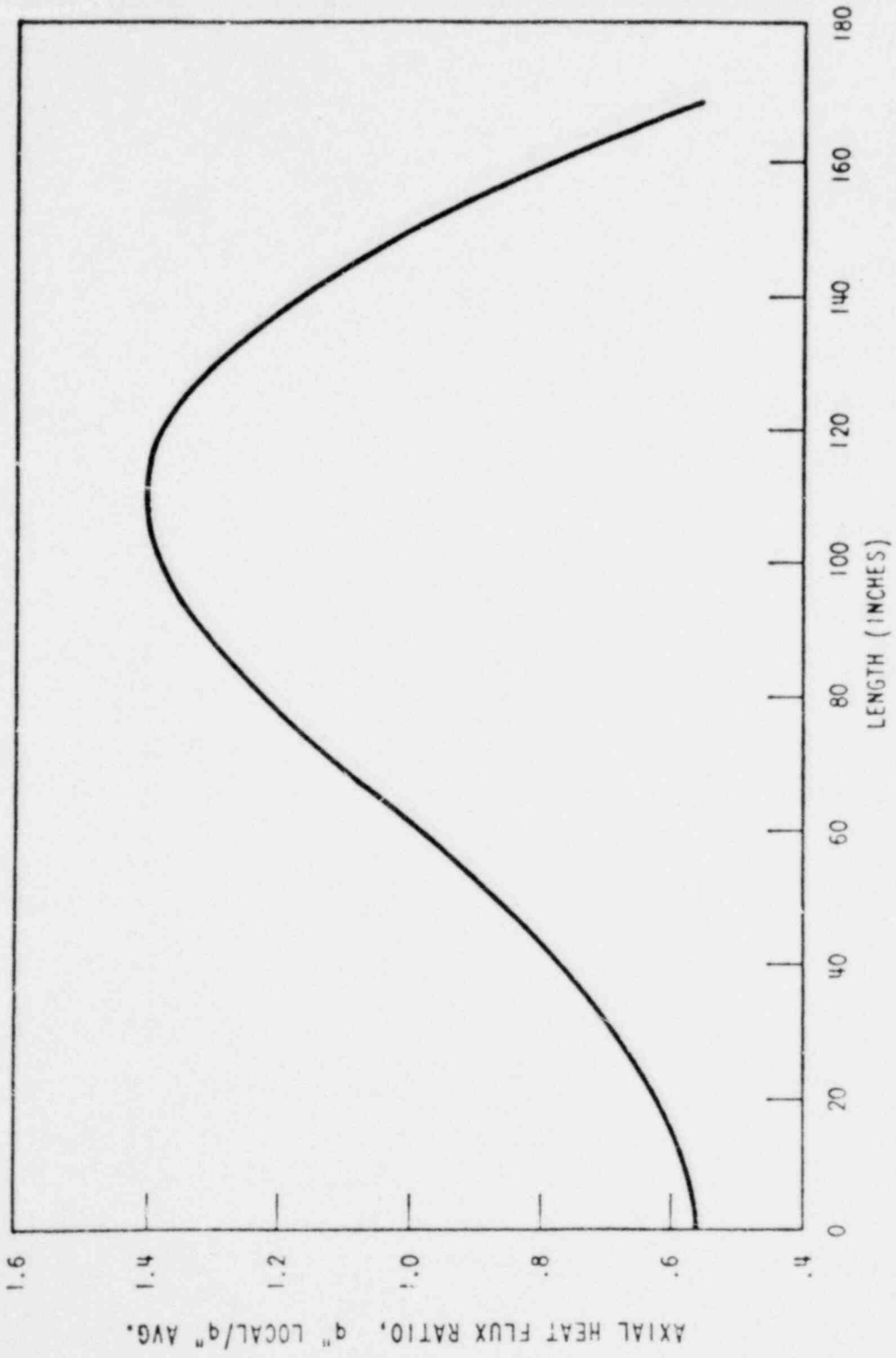
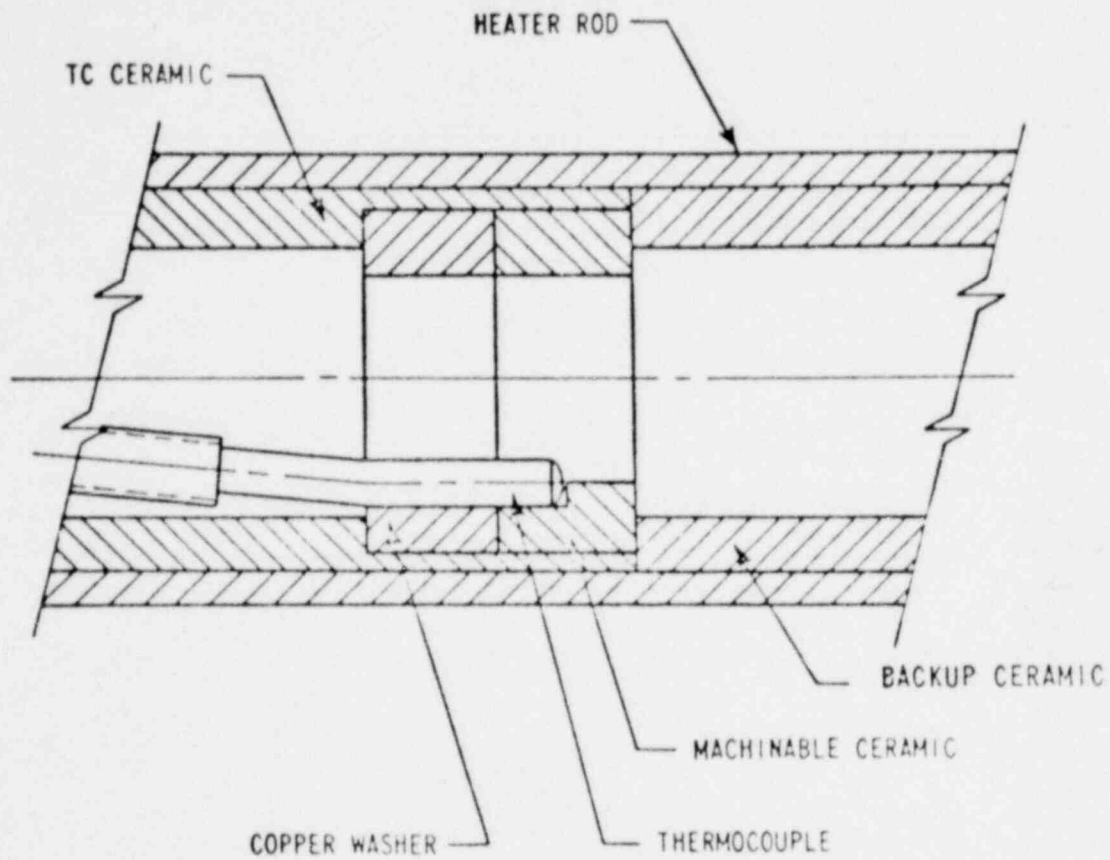Figure 2-6. Axial Heat Flux Distribution of 14-Foot Heater Rods

Figure 2-7. CHF Detector Assembly

1035 21

136" FROM BEGINNING OF HEATED LENGTH

HEATER ROD

COPPER THERMOCOUPLE POSITIONER

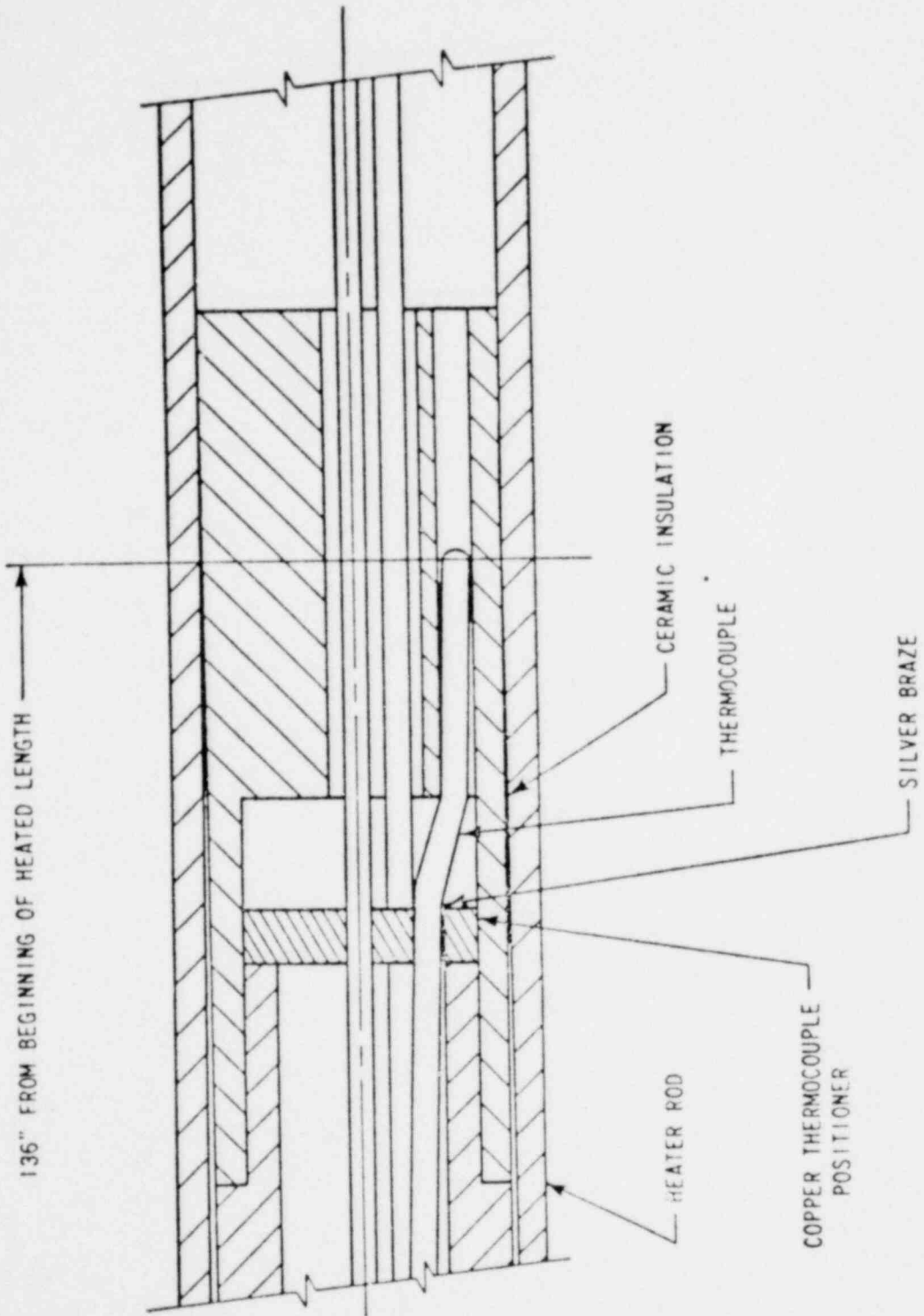SILVER BRAZE

THERMOCOUPLE

CERAMIC INSULATION

Figure 2-8. Special CHF Detector Assembly

1035 212

There are several characteristics of this installation which result in large uncertainties in surface temperature determination. These include radial and axial conduction of both the ceramic and heater tube wall, the gap between the heater tube wall and the ceramic, and the eccentricity of the thermocouple positioning ceramic. It should be pointed out, however, that the actual value of the surface temperature is not a key parameter in determining critical heat flux. Instead, CHF is indicated by a rapid rise in temperature as a consequence of the reduced heat transfer.

# SECTION 3
# TEST PROCEDURE

## 3-1. PRE-TEST CALIBRATION

Prior to each set of CHF tests with a particular test section, single phase (cold flow) pressure drop measurements are made to check test section inlet flow measurement and pressure drop instrumentation.

## 3-2. IN-TEST CALIBRATION

Periodically during each test program, heat balances are performed to check inlet and outlet temperatures, power instrumentation, and recording system performance. Typical heat balances show a negligible heat loss of 10 to 50 KW compared to test run powers of up to 7 MW.

## 3-3. DETERMINATION OF CHF

For a particular run, test section inlet temperature, mass velocity, and outlet pressure (at steady state conditions) are set with power at about 85 percent of the predicted CHF power. At this power level the thermocouples and Offner recorders (employed as CHF detectors) are checked for proper operation. The approach to CHF is accomplished by a sequence of steps, increasing the power in small increments (1 percent or less). A point is reached at which a rapid and continuous rise in temperature is indicated by one or more of the heater rod thermocouples. Once this happens, the test section power is quickly reduced manually (by perhaps 35 to 40 percent). During this approach to CHF the values of voltage and current through the test section, inlet temperature, inlet flow, outlet pressure, and test section pressure drop are automatically recorded. The set of measurements immediately before the power reduction is taken to be the recorded CHF conditions. Once all CHF thermocouples show a decrease in temperature, the power is reset for the next CHF run.

## 3-4. REPEATS

Periodically during testing, an earlier run will be repeated to check on the repeatability of the experiment and to reveal any changes which may have taken place in the test section.

# SECTION 4
# TEST RESULTS : ANALYSIS AND CORRELATION

## 4-1.    INTRODUCTION

The results of the 85 percent closure partial bow test are given in table 4-1. This table gives a complete tabulation of the measured test parameters of inlet pressure, inlet temperature, inlet mass velocity, and hot rod average critical heat flux as well as the location of measured CHF sites. Table 4-1 also contains values of the measured-to-predicted critical heat flux ratio $\left(\frac{M}{P}\right)_{PB}$, computed from a rod bundle subchannel analysis using the measured inlet conditions for each run. This analysis was carried out using the normal (unbowed) test section geometry as was done with the previously presented contact bow cases.[1,2]

Table 4-1 includes the run numbers and the values of $\left(\frac{M}{P}\right)_{no\ bow}$ for the matching unbowed runs, that is, those runs from the original[3] and repeat[1] unbowed thimble cell data sets which have inlet conditions that match the individual runs of this partial rod bow data set. In most cases there are matching unbowed runs from both original and repeat data sets, and the value of $\left(\frac{M}{P}\right)_{no\ bow}$ given in the table is the numerical average of the two. For cases where there is only one matching unbowed run, the value of $\left(\frac{M}{P}\right)_{no\ bow}$ for that single run is given in the table.

The last column in the table gives values of $\delta_{PB}$ defined by

$$\delta_{PB} = \frac{\left(\frac{M}{P}\right)_{no\ bow} - \left(\frac{M}{P}\right)_{PB}}{\left(\frac{M}{P}\right)_{no\ bow}}$$

This definition is consistent with that given for previous Westinghouse thimble and typical cell heated rod bowed to contact tests.[1,2]

---

1. Nagino, Y., et al., "Rod Bowed to Contact DNB Test Results from a Cold Wall Thimble Cell Geometry," to be published in the Journal of Nuclear Science and Technology.

2. Hill, K. W., et al., "Effect of a Rod Bowed to Contact on Critical Heat Flux in Pressurized Water Reactor Rod Bundles," ASME Paper 75-WA-HT-77.

3. Motley, F. E., and Cadek, F. F., "DNB Test Results for R-Grid Thimble Cold Wall Cells," WCAP-7958-A1-A, January, 1975.

1035 215

## TABLE 4-1
### EFFECT OF PARTIAL ROD BOW ON CHF, 85 PERCENT CLOSURE

| Run No. | Inlet Pressure (PSIA) | Inlet Temp (F) | Inlet Mass Velocity $\left(\frac{LBM}{hr \cdot ft^2}\right)$ | Hot Rod Average Heat Flux $\left(\frac{Btu}{hr \cdot ft^2}\right)$ | Elevation Of Measured CHF T/C No. h,c | $\left(\frac{M}{P}\right)_{PB}$ | Matching Run No Repeat | Matching Run No Original | $\left(\frac{M}{P}\right)_{no\ bow}$ | $\delta_{PB}$ |
|---|---|---|---|---|---|---|---|---|---|---|
| J0401 | | | | | | 1.2178 | J0014 | 1097 | 1.0452 | -0.1651 |
| J0402 | | | | | | .9837 | J0015 | 1099 | 0.9501 | -0.0347 |
| J0403 | | | | | | .9413 | J0016 | 1102 | 1.0179 | 0.0758 |
| J0404 | | | | | | 1.1587 | J0017 | 1104 | 1.1189 | 0.0445 |
| J0405 | | | | | | 1.0644 | J0016 | 1102 | 1.0179 | -0.0457 |
| J0406 | | | | | | .9085 | J0022 | 1109 | .9946 | 0.0866 |
| J0407 | | | | | | .9297 | J0021 | 1107 | 1.0122 | 0.0915 |
| J0408 | | | | | | .8657 | J0020 | 1116 | .8976 | 0.0355 |
| J0409 | | | | | | .9360 | J0019 | 1114 | 1.0035 | 0.0673 |
| J0410 | | | | | | 1.0131 | J0050 | 1106 | 1.0852 | 0.0664 |
| J0411 | | | | | | 1.0952 | J0023 | 1105 | 1.0522 | -0.0409 |
| J0412 | | | | | | .9914 | J0024 | 1113 | 1.0438 | 0.0502 |
| J0413 | | | | | | .9860 | J0025 | 1101 | 1.0797 | 0.0866 |
| J0414 | | | | | | 1.1545 | J0026 | 1103 | 1.0981 | -0.0514 |
| J0415 | | | | | | .8124 | J0027 | 1110 | .9355 | 0.1316 |
| J0416 | | | | | | .8383 | J0028 | 1120 | .9571 | 0.1241 |
| J0417 | | | | | | .9263 | J0029 | 1117 | 1.0005 | 0.0742 |
| J0418 | | | | | | .9010 | J0030 | 1108 | .9773 | 0.0781 |
| J0419 | | | | | | .8936 | J0052 | 1115 | 1.0160 | 0.1205 |
| J0420 | | | | | | .8098 | J0032 | 1127 | 0.8232 | 0.0275 |
| J0421 | | | | | | .9755 | J0033 | 1124 | .9349 | -0.0434 |
| J0422 | | | | | | 1.0322 | J0034 | 1098 | .9778 | -0.0555 |
| J0423 | | | | | | .8598 | J0036 | 1128 | .8960 | 0.0296 |
| J0424 | | | | | | .8819 | J0035 | 1133 | .8833 | 0.0016 |
| J0425 | | | | | | .9376 | J0054 | 1125 | .9254 | -0.0132 |
| J0426 | | | | | | .8240 | J0037 | --- | .8569 | 0.0384 |
| J0427 | | | | | | .7812 | J0040 | --- | .9089 | 0.1405 |
| J0428 | | | | | | .7922 | J0039 | 1111 | .9552 | 0.1706 |
| J0429 | | | | | | .8489 | J0038 | 1121 | .9557 | 0.1116 |
| J0430 | | | | | | .8524 | J0042 | --- | .9202 | 0.0737 |
| J0431 | | | | | | .7386 | J0041 | --- | 0.8874 | 0.1672 |
| J0432 | | | | | | .8511 | ----- | 1112 | 0.8739 | 0.0261 |
| J0433 | | | | | | .7820 | J0043 | 1123 | 0.9728 | 0.1961 |
| J0434 | | | | | | .7553 | ----- | 1112 | 0.8739 | 0.1357 |
| J0435 | | | | | | .8642 | J0044 | 1129 | 0.9295 | 0.0703 |
| J0436 | | | | | | .8780 | J0045 | 1134 | 0.9135 | 0.0399 |
| J0437 | | | | | | .9280 | ----- | 1126 | 0.9550 | 0.0283 |
| J0438 | | | | | | .8029 | J0047 | --- | 0.8690 | 0.0761 |
| J0439 | | | | | | .8567 | J0046 | --- | 0.8676 | 0.0063 |
| J0440 | | | | | | .8620 | J0048 | --- | 0.8791 | 0.0195 |
| J0441 | | | | | | .7516 | J0049 | --- | 0.9060 | 0.1695 |
| J0442 | | | | | | .8110 | ----- | --- | ----- | ---- |
| J0443 | | | | | | .8150 | J0047 | --- | 0.8690 | 0.0621 |
| J0444 | | | | | | .9068 | J0044 | 1129 | 0.9295 | 0.0243 |
| J0445 | | | | | | .8271 | J0037 | --- | 0.8569 | 0.0348 |
| J0446 | | | | | | .9450 | J0053 | 1100 | 0.9618 | 0.0175 |
| J0447 | | | | | | .9349 | J0057 | 1118 | 1.0148 | 0.0787 |
| J0448 | | | | | | .8849 | ----- | --- | ---- | ---- |

1035 216

In connection with the previous thimbel cell contact bow tests,[1] a repeatability test was carried out using two different but geometrically identical test sections. This test showed that CHF runs with the same inlet conditions are repeatable to within [ ]a,c percent of M/P (the measured-to-predicted CHF ratio). More precisely, this means that 95 percent of the runs in a repeatability test program should yield values of a repeatability parameter $\delta_R$ (defined similarly to $\delta_{PB}$ above) within a band of [ ]a,c

Thus, a bowed rod test program which results in a significant portion of the runs having values of $\delta_{PB}$ outside the [ ]a,c band can be said to display a measurable bow effect.

## 4-2.  RESULTS OF 85 PERCENT GAP CLOSURE TESTS

Figures 4-1 and 4-2 show plots of $\delta_{PB}$ for the 85 percent closure partial rod bow test against pressure and flow. These plots show that the 85 percent closure bow effect is small -- much smaller than was observed for the thimble cell contact bow.[1] Nevertheless, the effect is large enough to be measurable. The pressure effect shown in figure 4-1 is characteristic of rod bow, that is, there is no discernible effect at low pressures (1500, 1800 psia), but a definite effect at high pressures (2100, 2400 psia). [

]a,c

## 4-3.  CORRELATION OF THE 85 PERCENT CLOSURE PARTIAL BOW DATA

The plots of $\delta_{PB}$ versus the various test parameters indicate that the 85 percent partial bow data are qualitatively similar to the contact data, though much smaller in magnitude. It is thought, therefore, that these data can be correlated by a simple extension of the contact bow correlation, $(\delta_{bow})_{corr}$, which was fit to the thimble cell contact bow data:[1]

$$(\delta_{PB})_{corr} = F_{PB} \, (\delta_{bow})_{corr}$$

where

$(\delta_{PB})_{corr}$ is the partial bow effect parameter. (The subscript "corr" signifies $\delta_{PB}$ as computed by a correlation.)

$F_{PB}$ is the partial bow factor. Note that $F_{PB} = 0$ for unbowed rods (that is, no bow effect); $F_{PB} = 1.0$ for rods bowed to contact (that is, full bow effect)

---

1. Nagino, Y., et al., "Rod Bowed to Contact DNB Test Results from a Cold Wall Thimble Cell Geometry," to be published in the Journal of Nuclear Science and Technology.
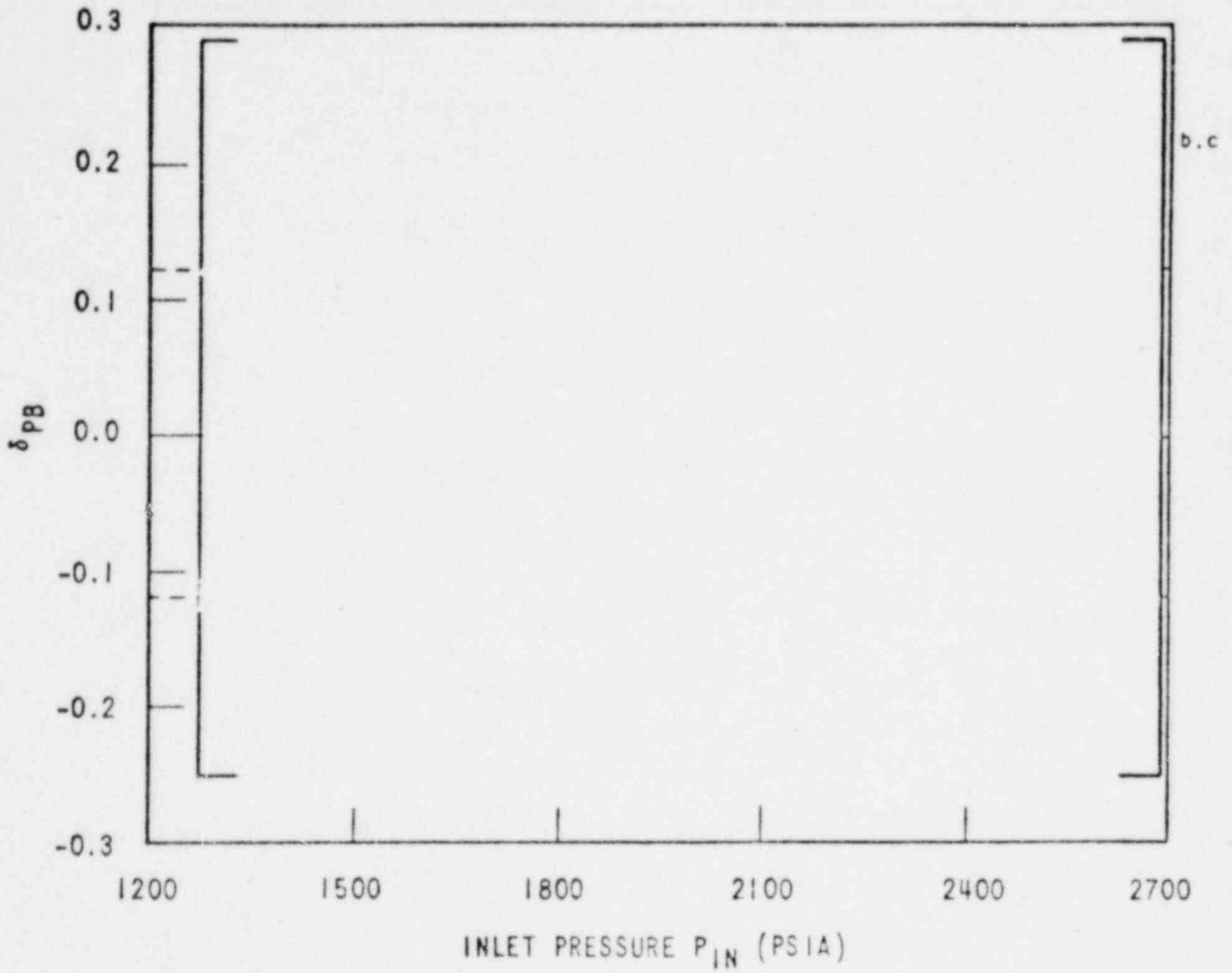
Figure 4-1. $\delta_{PB}$ Versus $P_{in}$, 85 Percent Gap Closure
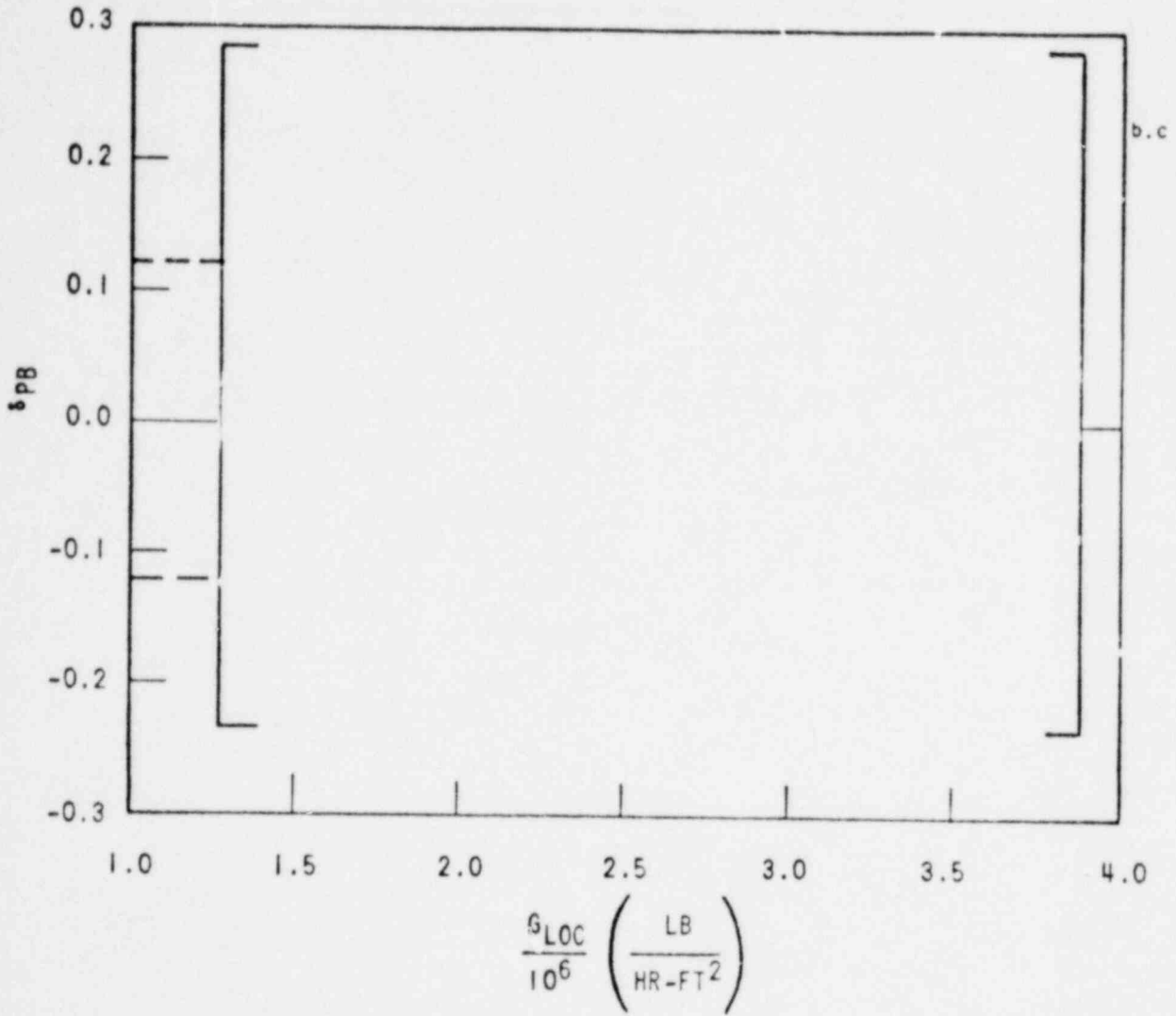
1035 216

Figure 4-2. $\delta_{PB}$ Versus $G_{loc}$, 85 Percent Gap Closure

$$(\delta_{bow})_{corr} = \left[ \phantom{xxxxxxxxxxxxxxxxxxxxxxxxxxxxxxxxxxxx} \right]^{a,c}$$

where

$Q''_{AVG}$ is the hot rod average critical heat flux $\left( \dfrac{Btu}{hr\text{-}ft^2} \right)$

P is the system pressure (psia)

The task of correlating the partial bow data thus becomes that of writing an appropriate expression for $F_{PB}$. The expression for $F_{PB}$ can be inferred from data by computing for each run in the partial bow data set

$$\bar{F}_{PB} = \frac{\delta_{PB}}{(\delta_{bow})_{corr}}$$

and plotting the results against various parameters. [
]$^{a,c}$ Figures 4-3 and 4-4 show plots for pressures of 2400 and 2100 psia.[1]

It should be pointed out that plotting the data in this manner exaggerates the data scatter because $(\delta_{bow})_{corr}$ appears in the denominator. $(\delta_{bow})_{corr}$ can have a small value for certain sets of conditions. This is especially true of the 2100 psia data, for which many of the predicted contact penalties are within repeatability. To show this more clearly, each data point in figures 4-3 and 4-4 has been plotted along with its range of most probable error.[2] As explained above, these error bands are larger for the 2100 psia data.

---

1. No such plots are presented for the low pressure (1500, 1800 psia) data since they show no bow effect and none is predicted by $(\delta_{bow})_{corr}$

2. The most probable error on $\delta_{PB}$ is given by

$$0.6745\sigma_\delta = \left[ \phantom{xxxxxxxxxxxxxxxx} \right] \qquad a,$$

where $\sigma_\delta$ is the standard deviation associated with repeatability (found to be [ ] percent in the thimble cell repeatability $\quad$ a, test)[3] Thus the most probable error range on $F_{PB}$ will be given by

$$F_{PB} = \frac{\delta_{PB} \pm 0.04}{(\delta_{bow})_{corr}}$$

3. Nagino, Y., et al., "Rod Bowed to Contact DNB Test Results from a Cold Wall Thimble Cell Geometry," to be published in the Journal of Nuclear Science and Technology.
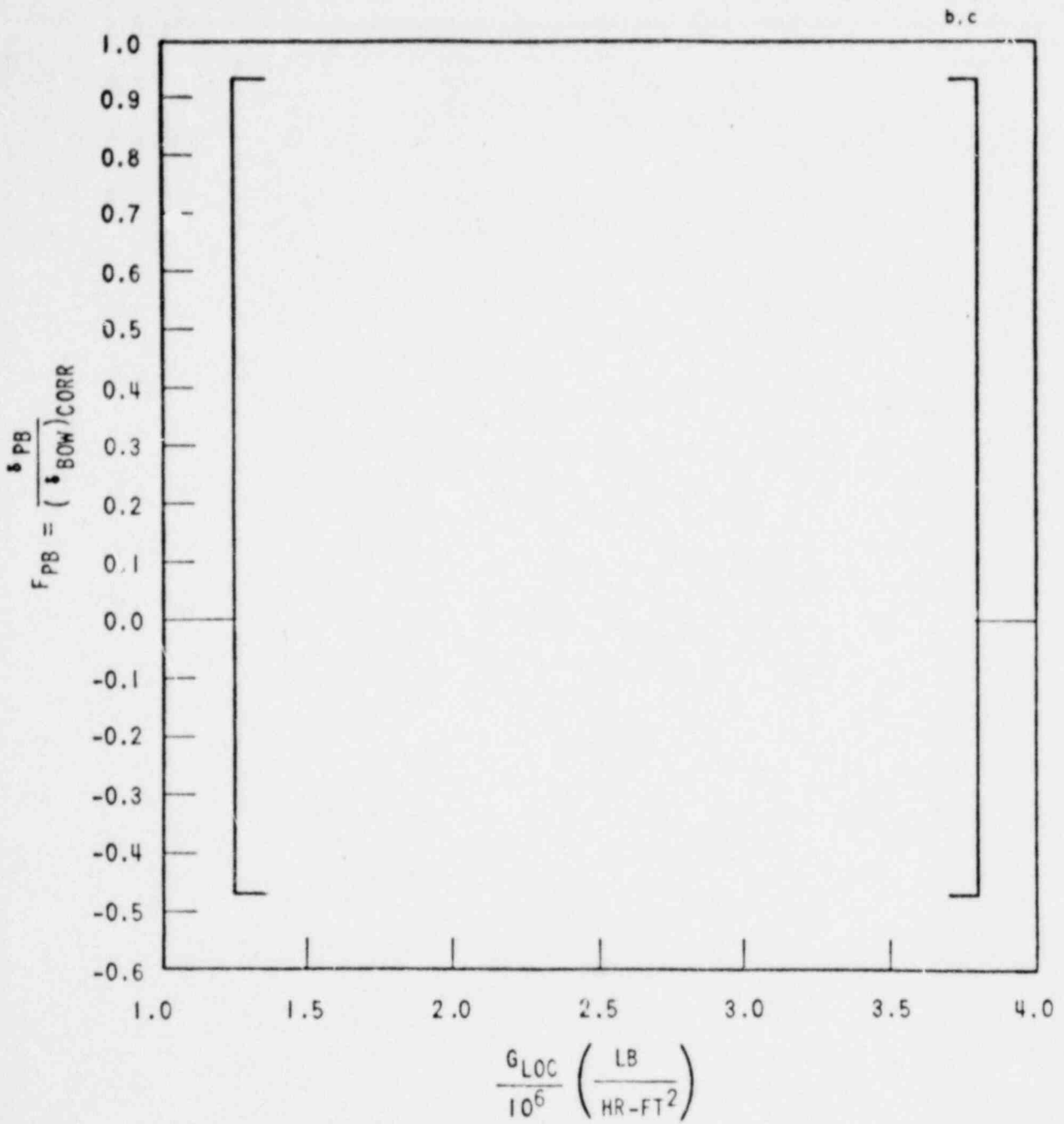
1035 210

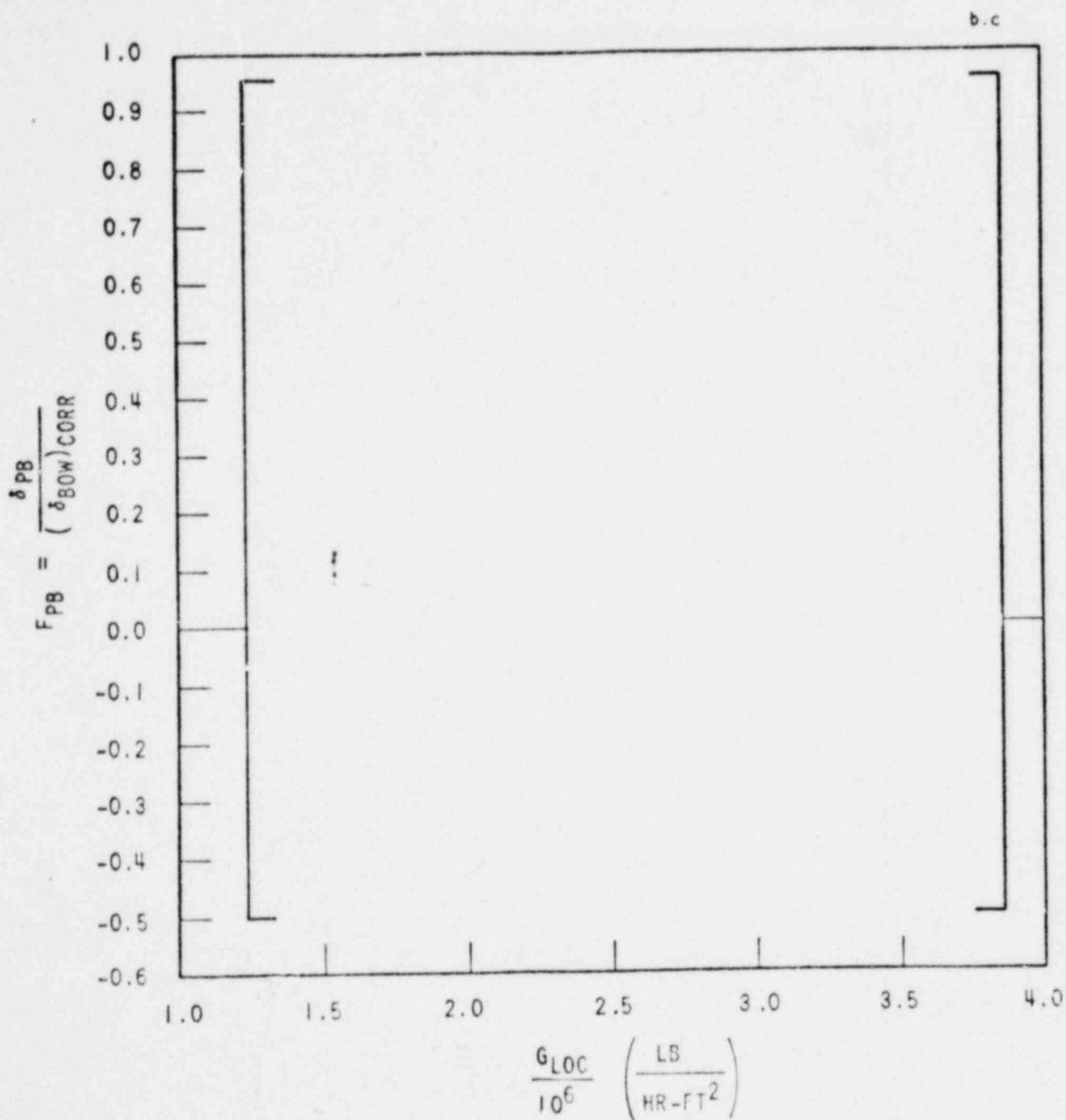Figure 4.3. $F_{PB}$ Versus $G_{loc}$. P = 2400 PSIA, 85% Gap Closure

Figure 4-4. $F_{PB}$ Versus $G_{loc}$, P = 2100 PSIA, 85% GAP CLOSURE

1035 224

Figure 4-5 shows a plot of $F_{PB}$ versus local mass flow for both the high pressure subsets. A linear best fit of these data is also shown, and is given by

$$\left[ \phantom{xxxxxxxxxxxxxxxxxxxxxxxxxxxxxxxxxxxx} \right]^{a,c}$$

When the measured values of $\delta_{PB}$ are corrected by the partial bow correlation, $(\delta_{PB})_{corr} = F_{PB}(\delta_{bow})_{corr}$, the resulting residue, $\Delta_{PB} = \delta_{PB} - (\delta_{PB})_{corr}$, should be no worse than repeatability data, that is, almost all the residues should fall within the repeatability band [ ]$^{a,c}$ when plotted against the various flow parameters. This is shown in figures 4-6 and 4-7 which are plots of $\Delta_{PB}$ versus pressure, flow, quality, and hot rod average heat flux.

Thus, it can be concluded that the 85 percent closure partial rod bow data is satisfactorily represented by the correlation
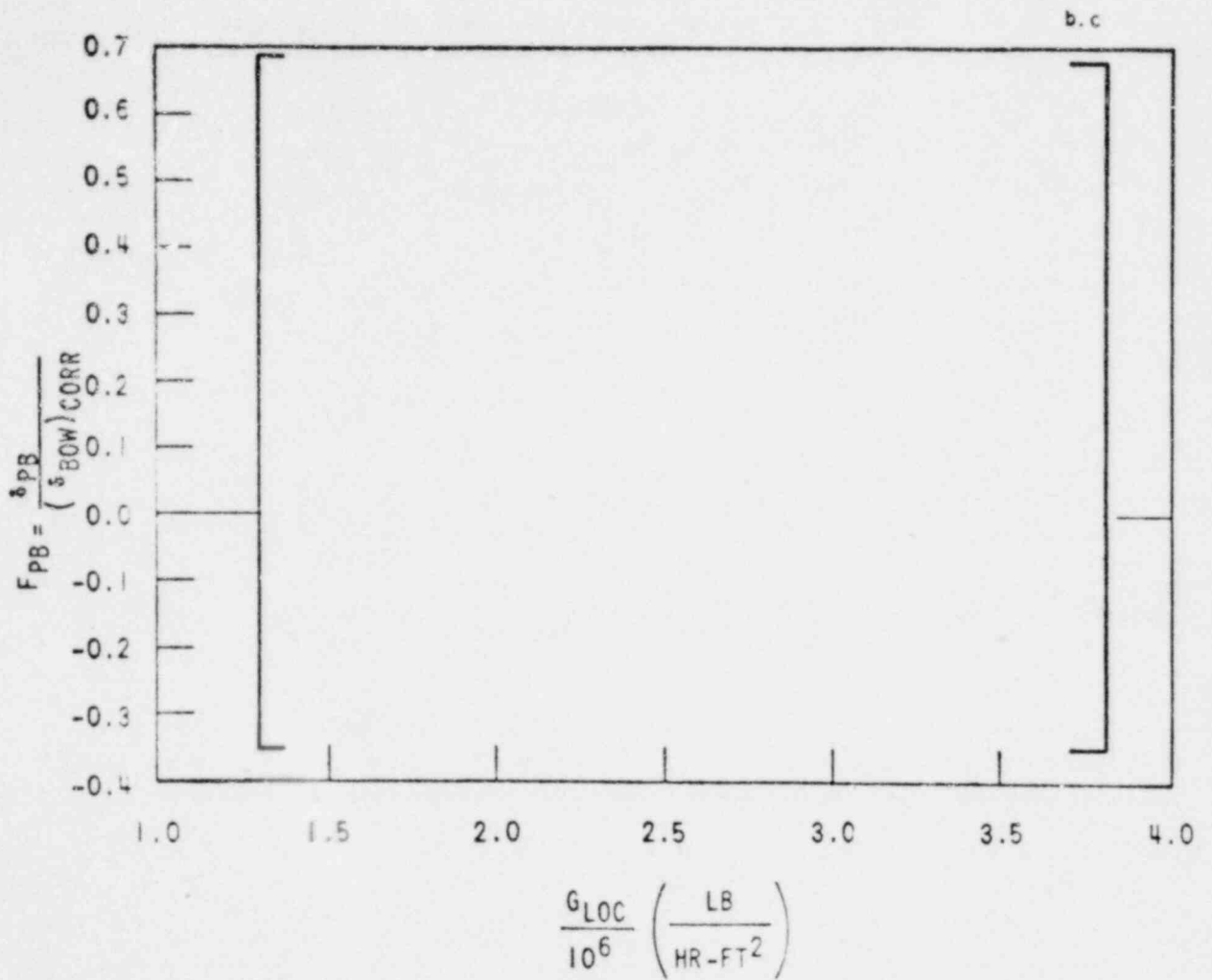
$$\left[ \phantom{xxxxxxxxxxxxxxxxxxxxxxxxxxxxxxxxxxxx} \right]^{a,c}$$

b.c



Figure 4-5. $F_{PB}$ Versus $G_{loc}$, P = 2400 and 2100 PSIA, 85% GAP CLOSURE
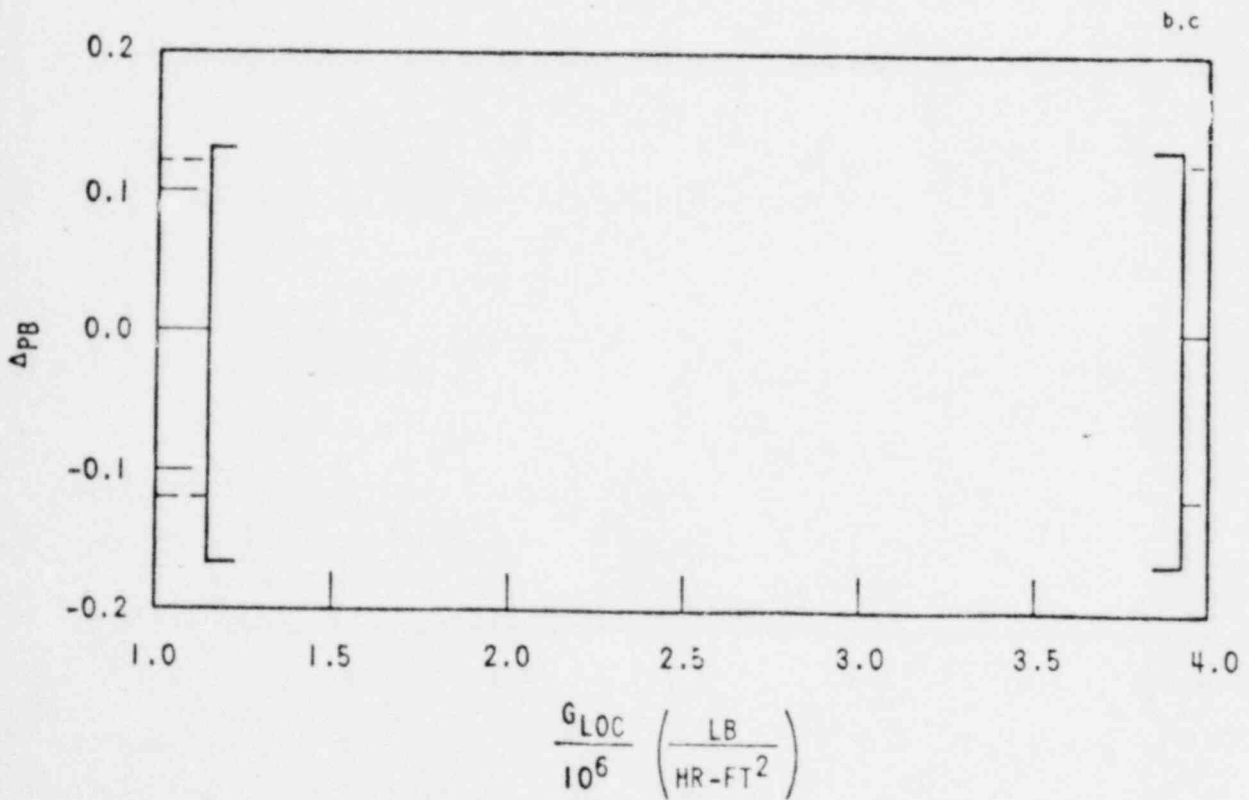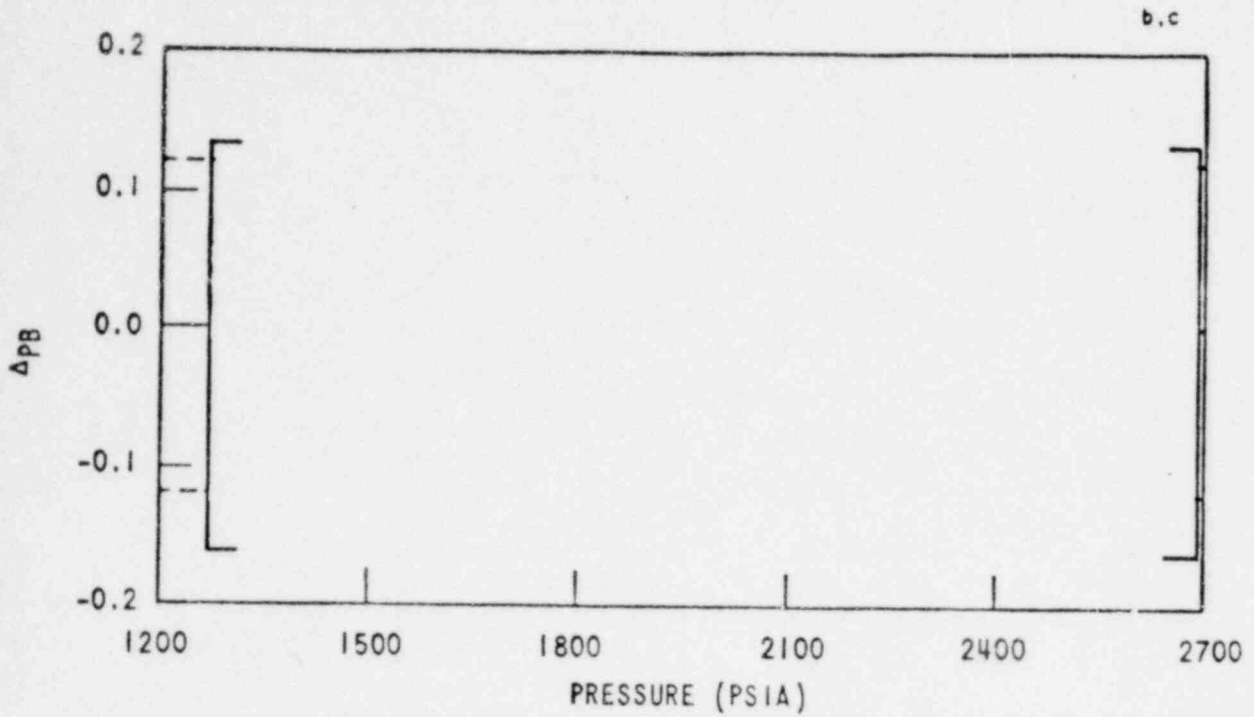
4-10

Figure 4-6. Partial Rod Bow Residuals, $\Delta_{PB} = \delta_{PB} - (\delta_{PB})_{corr}$, Versus Pressure and Flow, 85% Gap Closure
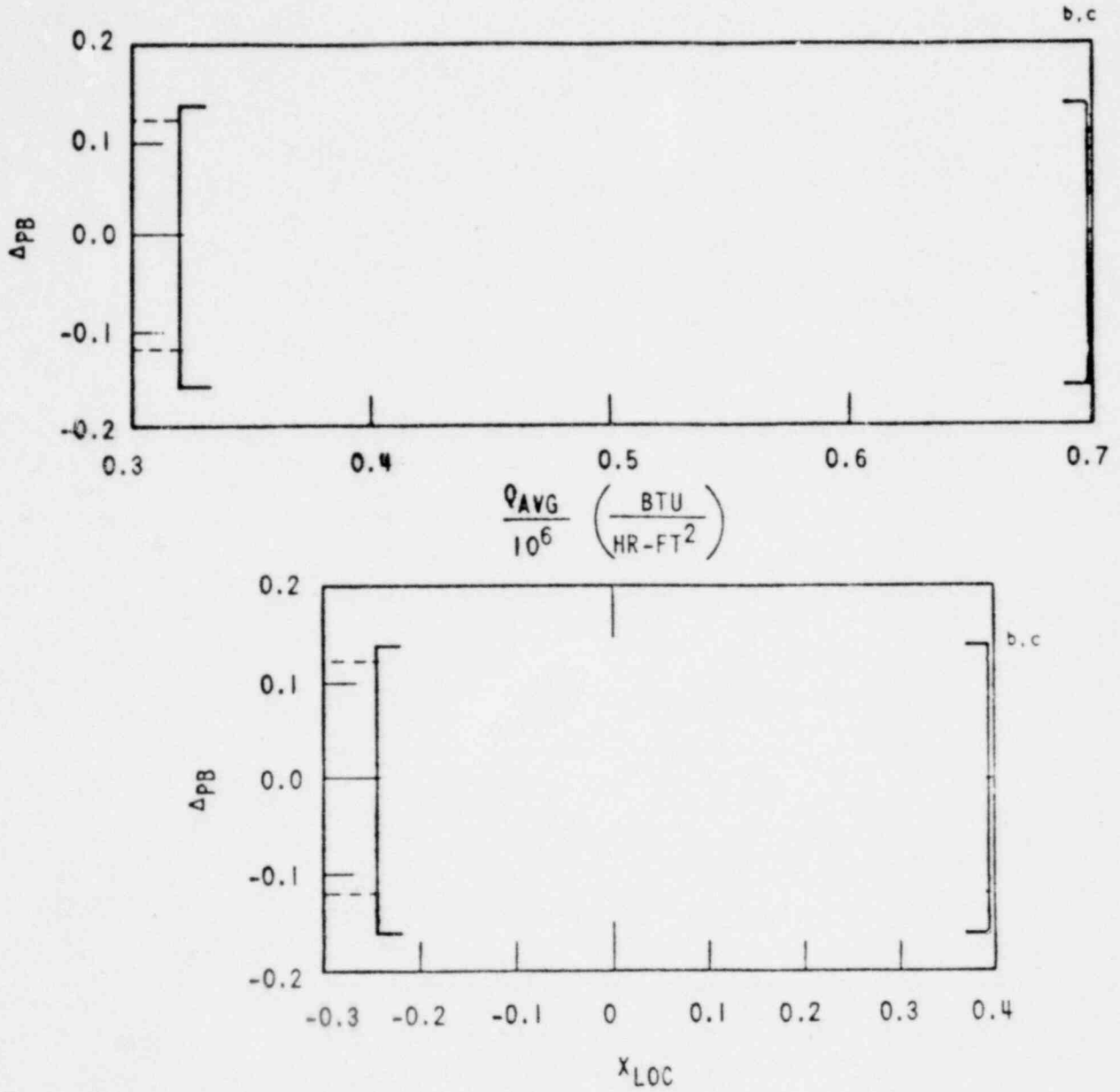
1035 225

Figure 4-7. Partial Rod Bow Residuals, $\Delta_{PB} = \delta_{PB} \cdot (\delta_{PB})_{corr}$, Versus Hot Rod Average Heat Flux and Quality, 85% Gap Closure

# SECTION 5
# CONCLUSIONS

The results of this test permit the following conclusions to be drawn:

- The effect of partially bowed heated rods on CHF is much smaller than that of heated rods bowed to contact. This effect is only slightly greater than repeatability.

- The effect of partially bowed heated rods resembles that of heated rods bowed to contact in that it is seen only at high pressures.

- The reduction of CHF caused by partially bowed heated rods can be correlated by a modification of the thimble cell contact bow correlation. This modification is in the form of a partial rod bow factor [which is a function of flow.] [a,c]